

Status and Objectives of Tokamak Systems for Fusion Research

S. O. Dean,¹ J. D. Callen,² H. P. Furth,³ J. F. Clarke,⁴ T. Ohkawa,⁵ and P. H. Rutherford³

This report had its beginnings at the Third International Symposium on Toroidal Plasma Confinement held in Garching/Munich, Federal Republic of Germany, March 26–30, 1973. The American scientists who attended this conference agreed to assist in preparing a summary of the status of the field. Since that time, the authors of this report have had the opportunity to incorporate progress reported at the VI European Conference on Plasma Physics and Controlled Fusion, held in Moscow, U.S.S.R., from July 29 to August 3, 1973. The report has been available previously only as U.S. Atomic Energy Commission Report WASH-1295 (1974). It was the first comprehensive survey of the status of the tokamak fusion research concept, which was to become the cornerstone of the world fusion effort for the next quarter century. It provided the basis for the rapid buildup of the U.S. tokamak program during the latter half of the 1970's and is published now to archive its historical significance.

KEY WORDS: Fusion; tokamak.

I. INTRODUCTION

Confinement of thermonuclear plasma in tokamak toroidal magnetic containers is a highly promising approach to the realization of fusion reactors for central station electrical generating plants. This report is devoted to a technical review of the present status and key near-term objectives of this program.

The basic tokamak apparatus is illustrated in Fig. 1. A toroidal body of plasma is confined in a strong toroidal magnetic field, generated by an external magnetic coil. The magnetic field lines are given a helical twist by the poloidal magnetic field generated by a current flowing

in the plasma torus. The plasma current, which is induced by transformer action, also serves to heat the plasma resistively.

The present world-wide research effort on tokamaks includes more than 15 major devices, in operation or under construction. Some representative parameters of these devices are summarized in Section II. The status of present-day knowledge about tokamaks and the most important remaining problems of physics and technology are outlined in Section III.

To minimize plasma leakage from the "magnetic bottle" of the tokamak, it would be desirable to make the plasma current as strong as possible; however, sufficiently high plasma currents cause the magnetic bottle itself to become grossly unstable. (Specifically, there is a safety factor $q = 5a^2B_t/RI$, where B_t is the toroidal field strength in kilogauss, I the plasma current in kiloamps, and a and R the minor and major radii of the plasma in cm. It appears that q must be kept greater than about 2.5 to insure gross stability.) Similarly, to maximize the fusion

¹ Fusion Power Associates, 2 Professional Drive, Suite 249, Gaithersburg, MD 20879.

² University of Wisconsin, Madison, WI, 53706-1087.

³ Princeton Plasma Physics Laboratory, Princeton, NJ.

⁴ Battelle Pacific Northwest Laboratories, Washington, DC.

⁵ Archimedes Technology, Inc., La Jolla, CA.

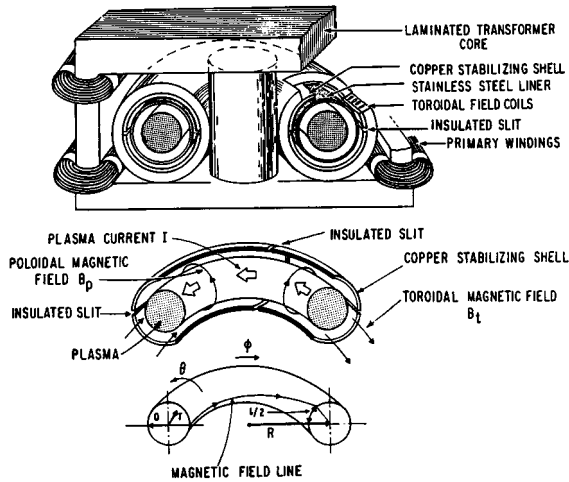


Fig. 1. Basic tokamak apparatus: a toroidal plasma confined in a helical magnetic field created by the superposition of a strong, externally generated toroidal field and the poloidal field generated by the plasma current. The plasma current, induced by transformer action, resistively heats the plasma.

energy generated in the plasma it would be desirable to make the plasma density as high as possible. However, for sufficiently high plasma density the magnetic bottle may lose its equilibrium or become grossly unstable. (The relevant parameter is $\beta_p = 8\pi n(T_e + T_i)/B_p^2$, where n is the plasma density, T_e and T_i are the electron and ion temperatures, and $B_p = 2I/a$ is the poloidal field strength. It appears the β_p must be kept below R/a .) The theory of these effects, the experimental evidence, and the possibilities for optimizing the tokamak configuration are discussed in Section III.A.

The rate of leakage of plasma from the tokamak magnetic bottle is found to be anomalous—that is, it cannot be explained by classical plasma diffusion theory. There are various theoretical explanations but the experiments do not as yet permit a unique identification of the loss mechanisms. Accordingly, there is presently considerable uncertainty about the scaling of plasma confinement in large tokamaks. It appears likely, however, that anomalous losses will not be strong enough to prevent thermonuclear ignition in a sufficiently large reactor of the tokamak type. Determining the minimum size required for ignition depends on successful development of the confinement scaling laws, as well as on the possibilities for optimizing the tokamak magnetic bottle, as discussed above. The theoretical and experimental problems of plasma energy and particle transport are discussed in Section III.B.

Resistive plasma heating by the tokamak current has raised the plasma temperature in present-day experiments to ~ 700 eV for the ions and ~ 2.5 keV for the electrons.

Since plasma resistivity decreases with rising temperature, it appears that the temperatures required for ignition (5–10 keV) cannot be achieved by ohmic heating alone. Development of auxiliary heating methods is therefore vital. The relative advantages of neutral beam injection, adiabatic compression, wave, and turbulent heating are discussed in Section III.C.

Even a plasma that is well confined in a magnetic bottle will interact with its material surroundings, by bombarding them with energetic particles and radiation. As a result, nonfusion particles are injected into the plasma, raising its radiation losses and diminishing its density of fusion nuclei. Impurities represent a major problem already in present-day high-current tokamaks, and must clearly be kept at low levels in tokamaks of the future if ignition conditions are to be reached. The basic features of the plasma boundary problem, and various means for ameliorating it, are discussed in Section III.D.

Based on the analyses of Section III, a set of key near-term objectives for the tokamak program are presented in Section IV. These include programs for answering the critical questions in each of the four major areas: configurational optimization, plasma transport and scaling, heating, and boundary effects.

II. SURVEY OF TOKAMAKS

There are now more than 15 tokamak or tokamak-like devices, worldwide, that have obtained routine operation; four of these are in the U. S. Several others are near completion or in the early stages of operation. Two large devices, PLT and T-10, are under construction. Thus, the base for tokamak research, in terms of the number of experiments, is very broad and indicates the global importance of this approach in understanding the physics of toroidal plasma confinement.

The design parameters of a number of operating tokamaks and several future tokamaks are tabulated in Tables 1 and 2 respectively. A pictorial display of a comparison of world tokamak parameters is presented in Figure 2. The design parameters of experimental devices are often not so important as the parameters that describe a characteristic plasma discharge. For a selected grouping of tokamaks, these “typical values” are shown in Table 3.

III. STATUS OF TOKAMAK RESEARCH

A. Configurational Stability

1. Elementary Theory

In a purely toroidal magnetic field B_t , a toroidal body of plasma would not be held in equilibrium: it would

Table 1. Design Parameters for Operating Tokamaks

	R	r	B_t	I_p	q
ORMAK - USA	80	23	25	340	2.4
TFR - FRANCE	98	20	60	490	2.5
PULSATOR-GERMANY	70	11	28	95	2.5
JFT-2 - JAPAN	90	28	10	180	2.4
CLEO - TOK - UK	90	18	20	150	2.4
ST - USA	109	13	50	130	3.0
ATC - USA	90-36	17-11	20-50	110-250	3.0
DOUBLET II - USA	59	doublet (12 × 15)	10	320	—
ALCATOR - USA	54	12	120	690	2.3
TTT - USA	60	10	35	90	2.4
TUMAN-2 - USSR	40	10 × 5	3-15	10	~4.0
TM-3 - USSR	40	8	40	80	4.0
T-4 - USSR	100	17	50	350	2.1
TO-1 - USSR	60	12	20	95	2.5
FINGER-RING - USSR	36	D-shaped	15	50	—
T-6 - USSR	70	25	15	270	2.5

R = major radius (cm)

r = plasma radius (cm)

B_t = toroidal field (kilogauss)

I_p = plasma current (kiloamps) design value at q listed

$$q = \text{safety factor} = \frac{5r^2B_t}{I_pR}$$

expand along its major radius. The possibility of MHD equilibrium is established in the tokamak by adding a poloidal field component B_p (Fig. 3), thus producing helical magnetic field lines. The poloidal field is generated principally by a toroidal current induced in the plasma, as in a transformer secondary. Equilibrium also requires the presence of an externally applied vertical magnetic field component B_v , which couples with the plasma current to produce an inward force along the major radius [1]. The B_v -field can be generated (transiently) by eddy

currents in a copper shell (Fig. 3(A)), or can be programmed by currents in external coils (Fig. 3(B)).

The rotational transform ι of the tokamak is defined as the angle through which a field line passes the short way around the torus (θ -direction) on passing once the long way around the torus (ϕ -direction). The “safety factor” q is defined as $q \equiv 2\pi/\iota = rB_t/RB_p$ where r and R are the minor and major radii. Thus, a magnetic field line makes q transits around the ϕ direction in making a single transit in the θ direction.

Table 2. Design Parameters of Future Tokamaks

	R	r	B_t	I_p	Estimated Operation Date
PETULA - GERMANY-FRANCE	72	16	15	105	1974
TOKAMAK - ITALY	80	22	100	1,210	1975
DITE - UK	112	23	30	280	1974
PLT - USA	130	45	45	1,400	1975
T-10-USSR	150	40	50	1,070	1975
JET (<i>tentative parameters</i>)	280	130 × 200	30	3,000	1978

R = major radius (cm)

r = plasma radius (cm)

B_t = toroidal field (kilogauss)

I_p = plasma current (kiloamps) - for a q of 2.5

$$\text{— where } q = \frac{5r^2B_t}{I_pR}$$

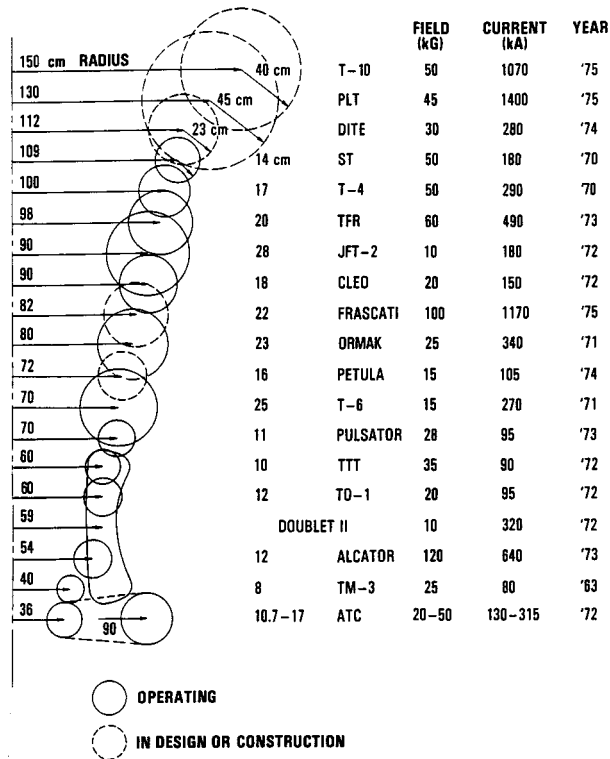


Fig. 2. A comparison of tokamak parameters throughout the world. U.S. tokamaks are ATC, Alcator, Doublet II, TTT, ORMAK, ST, and PLT. The plasma currents are calculated on the basis of $q = 2.5$.

The plasma may be unstable against a variety of “gross” or MHD instabilities, with space dependences $f(r) \exp[i(m\theta + n\phi)]$, where $m = 0, 1, 2, \dots$; $n = 0, 1, 2, \dots$. Consider first the axisymmetric $n = 0$ modes. These are stabilized (or at least slowed down) by eddy currents, when the equilibrium is provided by a copper shell. In an externally applied B_v -field, without copper shell, stability requires that the B_v -field must have a slight outward convexity [1], as in Fig. 3(B).

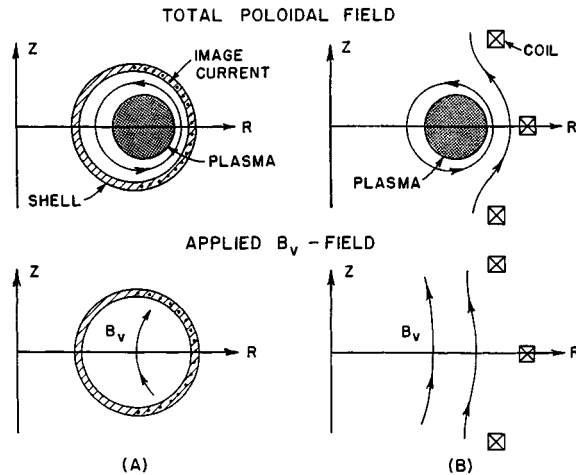


Fig. 3. Plasma equilibrium in major radius can be provided with a copper shell (A) or by external coils only (B). In either case, the required inward force (along-R) is due to the Lorentz force from plasma current flowing across the “vertical field” B_v in case (A), the B_v -field is produced by image currents in the copper shell; in case (B), the B_v -field is externally applied. Total poloidal field patterns are shown above; B_v -field patterns by themselves are shown below.

There can also be helical perturbations of the plasma column, so-called “kink” modes, with $q = m/n$, conforming with the helical magnetic field lines [2,3]. If the safety factor q drops to unity anywhere inside or outside the plasma, the $m = 1, n = 1$ kink mode is unstable, at least for monotonically decreasing J_z profiles and within a cylindrical analysis. The stability condition $q > 1$ against this mode imposes an upper limit on the plasma current flowing within the radius r : $I = rB_p/2 < r^2B_t/2R$. If the plasma edge radius is at $r = a$, and the current density is uniform, then $q > 1$ corresponds to the “Kruskal-Shafranov condition,” $I < a^2B_t/2R$. This is the basic limit on plasma current in tokamaks. Even if the condition $q > 1$ is satisfied everywhere, there can be unstable kink modes (with $m/n > 1$), provided the point $q(r) = m/n$

Table 3. “Typical Values” for Tokamak Discharges

	I_p (kA)	B_t (kG)	\bar{n}_g (cm^{-3})	n_{neu} (cm^{-3})	Central T_i (eV)	Central T_e (eV)	τ_E (msec)	β_p	q
ST	70	40	4×10^{13}	5×10^8	600	2,500	10	.8	5.1
ORMAK	120	18	3×10^{13}	3×10^8	300	700	11	.5	5.0
ATC (uncompressed)	60	15	1.5×10^{13}	10^9	250	1,000	5	.4	4.0
ATC (compressed)	140	35	8×10^{13}	—	750	2,500	~3	.2	4.0
Doublet II	130	8	1.3×10^{13}	10^9	250	550	2	.6	5.0
TFR	200	40	2×10^{13}	—	—	2,500	20	—	4.1
TM-3	70	40	7×10^{13}	$1-5 \times 10^9$	350	500	3-4	.8	4.6
T-4	120	40	4×10^{13}	2×10^8	700	1,500	16	.8	4.8
T-6	60	10	10^{13}	3×10^8	200	300	1	.3	7.4

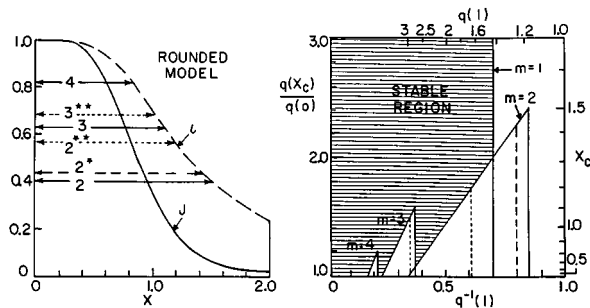


Fig. 4. Theoretical stability diagrams for the resistive kink mode (from Ref. 3), for “rounded model” of the current density profile J . At left are shown zones of possible instability for various mode numbers m . When $q(r) = m/n$ falls into such a zone, the mode can be unstable. At right are shown all unstable modes present for a given value of q at $x = 1$. (Note that the “effective plasma edge” designated by $r = a$ in typical experiments, would correspond to $x \sim 1.2$ in the present model.) As the conductivity increases, the unstable ranges of $q(I)$ are reduced. The basic diagram is for a copper shell at $x = 6$ (i.e., effectively at $x = \infty$). The stabilizing effect of shells at $x = 2.0$ and 1.33 is denoted by asterisk and double-asterisk cases on the left diagram and by long-dashed and short-dashed lines on the right diagram.

falls into the vacuum outside the plasma, or else into a plasma region of poor conductivity. In the latter case, the unstable kink is called a resistive (or “tearing”) mode.

Some typical predictions for the resistive tokamak kink instability [3] are illustrated in Fig. 4, for $n = 1$. Modes up to $m = 4$ are possible, provided the “singular surface” $q(r) = m$ falls into the appropriate unstable radial zone indicated in the left-hand diagram. The instability zones crossing the abscissa in the right-hand diagram show that, as the q -value at the characteristic plasma radius $x = 1$ is reduced (e.g., due to increasing current or shrinking current profile), the modes $m = 4, 3, 2, 1$ can appear successively. The unstable ranges of these modes can be narrowed by taking into account the condition that the plasma must be sufficiently resistive at the singular point so that the instability growth rate exceeds the “drift frequency” ω_* (c.f. Section III.B.1.b). A primitive version of this effect is illustrated schematically in Fig. 4, taken from Ref. 3. There appears to be a stable zone at about $q(a) \sim 2.5$, as well as stable zones for larger $q(a)$ values.

If $q > 1$ at all radii, the tokamak tends to be stable against flute modes (which are helical perturbations similar to kinks, but are driven principally by plasma pressure rather than by magnetic energy, and are located within the plasma column.). The stability of tokamak flutes is due to a geometric effect that causes “minimum-B stabilization” to occur on the average. For sufficiently high values of $\beta_p = 8\pi(T_e + T_i)/B_p^2$, however, the flutes can concentrate in local regions of unfavorable curvature, and thus become unstable “ballooning modes [4].” This effect

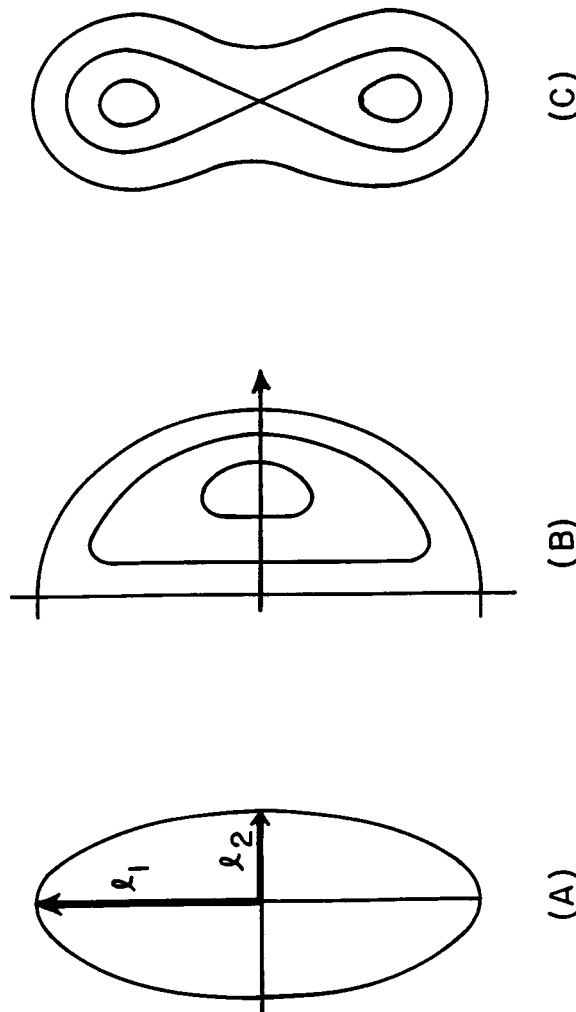


Fig. 5. Tokamaks with noncircular minor cross-section: (A), ellipse, (B) D-shape and (C) doublet. The axis of symmetry is to the left.

appears at about the same pressure level ($\beta_p \sim R/a$) at which it becomes difficult even to obtain a proper tokamak equilibrium configuration [5].

In summary, the two most important predictions of elementary tokamak MHD theory (including resistive effects) are that stability should require roughly $q(a) \geq 2.5$ and $\beta_p \lesssim R/a$. Thus we expect $B_p \lesssim B_t(a/2.5R)$ and for the important quantity $\beta = 8\pi(T_e + T_i)/B^2$ we estimate the rough limit $\beta \lesssim a/6R$.

All the above discussion is specialized to standard tokamaks, with approximately circular minor cross sections. It is of interest also to consider more general tokamak cross sections like those of Fig. 5. In the case of the ellipse (A), the poloidal field B_p has the approximate value $B_p \sim B_t(\ell_1^2 + \ell_2^2)/2qR\ell_1$ on the midplane. For a given q -value, it is thus advantageous to depart from the circular case $\ell_1 = \ell_2 = a$: if we take $\ell_1 \sim R \gg a$, then

we can have $B_p \sim B_t$, thus permitting higher values of β to be attained than in the circular case. One theoretical problem [4,6] is that stability requirements in the elliptic configuration force us to raise q , thus cancelling the advantageous effect of ellipticity on B_p/B_t . By modifying the ellipse to the D-shaped configuration (B), however, one can maintain flute stability [4] at low q -values and thus realize significant gains in β . Somewhat similar theoretical advantages are offered by the “doublet” configuration [6a] of (C). In all these cases, the problem of stability against vertical axisymmetric modes is a major consideration. The net effect of noncircular cross section on gross stability thus remains open to some question, but there is definite potential for advantage.

2. Experimental Results

The equilibrium position of the tokamak plasma column in a conventional copper-shell system (Fig. 3(A)) is found in general to conform well with the theory [7,8]. The position of the plasma can be centered within the copper shell by adding an electrically programmed vertical magnetic field component, based on external windings. In the absence of a copper shell [9–11] the externally programmed B_v (Fig. 3(B)) must do the entire job of positioning the plasma; this method appears to work equally well, though requiring a more sophisticated electrical system. In the absence of the copper shell, the requirements for stability against $n = 0$ perturbations (i.e., horizontal and vertical axisymmetric displacements) can be tested more sensitively; the ATC results are consistent with MHD theory and with an MHD simulation [9].

Nonaxisymmetric perturbations of the tokamak discharge column have been studied principally by means of magnetic pickup loops [12,13], and more recently with the heavy ion beam probe [13]. One finds rotating kink structures, typically with $n = 1$, $m = 4$, 3 and 2, as in the example of Fig. 6, which is taken from Ref. 12. There is evidently a qualitative correspondence between the experimental results and theoretical diagrams such as Fig. 4. For flatter current profiles than that in Fig. 4 — and especially for skin currents — one expects higher- m modes to appear, and this too is verified experimentally [8]. (Note incidentally, that the q -values in Fig. 6 are taken at the “plasma edge” radius a , which corresponds to the limiter radius a_L in well-centered plasmas, and is somewhat smaller in off-centered plasmas.)

The theoretical growth times of the linear modes are short compared with the times over which the oscillations are observed. It follows that the observations must be of nonlinearly saturated states of the instabilities.

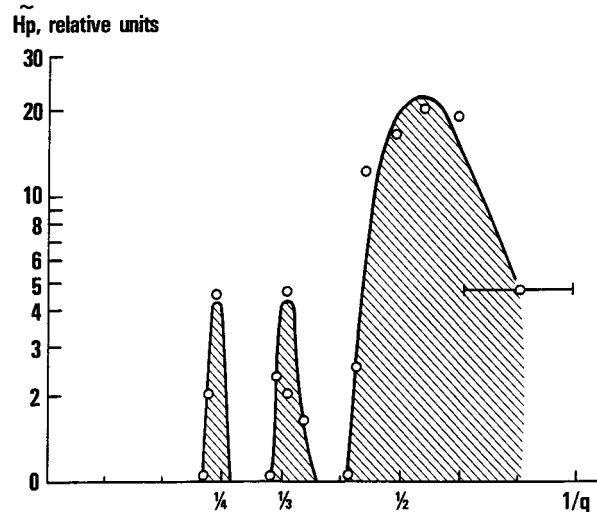


Fig. 6. Amplitude of poloidal magnetic field fluctuations in the T-3 device, as reported in Ref. 7.

The oscillations described above tend to rotate in the θ -direction at the electron diamagnetic drift velocity in the main magnetic field [8]. When there is a plasma electrostatic potential giving rise to a θ -rotation of the plasma, the corresponding velocity added to the electron diamagnetic velocity gives the correct rotation velocity of the oscillations [14]. When the plasma column is rapidly compressed in the ATC device, the rotation velocity of the oscillations speeds up in agreement with this picture [15]. The locking of the perturbations into the electron population is qualitatively consistent with theoretical expectation for resistive kink modes, particularly in the nonlinear range [16].

The oscillations (especially the $m = 2$) can be seen as density fluctuations on microwave interferometers. They have also been observed visually as bright helical bands on streak photographs. The structure of the density perturbations inside the plasma has now been examined by the thallium-ion-beam probing technique [14]. The observation that the plasma density profile may be flattened near the singular surface can be interpreted as resulting from the formation of magnetic islands inside the plasma.

The $m = 1$ mode is never seen as a slow-growing oscillation. When the plasma edge q -value has dropped sufficiently—generally below the threshold for $m = 2$ excitation—one sometimes encounters a sudden, large magnetic disturbance, associated with an explosive expansion of the plasma column, and often followed by termination of the discharge. This is known as the “disruptive instability [7,17].” It is generally accompanied initially by a negative spike of the discharge voltage (that is, the toroidal emf), though the voltage will often become

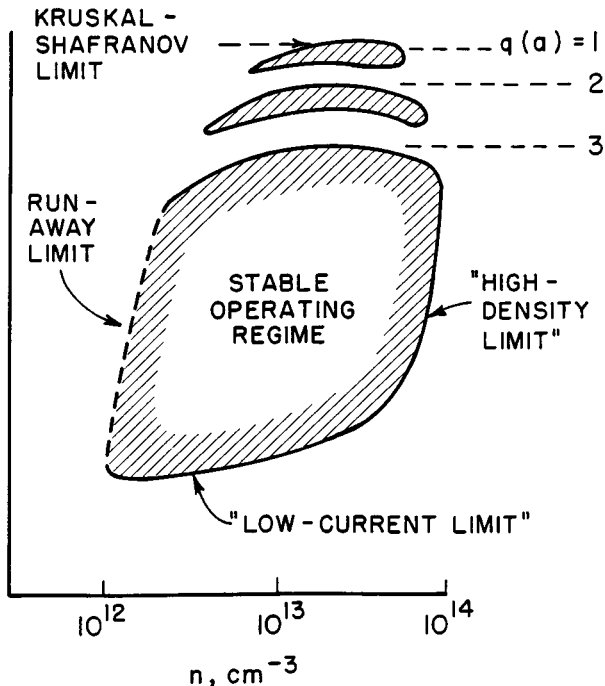


Fig. 7. Rough schematic of the stable operating regime in tokamaks. Disruptive instability sets in at both high and low currents and at high density. Electron runaway sets in at low density.

large and positive later in the course of the disruption. There is also generally a significant loss of plasma energy, and an inward shift in major radius.

The qualitative sketch of Fig. 7 illustrates the “traditional” picture of the stable tokamak operating regime. The disruptive instability limits the regime at both high and low currents. The high-current limit fits naturally into the theoretical kink-mode analysis. As the plasma edge q -value drops, one finds instability at decreasing m -numbers; after the oscillations (especially $m = 2$) reach large amplitude (typically $\sim 5\%$ perturbations in B_p), the disruptive instability appears. It is generally impossible to approach the Kruskal-Shafranov limit without being stopped by the disruptive instability. The onset of similar effects at the low-current boundary of the stable operating region is explained by a dramatic shrinking of the discharge radius (see Section III.B.2), which can outweigh the reduction of I in the safety factor ($q \approx a^2/I$), again causing the Kruskal-Shafranov limit to be approached. The attempt to reach high plasma densities aggravates the low-current shrinking and disruptive instability, thus imposing also a high-density boundary on the stable region (Fig. 7). At very low plasma densities, there are intense runaway electron phenomena, often accompanied by positive voltage spikes and sometimes by negative spikes—but it is unclear whether these effects are closely

related to the usual disruptive instability. An increase of the level of plasma impurities is found to shrink the stable operating zone of the tokamak discharge at all its frontiers—until it disappears entirely.

The structure of the disruptive instability [7,17] has now been observed by fast photography. Surprisingly, it is found that in a tangential view the minor discharge circumference remains quite circular [18] during the large and rapid plasma expansions, which may double the cross-section of the discharge in $\sim 20 \mu\text{sec}$; asymmetries, of order $>10\%$, do appear to be present just prior to disruption. These asymmetries are seen more clearly in streak pictures taken from the side [19].

While Fig. 7 indicates the maximum range of stable tokamak operation, as limited by the disruptive instability or by electron runaway phenomena, plasma energy confinement begins to deteriorate perceptibly even before the unstable boundary is reached. This is illustrated in Fig. 8, which gives schematically the behavior of the bulk energy confinement time τ_E , as observed in T-3 and ST experiments [7]. Typically, it is found that τ_E increases with rising plasma current I , but levels off for currents that cause q to fall below 2.5-3.5 at the plasma edge (or 4-5 at the limiter [7]). Alternatively, if B_t is varied for fixed I , there is little or no change in τ_E until q falls below 2.5-3.5; then there is a B_t -dependent decrease of τ_E [7,19a]. In some recent experiments with higher-currents [20], however, one finds a deterioration of τ_E setting in already at $q \sim 6$ (curve B in Fig. 6).

Additional evidence for the deterioration of confinement due to MHD-effects is provided by the escape of energetic electrons [17,22] on appearance of marked magnetic oscillations, and especially just before disruptive instability: this phenomenon is suggestive of disruption of magnetic surfaces by resistive modes.

Another interesting anomalous-transport effect, apparently related to MHD instability, has been observed on the ST. By careful adjustment of parameters, it is possible to produce discharges with q -values on axis (as calculated from $J \propto T_e^{3/2}$ and Thomson-scattering measured T_e -profiles) of about unity [21], but free from disruptive instability, and with nearly optimal energy confinement. One does observe a marked flattening of the central part of the T_e -profile, which becomes more severe as the edge q -value is reduced (by lowering B_t). The most plausible interpretation is that small-scale $m = 1$ kink and flute modes, localized near the axis, are responsible for enhanced energy transport, which causes the observed flattening of the temperature profile. This would be consistent with the theoretical finding that $m = 1$ modes localized near the axis are relatively weak.

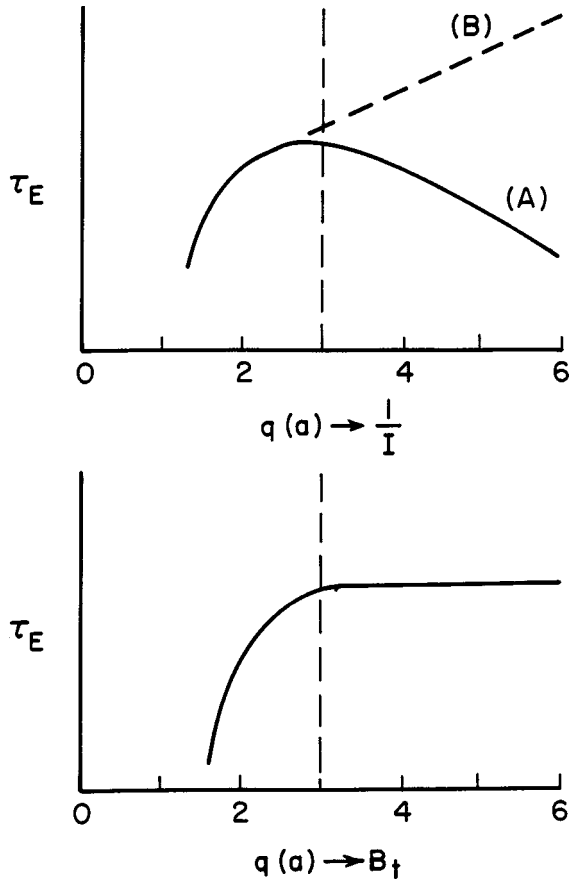


Fig. 8. Schematic of the typical q -dependence of the energy confinement time τ_E . If B_t is varied for fixed I , τ_E is unaffected in the standard operating regime ($q > 3$), but drops for small q -values. If I is varied for fixed B_t , τ_E rises for falling q , down to $q \sim 2.5$, then drops sharply (curve A). Some recent high-current experiments [20,21], however, show τ_E -deterioration with rising I setting in already at $q \sim 6$ (curve B).

Initial results are available on the stabilizing role of the tokamak copper shell. Addition of a very close-fitting shell on the T-6 device [23], (copper radius $b \lesssim 1.2$ times the limiter radius a_L) has permitted operation for short times down to q -values of ~ 1.2 at the plasma edge—a record never previously achieved in the more loose-fitting shells of T-3, T-4, and ST (where $b/a_L \sim 1.4$). The energy confinement time at low q -values in T-6, however, is rather poor, and it remains to be seen whether the ability to increase the current in T-6 above the usual q -levels is really advantageous for plasma confinement. At the other extreme, one finds in ATC [9] that the total removal of the copper shell does not lead to any evidence of inferior stability relative to the conventional tokamaks with loose-fitting shells. Grossly stable operation down to $q = 2.2$ is possible in ATC—again with an obvious deterioration in τ_E as soon as q falls below ~ 3 [23a].

With respect to the role of the copper shell, both the T-6 and ATC results are qualitatively consistent with the predictions of the simple MHD theory, as illustrated in Fig. 4: that is, the copper shell is not expected to be important *except* at very low q . The theoretically unstable ranges of the various modes are given on the left side of Fig. 4 for copper shells at $x = 1.33$ (two asterisks), $x = 2$ (one asterisk), and $x = 6$ (no asterisk). The reductions of the unstable zones on the right side of Fig. 4 are indicated by short and long dashed lines, corresponding to the cases $x = 1.33$ and 2 respectively. It is seen that even the extremely close-fitting shell at $x = 1.33$ has no substantial effect for $q(1) \gtrsim 2$ —the ATC case. A close-fitting shell, however, might play a vital role in reducing the $m = 2$ mode sufficiently so that a stable operating regime can be squeezed in for values of $q(1)$ below 1.6—an operating range that may indeed correspond to the T-6 regime.

On the whole, the experimental tokamak results on q -limitations can be said to bear a considerable resemblance to simple theoretical expectation, though many anomalies remain to be understood. As regards the β_p -limit, some initial experiments have been done on T-3 and ST, by heating the plasma resistively at high currents, and then reducing I before the plasma cools [23b,23c]. In this way, β_p -values of order 5 have been obtained transiently, without any evidence of gross instability. It should be noted, however, that such a transient demonstration of stability is not adequately convincing as to the existence of a long-lived stable configuration. Powerful auxiliary heating will be needed in order to drive β_p to R/a in steady state, so as to permit more definitive studies of attendant confinement limitations. The highest values of β obtained experimentally to date (on the compressed ATC plasma) [15] are below 1%.

Initial results have recently been obtained on noncircular tokamaks [24,25]. While we do not as yet have accurate data on the stability advantages with respect to confinement properties at low q -values and high β -values, the experiments to date show that it is clearly possible to realize the intended noncircular configurations with tokamak-like plasma parameters. These include the doublet of Ref. 24 and D-shape of Ref. 25, illustrated in Fig. 5.

3. Advanced Theory

While the MHD stability problem is well understood in principle, a great deal of analytic and computational work remains to be done in order to arrive at a detailed explanation of the present experimental results and at reliable predictions for large future tokamaks. The areas most in need of theoretical clarification are nonlinear

effects (such as the disruptive instability), the design of optimal noncircular cross sections, and the stabilization of resistive modes in high-conductivity, high-pressure plasmas.

The nonlinear theory of kink modes [26,27] has been applied to the magnetic oscillations and the disruptive instability, with considerable success in the former case. Thus far, however, it has proved difficult to account for many of the characteristic phenomena accompanying the disruption, and in particular, the conventional nonlinear MHD analysis has tended to show that the large “negative voltage spike” should not be there at all. An extremely nonlinear “vacuum bubble” model of the disruptive instability has recently been introduced [28]. Evidently, important advances remain to be made in the development of the nonlinear kink theory. The subject of magnetic-surface disruption due to nonlinear MHD effects is also still in its infancy.

Extensive theoretical work is now in progress on all the noncircular configurations shown in Fig. 5, especially the D-shaped model [29] and doublet [30], in respect to kink and flute stability. The problem of gross vertical stability can always be solved transiently by a copper shell (or an equivalent shunt-connected coil system). For steady externally-applied magnetic fields, the problem can apparently be eased by rectangularizing the ellipse: stable cases with $\ell_1/\ell_2 \lesssim 4$ are found to be possible for flat current profiles [31]. Similar techniques promise to work for the D-shape and the doublet. Very extensive numerical computations will be required to obtain fully practical MHD stability predictions for realistic current profiles, toroidal geometry, and finite β -values.

Considerable work remains to be done on the theory of resistive instabilities in future, higher-conductivity tokamak plasmas. It is well established [16] that, as the conductivity increases, the tearing modes become overstable, with frequencies corresponding to rotation in the sense of, and approaching the magnitude of, the electron diamagnetic drift speed. In this limit the growth rates are greatly reduced, and eventually the modes become either stable or, according to the most recent of the treatments in Refs. 16, radially convective. This occurs at conductivities somewhat higher than those in present experiments. The same criterion applied to a reactor, however, suggests that the lowest mode ($m = 2$ in particular) remains unstable, due to the reduction in diamagnetic drift at larger size. The experimental observation of mode rotation at about the electron diamagnetic drift speed should not be taken as evidence that the higher-conductivity regime has been reached, since in the nonlinearly saturated state of the tearing-mode instabilities [26] the ion inertia is unimportant, and the modes would be ex-

pected to rotate with the electron fluid even in the low-conductivity case. With respect to the effect of field curvature on resistive tearing modes, calculations in simple slab or cylindrical geometries [3,32] suggest that the average magnetic well of the tokamak should stabilize the modes (or, at least, greatly reduce their growth rates) in the high-conductivity limit. Current work for toroidal geometry suggests, however, that in view of their low azimuthal wave numbers and radially narrow singular layers, the modes more properly connect to geodesic-curvature resistive modes [33], which remain unstable even with an average magnetic well.

Finally, a word of caution should be expressed with regard to our understanding even of the MHD effects in tokamaks. The experimental observations indicate only that slow-growing “magnetic islands” [34] have arisen in the plasma, and that their m -values correlate with theoretical expectations based on the tearing mode stability criterion. Since these “islands” can be MHD equilibria, their onset is a transient whose mechanism may be resistivity or any other non-ideal-MHD effect. Investigation of the properties (stability, etc.) of these “islands” after the transient, even within ideal MHD theory, is a valid and potentially very profitable approach.

4. Outlook for Future Tokamaks

Present MHD stability theory predicts that β -values of order 4%—as required in typical tokamak reactor designs—should prove to be attainable for $R/a \sim 3$. Present experimental results generally show good qualitative agreement with the MHD theory, but direct experiments have not been carried out as yet on the high- β end of the tokamak parameter range. Furthermore, we do not as yet have experience with hot, high β tokamak discharges with aspect ratios as small as $R/a = 3$. In particular, for future tokamaks that lie in the collisionless (banana) regime (Section III.B.1.a), the trapping correction to the resistivity may tend to promote the concentration of the current density near the plasma axis for $\beta_p \sim 1$, thus making the simultaneous achievement of low R/a and low, stable q -value quite problematical. It is possible that practical limiting β -values for circular cross-section tokamaks might turn out to be as low as 1% - or as high as 10%.

It appears that about the same $\beta \sim 4\%$ estimate given above applies for a loose-fitting ($b/a \gg 1$) conductive shell, or with the conductive shell removed altogether—a technically convenient step for reactor purposes. On the other hand, technical inconvenience might be justified in the case of a close-fitting shell ($b/a \sim 1$), if it turns out that extremely low q -values, and

thus high β -values, can be attained. Alternatively, it might be possible to simulate the action of the copper shell by means of an appropriately designed system of feedback-stabilizing loops. The possibility of tokamaks with non-circular cross-section creates still another opportunity for raising β -values. On the basis of theory and initial experiments, several approaches of this type appear promising; but their advantages remain to be demonstrated.

There is, of course, a great continuing incentive to maximize β , even if the minimum requirements of a tokamak reactor can readily be met. The β -value is inversely proportional to the required magnetic energy of a device—which in turn is closely related to the cost.

B. Plasma Transport and Scaling

1. Elementary Theory

a. Classical Theory

Single Particle Orbits. In tokamak plasmas an individual charged particle is confined by a combination of a strong toroidal magnetic field and a weaker poloidal field. A particle is free to move along magnetic field lines, but since the field lines are essentially closed, in the absence of drifts this motion does not result in its loss from the system. The Lorentz force causes the particle to execute cyclotron orbits perpendicular to the magnetic field; the frequency Ω and gyroradius ρ of this motion are given by

$$\Omega = \frac{eB}{mc}, \quad \rho = \frac{v_{\perp}}{\Omega} \quad (1)$$

where v_{\perp} is the magnitude of the velocity component perpendicular to the magnetic field. In present experiments we have $T_i \sim 0.3$ keV, $B \sim 25$ kG, and so the ion gyroradius is about 0.1 cm.

As a particle moves along a field line into regions of varying magnetic field strength, it moves in such a way that the magnetic flux enclosed by the gyro-orbit remains constant, i.e.,

$$\pi \rho^2 B = \text{constant, or } \mu \equiv \frac{mv_{\perp}^2}{2B} = \text{constant,} \quad (2)$$

where μ is the magnetic moment of the particle. By conservation of particle energy

$$E = \frac{mv^2}{2} = \frac{mv_{\parallel}^2}{2} + \mu B; \quad v_{\parallel} = \sqrt{\frac{2}{m}(E - \mu B)} \quad (3)$$

where v_{\parallel} is the velocity parallel to the magnetic field at

a given point. The magnitude of B is approximately equal to the toroidal magnetic field, which varies as $B \cong (R_o + r \cos \theta)^{-1}$. Hence, it is minimum on the outside of the torus and maximum on the inner edge of the torus. For a maximum magnetic field strength B_{\max} on a given field line, a particle with $E > \mu B_{\max}$ will pass unidirectionally along the field line. This is called a “passing” or untrapped particle [35]. In contrast, a particle with $E < \mu B_{\max}$ finds the effective potential μB too strong and hence is “reflected” from the high magnetic field region. The latter is called a “blocked” or trapped particle [35], since it is trapped in the (weak) magnetic well along a field line. For a finite parallel velocity at the minimum magnetic field point, a particle must have $E > \mu B_{\min}$, and hence at that point a trapped particle has

$$\frac{v_{\parallel}}{v_{\perp}} \Big|_{\theta=0} \leq \sqrt{\frac{B_{\max}}{B_{\min}} - 1} \cong \sqrt{2\epsilon}, \quad \epsilon \equiv r/R_o. \quad (4)$$

The fraction f_T of the plasma particles that are trapped is just the fraction of velocity space occupied by such particles:

$$f_T \equiv \sqrt{\frac{B_{\max}}{B_{\min}} - 1} \cong \sqrt{2\epsilon}, \quad \text{fraction of trapped particles.} \quad (5)$$

Since $\epsilon \lesssim 1/4$ in most experiments, trapped particles comprise up to half the plasma. The “bounce” frequency for the periodic motion of a trapped particle in the magnetic well is approximately

$$\omega_b \cong \frac{v_T}{R_o q} \sqrt{2\epsilon}, \quad \text{trapped particle bounce frequency,} \quad (6)$$

where q is the “safety factor” defined in Section III.A.1 and v_T is a typical (thermal) particle velocity, $v_T \equiv \sqrt{2T/m}$.

In addition to the rapid gyromotion and streaming motion along the magnetic field, the particles experience an effective gravitational force due to the radial inhomogeneity of B . This force causes a particle to drift in the vertical (or z) direction with a drift velocity

$$V_D \cong \frac{c}{e} (mv_{\parallel}^2 + \mu B) \frac{B \times \nabla B}{B^3} \sim \frac{mc}{eB} \frac{v_T^2}{R} \quad (7)$$

The resultant combination of gyromotion, parallel streaming motion, and drift motion is shown in a constant toroidal angle projection in Fig. 9. For the trapped particles, the motion of the gyromotion guiding center produces the characteristic “banana” shape. The width of the banana is approximately twice the drift velocity divided by the bounce frequency:

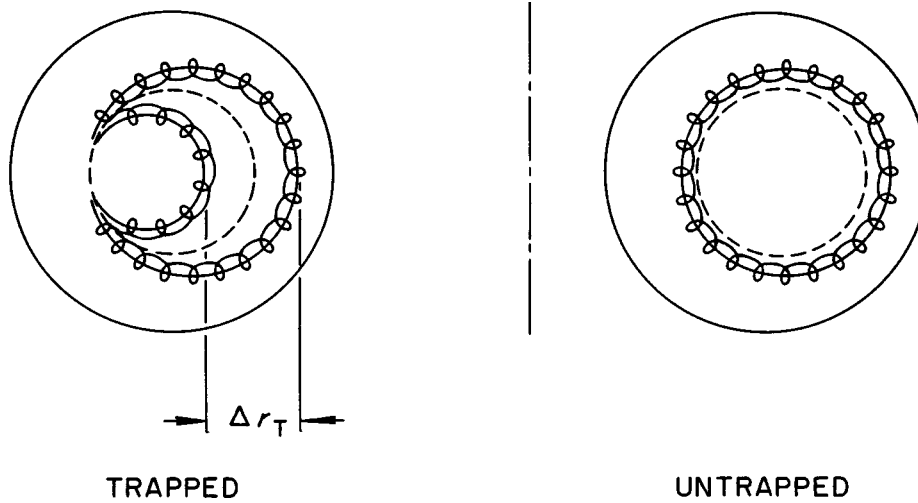


Fig. 9. Projection of particle orbits for trapped and untrapped particles into a given toroidal angle plane. Note typical “banana” shape of the trapped particle orbit. Dashed lines represent flux surfaces.

$$\Delta r_T \approx \frac{2V_D}{\omega_b} \approx 2\rho_\theta \sqrt{\epsilon} = 2q \rho' \sqrt{\epsilon},$$

trapped-particle banana width (8)

where ρ_θ is the gyroradius in the poloidal magnetic field. Note that this radial excursion is $2q/\sqrt{\epsilon}$ (~ 10) times larger than the gyroradius. The radial excursions of typical untrapped particles is only q (~ 2) times larger than the gyroradius and of no particular interest here.

The preceding discussion assumed implicitly that the magnetic field lines are closed within the plasma confinement region and that the toroidal magnetic field is homogeneous in the toroidal direction, i.e., the system is axisymmetric. From a primitive point of view when magnetic field errors or other non-axisymmetric magnetic fields are introduced, the field lines do not in general close within the confinement region. Rather, they often intersect a wall after many transits around the machine. Another significant magnetic imperfection is the bumpiness of the toroidal magnetic field caused by the use of a finite number of coils. This has the effect of creating very shallow local magnetic wells along a field line, which can “trap” a small fraction of the plasma particles [cf. Eqs. (4)–(5)]. Since such particles do not circulate around the minor cross section of the torus, nor are trapped symmetrically with respect to the horizontal mid-plane, they drift vertically out of the system at the rate given in Eq. (7). In addition to these magnetic trapping effects, an electric potential can, by itself or in combination with the magnetic field, cause particle trapping and thereby a wide variety of guiding center orbits [36]. In most present tokamak experiments, these field imperfec-

tion effects are relatively unimportant, primarily because the appropriate collisional mean free path is typically shorter than the “length” of a field line or drift trajectory to a wall [37]. The different types of effects have been demonstrated experimentally in ST [37a] by deliberately overpulsing the current in one of the toroidal field coils, thereby producing a nonaxisymmetric “magnetic mountain” of up to 30%. Then, it was found [37a] that while the bulk of the semi-collisional plasma was only slightly affected, the density of the collisionless ions in the high energy tail of the Maxwellian was significantly depressed or nonexistent. As we proceed to higher temperature plasmas, the mean free paths lengthen and more attention will have to be paid to coil design to minimize field errors [37].

Diffusion Due to Coulomb Collisions. If the plasma particles were affected only by the macroscopic fields discussed in the preceding, then plasma confinement would be simply a matter of ensuring that the plasma size be larger than the typical radial excursion Δr_T (\sim a few cm). However, the particles experience stochastic forces in the Coulomb scattering collisions they suffer with other particles in the plasma. In general we describe the particle diffusion due to the stochastic scattering by a diffusion coefficient

$$D \sim (\Delta x)^2 / \Delta t \quad (9)$$

where Δx is the mean spatial step size caused by the scattering process and Δt is the mean step time.

For a homogeneous magnetic field (i.e., straight field lines) the mean step size is the gyroradius ρ and the mean time is the Coulomb scattering time. Thus, the particle

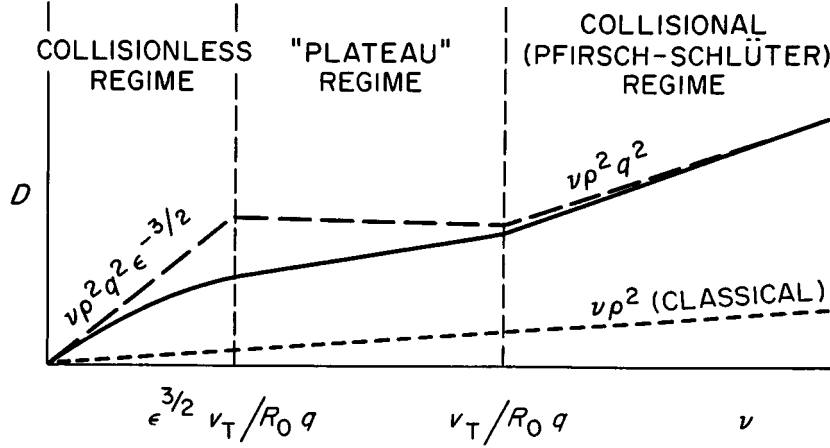


Fig. 10. Particle diffusion coefficient due to Coulomb collisions for various degrees of collisionlessness in a toroidal plasma.

diffusion caused by collisions of unlike particles (i.e., ions and electrons) is (for low β)

$$D \sim \nu \rho^2 \text{ classical diffusion} \quad (10)$$

where ν is the Coulomb collision frequency [38] for the accumulation of small angle scattering up to a complete 90° scattering [35]:

$$\begin{aligned} \nu_{ei} &= \frac{4\sqrt{2\pi} n_i Z^2 e^4 \ln \Lambda}{3 \sqrt{m_e} T_e^{3/2}} \\ &= 1.6 \times 10^4 \frac{\langle Z \rangle (n_e/10^{13} \text{ cm}^{-3})}{(T_e/1 \text{ keV})^{3/2}} \text{ sec}^{-1}. \end{aligned} \quad (11)$$

in which

$$\langle Z \rangle \equiv \frac{\sum_i n_i Z_i^2}{\sum_i n_i Z_i} = \frac{\sum_i n_i Z_i^2}{n_e} \quad (12)$$

is the mean effective charge of the plasma ions. In addition to particle diffusion, Coulomb collisions cause heat transport, viscous stress relief, etc., with similar transport coefficients [38].

The diffusion in a toroidal plasma is more complicated (cf. Fig. 10). For sufficiently long mean free paths (or low ν) the particles circulate around the drift orbits shown in Fig. 9, and thus the mean step size is not the gyroradius but the rather larger banana width Δr_T . The trapped particles can complete a banana orbit and hence have this step size only if the collision frequency for scattering particles out of the trapped-particle region of velocity space is small compared with the bounce frequency; i.e., if they are sufficiently “collisionless.” Since the trapped particle region of velocity space is small ($\sim \sqrt{\epsilon}$), and since Coulomb scattering is a cumulative

small angle scattering process, the appropriate collision frequency is

$$\nu_{eff} \sim \frac{\nu_{90^\circ}}{(\Delta\theta)^2} \sim \frac{\nu_{90^\circ}}{(v_{\parallel}/v_{\perp})_o^2} \sim \frac{\nu_{ei}}{\epsilon} \quad (13)$$

Hence, the condition that trapped particles are “collisionless” is that $\nu_{eff} < \omega_b$, or $\nu < \epsilon^{3/2} \nu_T/R_0 q$ (collisionless regime). In this “neoclassical” regime the diffusion coefficient due to the trapped particles is [39]

$$\begin{aligned} D &\sim \nu_{eff} (\Delta r_T)^2 f_T \\ &\sim \nu \rho^2 q^2 \epsilon^{-3/2}, \text{ neoclassical diffusion.} \end{aligned} \quad (14)$$

Note that this diffusion coefficient is $q^2 \epsilon^{-3/2} \sim 10^2$ larger than the classical one. Numerical coefficients for this and other neoclassical transport coefficients are derived in Ref. 6.

For higher collision frequencies, $\epsilon^{3/2} \nu_T/R_0 q < \nu < \nu_T/R_0 q$ (“plateau” or transition regime), the untrapped particles are “collisionless” but the trapped particles are scattered before they are able to “bounce.” In this intermediate regime, estimating the probability that a trapped particle completes its banana orbit to be ω_b/ν_{eff} , Eq. (9) gives

$$D \sim \frac{\nu_T}{R_0 q} \rho^2 q^2, \text{ Plateau regime [39].} \quad (15)$$

Finally, in the very collisional regime $\nu > \nu_T/R_0 q$, the particle motion along the magnetic field is impeded by the diffusive resistance to flow and the appropriate diffusion coefficient is approximately that first derived by Pfirsch and Schlüter:

$$D \sim \nu \rho^2 q^2 \text{ collisional (Pfirsch-Schlüter) regime [35].} \quad (16)$$

The transition of the transport rate from collisional to neoclassical has been experimentally observed in the dc Octopole at GGA [40a]. The transport coefficients show the scaling predicted by the theory.

The behavior of the diffusion coefficient in the various regimes of collisionality is summarized in Fig. 10. Here, the dashed line segments indicate the diffusion coefficients in Eqs. (14)–(16). The solid curve indicates the calculation by Hinton and Rosenbluth [41] where the transition regime $\nu_{eff} \sim \omega_b$ is computed more exactly. The improved curve can be inferred from Eqs. (9), (14) by multiplying Eq. (14) by the probability that a trapped particle completes a bounce orbit without scattering—a probability that decreases with increasing ν_{eff}/ω_b . The transition of the transport rate from collisional to neoclassical has been observed experimentally in the dc Octopole at General Atomic [41a]. The transport coefficients show the scaling predicted by the theory.

In the preceding, we have been discussing the particle diffusion due to collisions of unlike particles in the plasma. For an axisymmetric system it can be shown from the conservation of toroidal angular momentum that this diffusion is ambipolar [40]; i.e., the ions and electrons diffuse together, so that there is no net charge buildup. When the system is nonaxisymmetric, or magnetic field errors cause departures from axisymmetry, the ion and electron drift orbits are different, and the diffusion is not in general ambipolar. However, the diffusion-induced charge imbalance leads to a potential buildup that acts to make the diffusion ambipolar. The net result is usually to retard the diffusion to roughly twice that of the slower species and hence not to change significantly the diffusion picture developed above [37].

Coulomb collisions between like particles cause heat conduction. Since the diffusive step size is proportional to the gyroradius, which is larger for the heavy ions than for the light electrons, the ion heat conductivity is larger than that for the electrons for typical tokamak plasmas. In fact, the transport coefficient for ion heat conductivity is larger (typically by $\sqrt{\frac{m_i T_e}{m_e T_i}} \sim 10^2$ than either that for electron heat conductivity or particle diffusion. Thus, roughly speaking, the ion temperature profile in plasmas for which the transport processes are due to Coulomb scattering should be much flatter than either the electron temperature or plasma density profile [42].

While the Coulomb collision transport theory for equilibrium plasmas is in general well developed and reasonably precise, its principal predictions have been verified experimentally only for toroidal plasmas that do not carry a toroidal current [43,44]. In current-carrying

tokamak plasmas, the particle transport and electron heat conduction processes typically exceed the neoclassical predictions by several orders of magnitude (see Sec. III B.2). However, it has been found in T-3 [45] and ORMAK [45a] that the ion heat transport, after losses due to charge exchange (see Section III.B.1.c) are subtracted out, is reasonably consistent with the neoclassical prediction for the ion heat conductivity in the regime $\nu_{eff} \sim \omega_b$.

Neoclassical transport theory has some other implications beyond simple particle and heat transport. For example, the same frictional forces between trapped and untrapped particles that cause the radial particle diffusion cause a “bootstrap” current to flow in the plasma. When $\beta_p > \epsilon^{-1/2}$, this current can exceed the ohmic heating current. The bootstrap current is proportional to the pressure gradient and hence to the plasma β . The condition that the bootstrap current be kept weak enough so that $q > 1$ (for macroscopic stability—see Section III.A) leads to the limit [46] $\beta < \epsilon^{3/2}$. There is some speculation that the plasma current induced by neutral beam injection (see Sec. III.C.2) could act as the “seed” for the bootstrap current, and that the resultant system might be able to be run steady-state with an ohmic-heating transformer required only for the initial breakdown and heating phase. So far, the bootstrap current aspect of neoclassical theory has not been verified experimentally. In fact, it was not observed in the only experiment in which it has been searched for, the proto-CLEO stellarator experiment [43].

In an infinite, homogeneous plasma the electrical resistivity of the plasma is that calculated by Spitzer and Harm [48a]:

$$\eta_{Sp} = \alpha \frac{m_e \nu_{ei}}{n_e e^2} = \frac{2.8 \times 10^{-8}}{[T_e/1 \text{ keV}]^{3/2}} \left[\frac{\langle Z \rangle \alpha}{0.51} \right] \text{ Ohm-m} \quad (17)$$

where $\alpha = 0.51$ ($Z = 1$), 0.44 ($Z = 2$), 0.38 ($Z = 4$), 0.32 ($Z = 16$), or 0.30 ($Z = \infty$). In a “collisionless” ($\nu_{eff} < \omega_b$) tokamak plasma only the untrapped particles can carry the current. Also, there is a friction or momentum exchange between the untrapped (current-carrying) and trapped particles. Together [48b] these effects cause the resistivity in a tokamak to be increased by an additive factor proportional to the fraction of trapped particles [41]; the increase in plasma resistivity caused by these effects is typically less than 50%. For $\beta_p \sim 1$ the bootstrap current is an effect of comparable magnitude [48c] in Ohm’s law and it must be taken into account in calculating the relationship between the current and voltage in a tokamak. Experimentally the plasma voltage in tokamaks is found to exceed the neoclassical prediction for a hydrogenic plasma by a factor of 2–7; this factor, which we will label as A_R , is called the resistivity enhancement or

anomaly factor. If all the enhancement is attributed to impurities then this would imply an impurity level determined from the resistivity enhancement of

$$Z_{eff} \equiv \langle Z \rangle = A_R \left[\frac{0.51}{\alpha(Z_{eff})} \right] \sim 1.5A_R, \quad (18)$$

which is typically ~ 3 -10 in present tokamak experiments.

Another implication of neoclassical transport theory is that the ohmic-heating induction electric field causes enhanced plasma pinching. In classical (straight-field) plasmas the $c\mathbf{E} \times \mathbf{B}/B^2$ drift velocity causes the plasma as a whole to “pinch” toward the plasma center. In collisionless plasmas the untrapped particles pinch at this same rate, but the trapped particles pinch, by what is often called the Ware pinch effect [49], at a velocity of cE/B_p , i.e., $(B/B_p)^2 \sim 10^2$ times faster. This inward pinching is predicted to be faster than the outward diffusion, and thus lead to no net particle loss if $\beta_p \lesssim 1$. So far this effect has been neither systematically searched for nor experimentally observed.

As implied by the resistivity anomaly, tokamak plasmas are often plagued with a few high- Z impurity ions. When more than one ion species is present, the above picture is slightly modified in all collisional regimes, because the ion component with the higher Z feels a frictional force that causes it to concentrate near the center of the discharge [38,50]. The magnitude of the relevant diffusion coefficient is comparable to that for the ion heat conductivity. Hence, the diffusion of high- Z impurities to the plasma center should be a dominant transport process. An impurity peaking effect appears to have been observed experimentally [51]. The fact that the impurities may tend to concentrate near the hot plasma center is of some concern, as it is there that they can be most deleterious to plasma energy confinement through line radiation, enhanced Bremsstrahlung, and increased transport coefficients [cf. Eq. (12) and Sec. III.B.1.c].

In summary of the classical theory, it may be said that if Coulomb collisions were the only significant processes that led to plasma transport, then, since the resultant transport coefficients are small and decrease with increasing temperature (as $T^{-1/2}$), the plasma confinement would be ample by several orders of magnitude for fusion reactor requirements. Unfortunately, the particle and electron energy transport processes in present tokamaks (which operate in the regime $\nu_{eff} \sim \omega_b$) are not described by the classical theory. However, the part of the ion energy transport by conduction is apparently close to the neoclassical prediction.

b. Anomalous Transport

Since the only plasma distribution in thermodynamic equilibrium is a spatially uniform, Maxwellian velocity distribution, a confined plasma is necessarily out of equilibrium. As discussed in the preceding section, the most obvious relaxation mechanism is by Coulomb collisions, which fortunately have a cross section that does not exceed the fusion cross section by excessively large factors at high plasma temperatures: both cross sections are very small. However, in this “collisionless” regime the plasma can also relax toward equilibrium through various types of collective plasma instabilities. Plasma instabilities are customarily divided into two classes: macroinstabilities (derivable from a fluid description) and microinstabilities (derivable only from a kinetic description). The relevant macroinstabilities for a tokamak plasma have been discussed in Section III.A and shown to be unimportant as long as $q(a) \gtrsim 2.5$ -3.

In contrast to the macroinstabilities, we do not know how to stabilize all microinstabilities; in fact, we suspect that not all of them can be stabilized. Because of their generally short wavelengths, high frequencies, and the small amounts of energy driving them, the microinstabilities are generally expected to grow rapidly into the nonlinear regime, where their growth is limited. They are thus not expected to be as large-scale and chaotic as the macroinstabilities. However, they can cause rapid, small-scale, but relatively ordered plasma transport, and hence be very detrimental to plasma confinement. Since the transport caused by microinstabilities is in general in excess of, and relatively unrelated to, classical transport, it is usually referred to as “anomalous” transport.

The main sources of free energy that drive plasma microinstabilities are:

- 1) *Velocity-space anisotropy*, specifically the distribution function distortion caused by the current in the plasma, and, perhaps, differences between the distribution functions for trapped and untrapped particles.
- 2) *Plasma expansion energy* due to the fact that a confined plasma necessarily has gradients of density, temperature and more generally, of pressure.
- 3) *Magnetic energy*, stored in the distortions of the magnetic field from its vacuum state. (While microinstabilities driven by this source of free energy are certainly possible, in addition to the kink-tearing macroscopic modes discussed in Section III.A, no particularly important ones have been identified as being relevant in toroidally confined plasmas. Thus, we will neglect this free

energy source in the remainder of our discussion of microinstabilities.)

There are three main types of nonlinear effects that lead to a saturation of the linear growth phase of the microinstabilities:

- 1) *Quasilinear* [52,53]: As linearly unstable modes grow in amplitude, they modify the nonequilibrium distribution function that provides their growth. Quasilinear theory is the part of nonlinear theory that takes the perturbative first order distribution-function modifications into account to produce conservation of energy and momentum for the perturbed system. The resultant modifications generally relax the distribution function to a stable state; however, the instability amplitudes required to effect this are often only marginally within the range of validity of the perturbation expansion.
- 2) *Mode-coupling*: The coupling of a particular linearly-unstable mode of a plasma to other modes of oscillation of a plasma is called mode-coupling theory [54]. This coupling can be of the stabilizing or destabilizing [55] type. This saturation mechanism applies only for a few special types of modes, and even there, as with the quasi-linear theory, the instability amplitudes required for nonlinear saturation are often larger than is allowed by the perturbation expansion.
- 3) *Strong turbulence*: Unstable modes in a plasma often reach amplitudes where they affect, in a nonperturbative manner, the orbits of the particles in the plasma [56,57]. This orbit modification then leads to a modification of the wave-particle resonance that was responsible for the microinstability in the first place, and, ultimately, to the nonlinear saturation of the instability. The effective damping rate due to this effect is of order $k_{\perp}^2 D$, where we have taken for the reciprocal step size the relevant perpendicular wave number of the modes giving rise to the orbit diffusion, and where D is the appropriate diffusion coefficient. Nonlinear saturation occurs when this damping is greater than the linear growth, and this equality leads to the commonly used formula $D \sim \gamma/k_{\perp}^2$ for a very rough upper bound on the diffusion due to a given group of modes. This strong-turbulence orbit-diffusion is the mechanism thought to be responsible for the ultimate saturation of most of the micro-instabilities encountered in toroidally confined plasmas.

Among the various microinstabilities, the first types we will consider are those whose source of free energy is the velocity-space anisotropy. Such microinstabilities must have phase velocities that resonate with the portions of velocity-space that are the source of free energy. Also, the most unstable ones are invariably characterized by the highest possible frequencies. They generally have frequencies comparable to the electron or ion plasma frequency, and wavelengths slightly greater than the Debye length.

A prominent velocity-space anisotropy microinstability is the current-driven ion acoustic instability [58]. (A related instability is the current-driven ion cyclotron mode [59].) This mode has a frequency near the ion plasma frequency. It is unstable only if the current drift velocity $u = j/ne$ is large enough so that [60,61]

$$u > V_s \sqrt{\frac{m_i}{m_e}} \left(\frac{T_i}{T_e}\right)^{3/2} e^{-T_e/2T_i} \quad (19)$$

where $V_s \equiv \sqrt{T_e/m_i}$ is the ion sound speed. This mode is often invoked as a source of anomalous resistivity in tokamak experiments. However, since most present experiments have $T_e/T_i \lesssim 4$ and $u/V_s \lesssim 2$, we see from condition (19) that this mode should be stable. There is also the possibility that, even when these modes are stable, but weakly damped, they might cause an anomalous resistivity. However, a specific calculation in this regime [62] has shown that there is no significant enhancement of the resistivity unless the instability condition, (19), is satisfied. In addition, since the true velocity distribution function in a tokamak plasma is not of the shifted Maxwellian type, as is assumed in the usual calculations, but, rather, carries a large amount of the current in untrapped particles at high velocities, condition (19) would seem to be a necessary, but not sufficient, condition for instability.

Another velocity-space anisotropy instability of interest is an electron-plasma mode that is driven by a gradient in the current drift velocity u over the cross-section of the plasma [63]. This mode may play a role in the anomalous skin effect observed in most tokamaks, by the introduction of an anomalous electron viscosity in the plasma.

The most important class of microinstabilities in tokamaks is that driven by the expansion free energy. Here, most of the relevant instabilities are related to the drift waves. In a plasma that has an inhomogeneous (in the r direction) distribution of gyromotion guiding centers, there is an apparent drift of the particles in the $\underline{B} \times \nabla n$ direction. This diamagnetic drift velocity is given by

$$V_d = \frac{cT}{eB} \frac{1}{n} \frac{dn}{dr} = \frac{\rho}{r_n} v_T, \text{ diamagnetic drift velocity} \quad (20)$$

where we have defined the effective plasma radius $r_n = \left(\frac{1}{n} \frac{dn}{dr}\right)^{-1}$. Now, when there is a fluctuating electric field \tilde{E}_θ in the $\underline{B} \times \nabla_n(\theta)$ direction that has a wave number k_θ , this produces a drift wave with frequency

$$\omega_* = k_\theta V_d, \text{ drift wave frequency.} \quad (21)$$

Since k_θ has a minimum value of $1/r$ and a maximum effective value of ρ_i^{-1} , the range of possible drift frequencies always lies between

$$\omega_{*min} \approx \frac{V_d}{r} \sim \frac{cT}{eB} \frac{1}{r r_n} \sim \frac{v T_i \rho_i}{r r_n}, \text{ and} \quad (22)$$

$$\omega_{*max} \approx \frac{V_d}{\rho_i} \sim \frac{v T_i}{r_n} \quad (23)$$

In a more physical manner, we can say that the \tilde{E}_θ causes particles to move in the $\underline{E}_\theta \times \underline{B}$ or r direction in an oscillatory manner at the natural frequency ω_* and hence to sample a limited region of spatial density variation. Since the simple $\underline{E} \times \underline{B}$ drifts of electrons and ions are the same, this process alone does not cause any momentum or energy exchange, and hence there is no instability. However, if there is some process that can retard the $\underline{E} \times \underline{B}$ motion of either particle species, then this causes the species to get out of phase. The particles exchange energy and momentum with the wave, and, if the conditions are right, the wave grows. Thus, a discussion of the various types of drift waves basically reduces to a discussion of the mechanisms by which the $\underline{E} \times \underline{B}$ drifts of ions and electrons can be slightly out of phase. In turn, the various mechanisms that occur can be delineated by the relationships that exist between the natural frequencies of the confined plasma: the collision frequency ν ; the minimum and maximum drift frequencies ω_{*min} , ω_{*max} ; the bounce frequency ω_b ; and the curvature drift frequency $\omega_D \equiv k_\theta V_d$.

First, we consider the regime where $\nu \sim \omega_* > \omega_{*min} > \omega_{be}$, in which we encounter modes that are called either resistive drift waves [64] or drift-dissipative [65] modes. Here, the particle collisions are sufficiently frequent so that they drastically modify the $\underline{E} \times \underline{B}$ drifts of the electrons. The growth rate of this mode is $\gamma \sim \omega_*$, with the maximum resultant diffusion apparently being

$$D_{max} \sim \frac{\gamma}{k_\perp^2} \Big|_{max} \sim \frac{\omega_{*e}}{k_\perp^2} \Big|_{max} \sim \frac{cT}{eB} \frac{1}{k_\perp r_n} \Big|_{max} \quad (24)$$

For $k_\perp r_n \sim 1$, this is the Bohm diffusion rate, which was

so ubiquitous in the C-Stellarator experiments [66]. Thus, the resistive drift instabilities have often been advanced as the cause of Bohm diffusion in the C-Stellarator. However, direct measurements of the correlated density and potential fluctuations and the resultant plasma transport by Young [67] were inconclusive on this point; i.e., they neither proved nor disproved this hypothesis conclusively. A necessary condition for the regime of Eq. (24) is $\omega_{*min} > \omega_{be}$ or, $r/R_o q < \rho_i/r$. [The condition [68] that the magnetic shear be weak enough so that a radially localized standing wave mode exists, $(r_n/L_s < \rho_i/r_n)$, is quite similar, since the shear length $L_s^{-1} \equiv (r/R_o q^2)(\partial q/\partial r)$ is often of order $R_o q$.] This necessary condition was apparently satisfied in the C-Stellarator but is not satisfied in tokamak experiments. Tokamaks and a number of stellarators with fairly large rotational transforms (or low q) do not seem to exhibit the unfavorable Bohm diffusion.

In tokamak experiments, the relationship between the various natural frequencies of the plasma is typically

$$\omega_{Dmin} < \omega_{*min} \ll \omega_{bi} \ll \omega_{*max} < \omega_{be}.$$

Thus, the various types of drift waves that occur in tokamaks can be arranged in order of their appearance as the collision frequency decreases.

A) $\nu_{eff} > \omega_{be}$, but $\nu < \omega_{*max}$. Here, collisions are sufficiently rapid so that trapped particles collide before they bounce and hence do not really know they are trapped. Drift dissipative modes develop, as above, from the collisional modification of the electron $\underline{E} \times \underline{B}$ drifts. The radial excursion of the electrons caused by a drift wave fluctuation potential of $e\varphi$ has been estimated by Pogutse [69] to be

$$\Delta x \sim \rho \sqrt{\frac{e\varphi}{T}} \left(\frac{k_\theta}{k_\parallel}\right) \quad (25)$$

where k_\parallel is the wave number along the magnetic field of the relevant fluctuation. The resultant heat transport coefficient for the electrons is estimated to be [69]

$$\chi_e \sim \sqrt{\frac{e\varphi}{T_e}} \nu_{ei} \rho^2 \left(\frac{k_\theta}{k_\parallel}\right)^2 \sim \sqrt{\frac{\Delta n}{n}} (k_\theta r)^2 \nu_{ei} \rho_{be}^2 \sim C_o \nu_{ei} \rho^2 \theta_e \quad (26)$$

where in the next-to-last approximate equality we have made use of the fact that for a tokamak $k_\parallel \approx 1/qR_o$, and in the last expression the numerical coefficient C_o is chosen empirically; it is typically in the range 4–10. A similar coefficient has been obtained for a particle diffusion coefficient, $D \sim C_1 \nu \rho^2 \theta_e$, from a similar basis by Yoshikawa [70]. The particular empirical constants C_o and C_1 used in describing pseudoclassical diffusion are

somewhat different for various tokamak groups. In the origination of pseudoclassical diffusion Artsimovich [71] inferred $C_0 \approx 10$, $C_1 \approx 0$ from experimental data (cf. Sec. III.B.2). At present the commonly used values are $C_0 \approx 10$, $C_1 \approx 3$ (ORNL), and $C_0 \approx 1-4$, $C_1 \approx C_0/3$ (PPPL). It is very important to realize that pseudoclassical diffusion has been derived from a phenomenological picture and not from first principles. Thus, its extrapolatability and perhaps even its validity are subject to considerable debate.

B) $\nu_{eff_e} < \omega_{be}$, $\nu_{eff_e} > \omega_{*min}$, dissipative trapped-electron mode. In this case, the trapped electrons are “collisionless” in the sense that they bounce before colliding. However, the collisions do retard the $\underline{E} \times \underline{B}$ drift of the trapped electrons and thereby cause an instability if there is a temperature gradient. The maximum growth rate of the mode occurs for $\gamma \sim \nu_{eff} \sim \omega_*$, which determines the relevant $k_\perp (> 1/r)$. Thus, the electron heat transport and diffusion coefficients estimated from a strong turbulence theory are [72,73]

$$\chi_e \sim \frac{\gamma}{k_\perp^2} \sim \frac{\nu_{eff}}{k_\perp^2} \sim 3\epsilon^{3/2} r^2 \frac{\omega_{*min} \omega_{*min}^T}{\nu_{ei}}, D \sim \epsilon \chi_e \quad (27)$$

where ω_{*min}^T is the minimum electron-temperature-gradient drift-frequency $\frac{c}{eBr} \frac{\partial T}{\partial r}$. This transport has an “unfavorable” scaling with collision frequency, since it increases in magnitude as the plasma temperature increases and the collision frequency corresponding falls.

C) $(\nu_{eff})_e < \omega_{be}$, $(\nu_{eff})_e < \omega_o \approx 0.1 (r/\rho_{\theta e}) \omega_{*min}$ (cf. Fig. 3), dissipative trapped-electron mode [72,73]. This is really just a lower collision frequency regime of the preceding mode. In this regime, the effective k is not determined by the condition $\nu_{eff} \sim \omega_*$, but rather by the radial localization properties of the mode [73] and hence by the magnetic shear. The growth rate of this mode is $\gamma \sim \epsilon^{3/2} \omega_* \omega_*^T / \nu_e$, and the electron heat conductivity is estimated to be [74]

$$\chi_e \sim c_2 \nu_{ei} \rho_{\theta e}^2 \quad (28)$$

collision frequency correspondingly falls.

where $c_2 \approx 0.06 \epsilon^{1/2} (d \ln T / d \ln n) (m_i / m_e) (B_\theta / \theta B)$ a constant of order 10^2 , depending on the magnetic shear strength $\theta \equiv r_n / L_s$.

D) $(\nu_{eff})_i \ll \omega_{bi}$, dissipative trapped-ion mode [72]. Here, the frequency of the mode drops below the ion bounce frequency, and the drift wave is supported by just the trapped particles. As with the dissipative trapped-electron modes, the trapped-electron collisions have a destabilizing effect. However, trapped ions [75,76] and

ion-bounce resonances [76,77] have a stabilizing effect, and can completely stabilize the mode if [75,78]

$$\frac{\nu_{ii}}{\epsilon \omega_{bi}} > 0.4 \left(\frac{m_e}{m_i} \right)^{7/18} \left(\frac{T_e}{T_i} \right)^{7/6} \quad (29)$$

For lower collision frequencies, this mode is unstable, and using the strong turbulence relation $D \sim \gamma / k_\perp^2$ with $k_\perp \sim 1/r$ yields [72]

$$D \sim \chi_e \sim \chi_i \sim \frac{\epsilon^{5/2} r^2 \omega_{*min}^2}{\nu_{ei} (1 + T_e / T_i)^2}. \quad (30)$$

Recently [76], the localization effects caused by magnetic shear have been investigated. Since these effects cause the mode to be localized to the region between mode rational surfaces, which is a region smaller than the full radius of the plasma, the diffusion may be considerably smaller [76] than that estimated in Eq. (30). On the other hand, proper consideration of profiles self-consistent with a diffusion process of this kind [79] indicates that the loss rates may be larger than simple parabolic density profile estimates would indicate. However, the profiles, and consequently the loss rates, may be able to be tailored by adjusting the spatial distribution of the source of plasma particles [80].

E) $(\nu_{eff})_i < \epsilon^{1/2} \omega_{*min}$, trapped-particle interchange mode. In this very collisionless regime the instability resembles the ordinary MHD flute instability in a mirror machine, in that it is driven unstable by the combination of the radial pressure gradient and the unfavorable drifts of the trapped particles. The only difference is due to the fact that in toroidal systems the trapped particles are embedded in the plasma of untrapped particles, which, because of its high dielectric constant $\epsilon_{||} = 1 + 1/k^2 \lambda_D^2 \gg 1$, strongly diminishes the effect of charge separations. However, since $\epsilon_{||} \neq \infty$, a flute mode with

$$\omega^2 = \epsilon^{1/2} \omega_* \omega_D, \gamma = \sqrt{-\epsilon^{1/2} \omega_* \omega_D}$$

does take place. (The mode can be derived from fluid-type equations [72] if proper account is taken of the differences between the trapped and untrapped “fluids”.) These instabilities can be stabilized by making the trapped particle drifts favorable rather than unfavorable, e.g., by using very non-circular cross sections [81,82] or [83] high $\beta_\theta (\gtrsim \epsilon^{-1})$. Presuming this mode to be localized radially [81] to a region of width $\Delta r (< r_n)$, a strong-turbulence-theory estimate of the diffusion caused by the mode is given by

$$D \sim \sqrt{-\epsilon^{1/2} \omega_* \omega_D} (\Delta r)^2 \sim \epsilon^{3/4} \frac{c T_e}{e B} \frac{(\Delta r)^2}{r r_n} \quad (31)$$

Note that this diffusion coefficient is apparently some

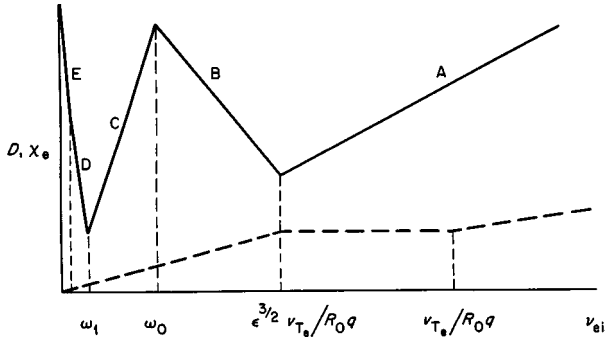


Fig. 11. Scaling with collision frequency of the estimates of the transport coefficient arising from the drift wave instabilities which obtain in the various collision frequency regimes. The letters on the various line segments refer to the descriptive sections in the text. The dashed line at the bottom indicates the predictions of the neoclassical transport theory (cf. Fig.10). The break points ω_0 and ω_1 are given roughly by

$$\omega_0 \approx \omega_{*min} \left(\frac{r}{\rho\theta_e} \right) \sqrt{\frac{3\epsilon^{3/2}}{C_2} \frac{\partial \ln T}{\partial \ln n}},$$

$$\omega_1 \approx \omega_{*min} \left(\frac{r}{\rho\theta_e} \right) \left(\frac{T_i/T_e}{1 + T_e/T_i} \right) \sqrt{\epsilon^{3/2}}.$$

small fraction of the unfavorable Bohm diffusion coefficient.

The scaling with collision frequency of the transport coefficient for the various trapped-particle drift wave instabilities is summarized in Fig. 11. Present tokamaks operate near the transition region between A and B, and a reactor would operate in the transition region between C and D, or a bit into region D. The important things to note from Fig. 3 are that the transport coefficients can be significantly larger than the neoclassical values, and that they do not scale the same way with collision frequency.

The preceding discussion of trapped-particle instabilities has concentrated on the flutelike modes, i.e., those which have nearly constant perturbed potentials along the magnetic field lines. Trapped-particle instabilities with other standing-wave characteristics may also exist. At present the possible mode geometries of the trapped particle modes have not been completely elucidated. However, odd modes, for which the perturbed potential changes sign somewhere along a magnetic field line, have been found in both collisional [84] and collisionless [85] regimes.

We must point out, of course, that the theoretical formulas given here are only order-of-magnitude estimates, which are continually being refined, and that some are sufficiently crude that the existence of the phenomena is not even certain. Since no part of the trapped-particle instability theory has ever been compared successfully with experiment in a detailed manner, it does not seem appropriate to take the specific theoretical predictions too

seriously. However, it is important to realize that the further we penetrate into the collisionless regime ($\nu \rightarrow 0$) the more likely it is that collective plasma microinstabilities will cause significant (perhaps catastrophic) enhancement of the transport coefficients. It is therefore fortunate that the conditions for a toroidal reactor can apparently be met without going deep into the collisionless range. Future experiments in internal ring devices may yield quantitative results on the transport coefficients in the trapped particle regime. Note, incidentally that the meaning of "collisionless" in the sense of Eq. (29) of the present section is somewhat different from the meaning of "collisionless" in the sense of Section III.B.1.a; the present meaning is more relevant for reactor considerations.

In addition to these estimates of the transport due to standing-wave instabilities in a plasma, there can be "anomalous" transport due to an enhancement of portions of the thermal fluctuation spectrum in a toroidal plasma. In general there are two classes of such enhancements. First, there is the so-called quasiclassical scattering process [86], due to the long-range polarization fields arising from convectively unstable (but globally stable) waves. As a plasma becomes unstable, it typically first goes through a convectively (nonzero group velocity) unstable state before becoming globally unstable; the quasiclassical scattering process is effectively the transition process between the completely stable, Coulomb-collision-dominated plasma and the case of fully developed turbulence. In a specific calculation of this transition for collisionless drift waves [62], it was found that this transition region is quite narrow and apparently not too significant.

The second class of enhancements of portions of the thermal fluctuation spectrum arises because plasmas that are infinitely extended and homogeneous along the magnetic field lines (i.e., "two-dimensional" plasmas) have a considerably different fluctuation spectrum from an unmagnetized, three-dimensional plasma [87]. In fact, the fluctuation spectrum in a low density ($\omega_{pi} < \Omega_i$), "two-dimensional" plasma with a spatially uniform Maxwellian distribution (i.e., a plasma in thermodynamic equilibrium) is such as to produce Bohm diffusion as a natural consequence of the (non-linear) interaction of the line charges on the various magnetic field lines. This process is often called vortex diffusion, because of its intrinsic two-dimensional character, and in fact is quite similar to the orbit-diffusion considerations of strong turbulence theory. The important thing to realize about it is that, to the extent that a plasma is effectively two-dimensional, Bohm diffusion is a natural consequence. The implications of this physical phenomenon for tokamak plasmas, where the plasma is effectively two-dimensional in only a very small

portion of the thermal fluctuation spectrum [88–91], namely $k_{\parallel}' \approx 1/R_0 q$ and $k_{\perp}' \rho < 1$, and where the plasma is not in thermodynamic equilibrium, but has expansion free energy, is yet to be worked out in detail. However, it appears that the net result of working this out may well be another means of obtaining the same results as those from strong turbulence theory noted in Eqs. (25)–(31) above. The calculation may serve to refine the strong-turbulence-theory estimates and put them on a firmer physical basis.

Another possible source of anomalous transport is the breakup of the flux surfaces caused by the development of kink/tearing modes in the plasma (see Section III.A.3). When there exist magnetic island structures within the plasma, the transport is very rapid across the width of the island. This effect may contribute to the lack of increase of the experimentally observed energy containment time as the current is increased and $q(a)$ is lowered below about 2.5–3.5 (see Section III.B.2). It has, however, not yet been worked out in detail. In addition, if there are adjacent magnetic island structures having different periodicities then “magnetic braiding” can occur [92]; field lines can have large radial excursions and maybe even connect the plasma center to the containment vessel wall. Breakup of the flux surfaces may also modify, eliminate, or exacerbate trapped-particle instabilities, since the basic particle orbits in regions of non-circular flux surfaces may be greatly modified.

In summary, there are many known mechanisms of anomalous transport; furthermore, it is not certain that all of the relevant linear instability and limiting nonlinear mechanisms have been identified. On the positive side, we note that the maximum loss rates can be estimated at least roughly for the known microinstabilities; in Section III.B.3 it is shown that these estimates appear to be consistent with reactor confinement requirements. Future experiments with the internal ring device may yield quantitative information on the transport coefficients in the trapped particle regime.

c. Atomic Physics

Plasma Impurities. The major source of impurities is presumably from the plasma containment vessel walls (See Sec. III.D.1), and hence is at the plasma edge. As impurities impinge upon the plasma they become alternately ionized, recombined, excited and de-excited, giving rise to copious amounts of radiation [93]. They also apparently feel a frictional force which tends to concentrate them in the center of the plasma (see III.B.1.a.). In addition to line radiation from partially stripped ions, all impurities cause increased Bremsstrahlung losses [94]

and increased Coulomb collision frequencies in the plasma [cf. Eqs. (11), (12)].

For low-Z materials, the plasma temperature typically exceeds the ionization potential of the most closely bound electron [95]. Hence, any such impurity ions in the hot plasma region are completely stripped and do not give rise to any significant line radiation. However, there is line radiation from the plasma edge, where the temperature is lower [96]. The plasma heat loss due to the line radiation in this outer region is effectively in series with the plasma conduction and convection heat losses from the plasma center. Hence, it influences only this outer region.

In addition to the low-Z impurities discussed in the preceding paragraph, there can be high-Z impurities (e.g., tungsten, molybdenum, from the liner, limiter, etc.) which are not fully stripped [95,97] even at the hot plasma center. Since: 1) as noted in Section III. B.1.a. the high-Z ions tend to concentrate near the plasma center; and 2) the radiated power [97] for the relevant charge state ($Z_{ion} \sim \sqrt{2T_e/13.6 \text{ eV}}$) is proportional to $T_e^{3/2}$, the heat losses from this line radiation will be primarily from the hot plasma core. These will be in parallel with other heat losses from this region and could be quite serious. Some estimates of the severity of these effects for reactor considerations are given in Section III.B.3.

In addition to the line radiation losses from the plasma, impurities enhance the Bremsstrahlung radiation losses [94] from the plasma. Strictly speaking, Bremsstrahlung is only the radiation process caused by acceleration of electrons in the Coulomb field of an ion nucleus. This “free-free” radiation exceeds that of a pure hydrogenic plasma by a factor of $\sum n_i Z_i^2/n_e$, which is similar to the resistivity anomaly factor (see Section III.B.1.a). However, radiation from inelastic “free-bound” collisions [94] between electrons and high-Z ions that are not fully stripped—sometimes called recombination radiation—has the same energy spectrum but depends on $n_i(Z_{ion})$ [38]. The latter process is distinguished from line radiation by the fact that it is caused by de-excitation from the continuum rather than bound states of the high Z ion and is sometimes quite significant in present experiments. For a plasma containing incompletely stripped ions both the “free-free” and “free-bound” radiation processes contribute to the ratio $\langle Z_x \rangle$ by which the experimentally measured “Bremsstrahlung” exceeds that of a pure hydrogenic plasma. Thus, this radiation loss from the plasma can be quite sensitive to a minute quantity of very high Z impurities.

Synchrotron Radiation. Another important radiation loss mechanism is synchrotron radiation [98,99]. Since the radiated power increases as $T_e^{11/4}$ for a homogeneous

plasma, this loss becomes increasingly important as the electron temperature increases. The fact that the magnetic field is inhomogeneous in tokamaks causes a spread in emission frequencies and an increase in the effective power loss by synchrotron radiation relative to that in a large homogeneous plasma [100]. A diffusive transport model [101] has been suggested for the realistic case where plasma parameters vary strongly across the plasma. For electron temperatures exceeding 5–10 keV, relativistic corrections to the gyrofrequency lead to increased synchrotron radiation [102]. In order to cut down on the radiation losses it has been proposed that the walls be made of materials which have a high reflection coefficient for this radiation [99].

As a numerical illustration, the author of Ref. 66 estimates for the parameters $R_o = 600$ cm, $T_e = 15$ keV, $\beta = 2\%$, $B = 50$ kG, and wall reflectivity 90% that the energy loss by synchrotron radiation would be 5 times the hydrogenic Bremsstrahlung loss, and would remove about 30% of the energy input into the plasma from D-T reactions. At β values below 1% (corresponding to $n < 2 \times 10^{13}$ cm⁻³), the synchrotron radiation loss exceeds the thermonuclear heating power, for the parameters stated above.

Providing the impurity content can be kept low enough, synchrotron radiation is expected to be the dominant energy loss (or cooling mechanism) in a reactor-like regime. It has not been significant in plasma confinement experiments yet because the electron temperatures are not hot enough.

Neutral Atoms. During the time when a plasma is confined away from material walls, it is emitting not only radiation, but also high-energy neutrals. The plasma emissions hit the walls of the containment vessel or limiter and dislodge hydrogenic or other atoms and molecules adsorbed on the surface. This produces a source of relatively cold (typically room temperature ~ 0.25 eV) neutrals at the plasma edge.

As neutral hydrogen molecules impinge upon the plasma edge they are usually first ionized (in a few millimeters) to an H_2^+ ion and then, when struck by another electron, suffer a Frank-Condon dissociative ionization process [103] which produces a neutral that has an energy of a few eV. Similarly, atomic hydrogen can be energized to an eV or so by collisions with the plasma ions. Since the low eV range neutrals thus produced are roughly randomly distributed in direction, about half of them are directed into the hot plasma region. They have a mean free path for ionization of about 5–10 cm, depending on the plasma density. At this new absorption point a fraction of the neutrals suffer a charge-exchange collision with a plasma ion, and the new neutrals have a higher energy.

A fraction of these higher energy neutrals penetrate more deeply into the plasma, get absorbed, produce a new, higher-energy generation of neutrals, etc. The net result [104] of such a cascading process is to produce a significant density of fast neutrals at the plasma center, which have energies that are a significant fraction of the ion temperature there. For example, in ORMAK the neutral density at the magnetic axis is in the range [105] of 3×10^8 /cm³ to 2×10^9 /cm³. Note that since the cascading process produces successively higher energy neutrals and the charge exchange mean free path increases roughly as $E^{1/4}$, the neutral density is not simply exponentially attenuated as we move from the outside to the plasma center. However, the neutral density at the plasma center should decrease with increasing plasma size and density.

The main effect that neutrals at the plasma center have on plasma confinement is that, through charge exchange, they limit the lifetime of the plasma ions near the axis. Thus, they can be an important mechanism for the heat loss from the central core region, if the charge exchange loss time is shorter than the plasma energy containment time from other processes.

2. Experimental Results

a. Characteristics of the Plasma

By way of introduction to the experimental results on plasma confinement, it may be helpful to review briefly some of the general features of the tokamak discharge. In Fig. 12 we illustrate schematically the time-dependences and magnitudes of the plasma current I , voltage (emf) V , density n , temperatures T_e and T_i , and plasma β_p -value. Density is measured by microwave interferometry and Thomson scattering; electron temperature by Thomson scattering and Bremsstrahlung; ion temperature (somewhat less reliably) from charge-exchange neutrals and spectroscopic data. The β_p -value can be measured by a diamagnetic loop, giving $\beta_p = 8\pi \langle n(T_e + T_i) \rangle / B_p^2$ (a). The β_p -value equals $2W_\perp / I^2$, where W_\perp is the perpendicular plasma energy per unit length, and can be calculated from measured values of n , T_e , and T_i .

The typical radial profiles [106–109,128] of various plasma parameters are illustrated in Fig. 13. In steady state, the density profiles tend to be somewhat broader than the T_e -profiles. Beyond the low-current and high-density limits of the standard tokamak operating regime (see Fig. 7), the T_e -profile tends to become very sharp and narrow. There also appear to be significant variations among the T_e -profiles obtained in the “standard operating regime” of various devices: T-3 and ORMAK have some-

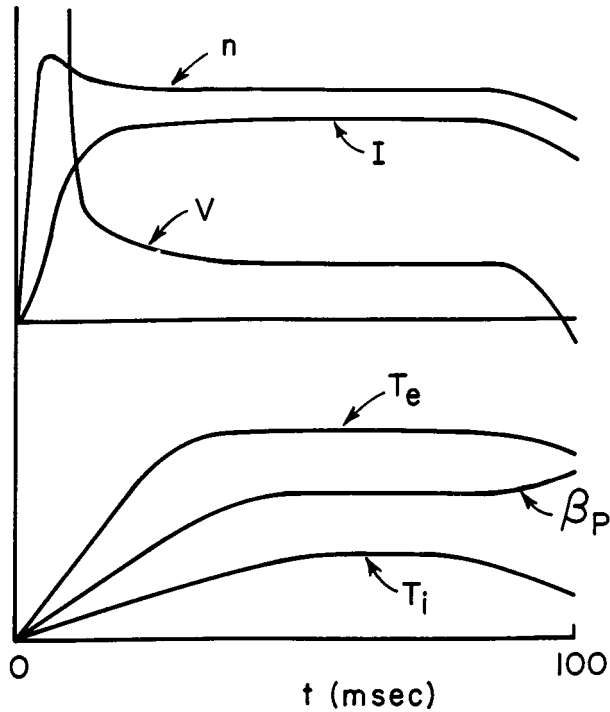


Fig. 12. Representative time-variation of current, voltage, density, temperature, and β_p in the standard tokamak regime.

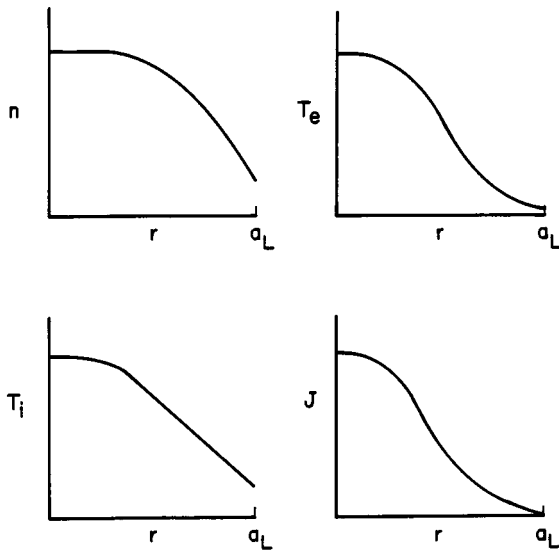


Fig. 13. Representative radial profiles of density, temperature, and current-density [as inferred from $T_e(r)$].

what flatter profiles than ST, ATC, or T-4. The T_i -profile is not accurately known from direct measurement, but appears to be less peaked than the T_e -profile. In present experiments the peak value of $n(T_e + T_i)$ is generally ≈ 3 times $\langle n(T_e + T_i) \rangle$, so that β_p is quite sensitive to the nature of the plasma profile.

The radial profile of the current density has not as yet been obtained by accurate direct measurement. If the effective ionic charge Z (see Section III.B.1.c) is assumed to be constant in radius, and if the toroidal electric field E_t is also constant (“steady state”), then $J(r)$ should follow the distribution of $T_e^{3/2}(r)$ (Fig. 13). As noted in Section III.B.2.1.c, however, there is some indication that Z_{eff} may be centrally peaked. Direct measurements of $J(r)$ on ST, using a heavy ion (thallium) beam [110] and polarized microwave beams [111] have demonstrated the feasibility of these two methods, but have not yet yielded data sufficiently precise to document deviations of $J(r)$ from $T_e^{3/2}(r)$ —if there are any. During the first few milliseconds of the discharge, one typically finds outwardly peaked T_e -profiles [113], which imply the presence of a skin effect—i.e., an outwardly peaked $E_t(r)$ and a peaking of $J(r)$ even stronger than $T_e^{3/2}(r)$. The magnitude and duration of this effect are at least roughly consistent with expectation from the initial bulk resistivity of the plasma. On the other hand, if the “steady state” plasma current of a hot discharge is suddenly raised by a current step [112], the associated skin effect appears to relax too rapidly to be consistent with ordinary bulk resistivity.

The electrostatic potential inside the tokamak discharge has been measured on ST for currents up to 130 kA by the thallium beam method [114], and was found to be typically negative and smaller than T_e . The plasma rotation has also been measured on ST from the Doppler shift of the O VII and C IV lines [115]; the poloidal rotation is found to agree with the electrostatic potential result in cases of simultaneous measurement. The poloidal and toroidal plasma rotation velocities are generally found to lie below $3 \cdot 10^5$ cm per sec. Doppler measurements on neutral charge-exchange hydrogen atoms in ORMAK [128], on the other hand, show poloidal and toroidal velocities in the range $10^6 - 10^7$ cm/sec. This diagnostic appears to provide information concerning the interaction of the ion banana orbits with sharp neutral density gradients at the edge of the discharge.

The magnitude and radial distribution of the neutral hydrogen atom density is obtained from spectroscopy and charge-exchange neutral measurements [106–108,128], and from the lifetime of injected energetic ions [116]. The central neutral density is depressed by as much as an order of magnitude relative to the edge value (see Section III.B.1.c), and appears to vary from $2 \cdot 10^8$ to $2 \cdot 10^9$ cm^{-3} , with the higher values being obtained in discharges with lower plasma densities. The neutral density is peaked (as a function of ϕ) in the vicinity of the limiter, where up to half of the neutral influx takes place in typical cases [108].

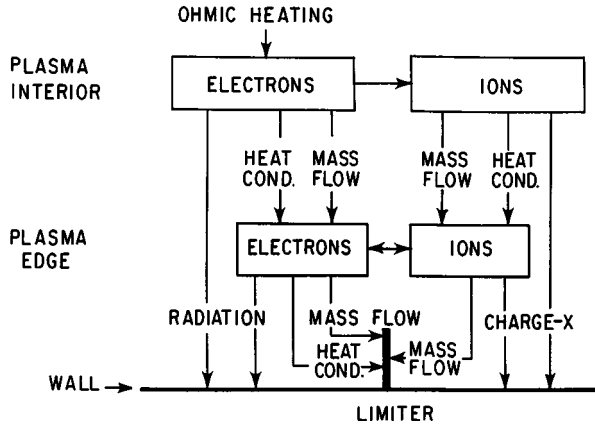


Fig. 14. Energy flow pattern in the tokamak discharge.

The magnitude, radial distribution, and ionization state of impurity ions is measured by absolutely calibrated ultraviolet and x-ray spectroscopy. The two methods give consistent results when one takes into account the calculated effect of recombination radiation in enhancing Bremsstrahlung [117]. In cases where light ions, such as oxygen, are the principal contributors to the plasma resistivity, agreement is reasonably good between the spectroscopic and resistivity-determined values of Z_{eff} [108,113,117,118], implying that the bulk resistivity anomaly, if there is one, may be small for standard-density-range tokamak discharges. The resistance enhancement or anomaly factor A_R (see Section III B.1.a) is often found to be inversely proportional to the plasma density [109,119,120].

The relationship between plasma density and neutral gas filling density is complex. The plasma density reached during the initial few milliseconds of the discharge tends to be proportional to the gas filling density; the plasma density reached later in the discharge is apparently related to wall-evolved neutrals (cf. Section III.D.1) and the current density. The percentage of light impurities is typically constant during the discharge, but the percentage of heavy (metallic) impurities tends to increase with time.

b. Energy Flow Pattern

The energy flow pattern of the tokamak discharge is illustrated in Fig. 14. Ohmic heating power goes into the electrons, and is transmitted to the ions by Coulomb collisions, on a time-scale $\tau_{ie}^{-1} = d \log T_i / dt \propto n T_i^{-3/2} f(T_e/T_i)$, where f is roughly constant [106] for $1.6 < T_e/T_i < 10$. In large devices, where the gross energy confinement time τ_E will become long relative to τ_{ie} , the electrons and ions will be closely equilibrated; in present day devices one has typically $\langle T_i \rangle / \langle T_e \rangle \sim 1/3$ at standard

plasma densities (and less at lower densities). The highest central temperatures obtained with Ohmic heating thus far are about 2.5 keV for T_e and 700 eV for T_i at peak densities $n \sim 3 - 6 \times 10^{13} \text{ cm}^{-3}$.

From the hot interior region of the plasma, the electrons lose energy to the plasma edge principally by heat conduction and by the energy transport that accompanies mass transport. (In steady state, the latter effect is equivalent to the energy consumed in heating the electrons of newly ionized neutral atoms to the ambient electron temperature.) The energy lost by radiation from the plasma interior is typically negligible, unless the plasma is severely contaminated with heavy ions (cf. Section III.B.1.c). Similarly, the ion energy loss from the plasma interior is in general dominated by heat conduction and mass flow to the plasma edge, but charge-exchange is of comparable magnitude as an energy loss mechanism. Under typical conditions, about 70% of the input power flows out of the hot region through the electrons, and about 30% through the ions.

At the plasma edge, electrons and ions may actually be equilibrated more closely than in the interior, if the density profile is flatter than the temperature profiles. Electron and ion energy can go from the plasma edge to the limiter by mass flow, but since the edge temperatures are much lower than the average plasma temperatures, this is a weak mechanism for heat removal unless the particle confinement time τ_p is much shorter than τ_E . Electron energy can also flow to the limiter by heat conduction, provided that the limiter emits enough cold secondary electrons. There is evidence that heat loss to the limiter accounts for about half of the total plasma energy loss, under standard operating conditions [121,122] (Section III.D). On the other hand, it is also possible to obtain regimes where there appears to be little heat loss to the limiter, with virtually the entire input power of the discharge being lost by radiation and charge-exchange from the plasma edge [123]. The latter regimes can be induced by adding impurity atoms and/or attempting to operate at very high plasma densities; these regimes are characterized by shrinkage of the plasma edge away from limiter contact, and tend to lead into the disruptive instability of Section III.A.1.

c. Gross Plasma Confinement

The gross energy confinement time of the discharge is $\tau_E = W/P$, where $W = (3/2)W_\perp$ is the total plasma energy per unit length, and P is the Ohmic heating power per unit length. In terms of the discharge resistance per unit length R_D we thus have $P = I^2 R_D$ and $\tau_E = (3/4)\beta_p / R_D$. In the T-3 experiments [119] conducted in

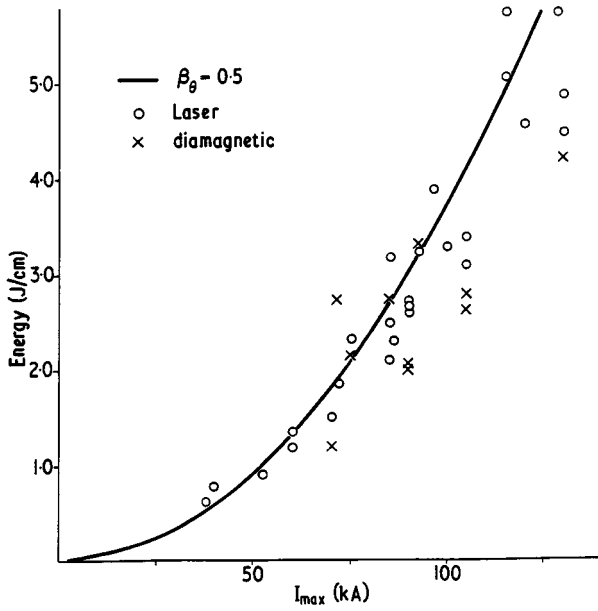


Fig. 15. Total plasma energy W per unit length as a function of I , for the T-3 device, from Ref. 86.

the period 1968-9 at currents up to 130 kA, it was found that $\beta_p \approx 1/2$ was obeyed for a wide range of discharge parameters (Fig. 15). This result is consistent with the calculated β_p -value for ohmic-heating equilibrium in the presence of pseudo-classical electron energy loss rate (Section III.B.1.b), assuming fixed plasma parameter profiles. The energy confinement time then depends simply on plasma resistance $\tau_E \approx 3/(8 R_D)$. Alternatively, the empirical formula $\tau_E \propto a^2 B_p n [(1/4 \pm (1/4))]$ was proposed to fit the T-3 data [120].

Recent results from the ST, ORMAK, ATC, and T-4 tokamaks (Fig. 16) show considerably more variation in β_p , with values ranging from 0.2 to about 1.0. The general trend of β_p is toward higher values at lower currents and at higher densities ($\beta_p \approx n/I$). The energy confinement time τ_E shows a similar tendency to improve with rising density; it also improves initially with rising current, but falls off for very large currents. Both β_p and τ_E tend to be somewhat higher in devices that operate at higher toroidal fields [107,124] (ST, T-4).

Energy confinement in nonhydrogenic plasmas has been studied on ST. Helium typically has somewhat larger β_p -values and confinement times than hydrogen [108]. Neon [125] and oxygen discharges also have good β_p -values and give record plasma temperatures, but since the plasma resistance RD is increased by the larger Z_{eff} of these plasmas, the τ_E -values are shortened correspondingly. Heavy gases, such as krypton, which do not become fully ionized on the plasma interior, do not form stable

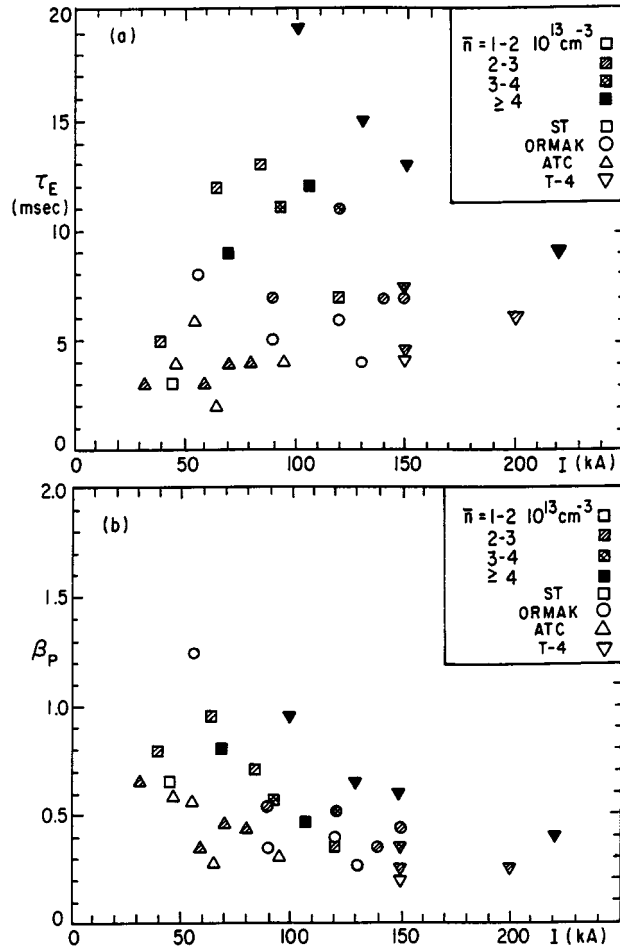


Fig. 16. Energy confinement time τ_E and β_p -value, versus I and n , for typical discharges in ST, ORMAK, ATC, and T-4. U.S. data are contributed by E. Hinnov (ST); M. Murakami (ORMAK); E. Mazzucato (ATC). They are based on Thomson scattering, with the assumption that $\langle T_i \rangle / \langle T_e \rangle \sim 1/3$, and β_p and τ_E enhanced accordingly. T-4 data are from Ref. 90.

tokamak discharges; indeed, an admixture of one part in 10^3 to a hydrogen discharge has a markedly adverse effect on τ_E -larger than expected from the contribution to Z_{eff} , or from the calculated radiation loss.

The ion energy confinement time τ_{Ei} can be determined separately from the electron energy confinement time τ_{Ee} , by dividing the ion energy content by the calculated rate of electron-ion energy transfer, which is assumed to be classical. The ion energy confinement time is typically several times longer than that of the electrons.

The plasma particle confinement time $\tau_p(0)$ in the interior region of the plasma can be determined in steady state from measurement of the neutral gas density, since the computed ionization time must also equal $\tau_p(0)$. Typically, $\tau_p(0)$ is found to be considerably longer than τ_{Ei} or

τ_{Ee} , though not nearly as long as would be expected from classical theory (Section III.B.1.a). On the other hand, at the plasma edge, where the neutral density is much higher, the particle confinement time $\tau_p(a)$ (defined as the total particle content of the discharge, divided by the rate of outflow at the edge) becomes comparable to τ_E .

d. Interpretation of Plasma Confinement

In view of the great complexity of the plasma energy flow pattern (Fig. 14), it is not surprising that a fairly wide variety of confinement results are obtained under different discharge conditions and in different devices (Fig. 16). In order to relate the gross measured confinement results to plasma transport coefficients, elaborate computer codes [126–128] are required.

The particular strength of these codes lies in their ability to take into account atomic effects with complex but well-known coefficients (ionization, charge-exchange, radiation, etc.), and to solve diffusion equations with a multiplicity of different transport coefficients, with various ranges of validity. It turns out that the computed plasma *profiles* exhibit considerable sensitivity to plasma parameters; the computed “gross energy confinement times” may consequently follow scaling laws that differ markedly from simple expectation based on a fixed-profile model.

Even the most elaborate tokamak simulation codes at present do not provide a natural fit of all the experimental data, and even in those cases where the fit is reasonably accurate, it is difficult to conclude whether the computer model is unique. Accordingly, present-day computer codes must still be regarded more as tools for investigating the behavior of the plasma than as a means of predicting the confinement properties of larger and hotter tokamaks.

The observed behavior of β_p and τ_E as a function of density and current is connected principally with electron energy flow, and can be interpreted in several ways:

- i. Using pseudoclassical transport coefficients (Section III.B.1.b) and “realistic” atomic processes, one finds that the shape of the electron temperature and density profiles can vary considerably, and that β_p is greater at lower I and at higher n . Whether the actual plasma profile changes that accompany the measured changes of β_p can support this model in detail, remains to be verified experimentally. In order to fit the data from a wide range of experiments, one must add the condition that plasma resistivity increases with falling density; this is consistent

with observation, and appears to reflect an increase of the percentage of impurities at lower densities, and the onset of a genuine resistivity anomaly at very low densities. The computer fit is not sensitive to the exact relative magnitude assumed for pseudoclassical heat and particle transport coefficients; the latter coefficient is generally taken to be several times larger.

- ii. The tendency of τ_E to diminish at low densities and high currents can also be interpreted as reflecting a deterioration of plasma transport, with the favorable T_e -dependence of the pseudoclassical model going over into an unfavorable dependence in the limit of large particle mean free paths. The onset of the trapped-electron mode (Section III.B.1.b) could be a phenomenon of this type; the present experimental evidence appears insufficient either to verify this possibility or to rule it out.
- iii. The decrease of τ_E at large currents may simply reflect the appearance of MHD instabilities (Section III.A., Fig. 6). This interpretation would be at least qualitatively consistent with the favorable effect of increasing B_r . On the other hand, the adverse effect of increasing I has been observed even for large q -values [124], and in the absence of observable magnetic oscillations. It is possible that very weak MHD modes may play a significant role in electron energy transport, and that the computer codes must be modified to include this effect.

If one considers the ion energy flow by itself, the task of interpretation appears to be relatively straightforward. For low neutral densities inside the plasma, the ion heat conductivity dominates and is close to classical [129,130]. For higher neutral densities, charge-exchange and mass flow play an increasing role. The accuracy of present experiments, however, is still insufficient to rule out the presence of an anomalous ion heat conductivity comparable in magnitude to the classical plateau value (Section III.B.1).

e. Evidence from Internal-Ring Experiments

While present-day tokamak experiments have not yet become sufficiently collisionless to explore beyond the edge of the trapped particle regime, considerable experimental evidence on long-mean-free path confinement is available from internal-ring devices. The degree to which the effects of trapped particle modes in a tokamak can be simulated in internal ring devices is not

clear. Nonetheless, diagnosing and understanding trapped particle instabilities in internal ring devices is a valuable tool in assessing the role of these modes in tokamaks.

Experiments on FM-1 have shown that plasma turbulence can limit plasma confinement at levels determined in large part by the collisionality of the plasma [131]. When the plasma is fairly collisional, the confinement exhibits a pseudoclassical behavior; the confinement times range from as little as 5 Bohm times to 500 Bohm times as the temperature is increased and the collisionality is reduced. Eventually the confinement enters a regime with an unfavorable, Bohm-like dependence on electron temperature. The magnitude of the confinement in the Bohm-like regime is strongly dependent on stability properties of the particle trapping region.

The magnitude and parametric dependence of the plasma confinement in the various regimes can be explained by the presence of resistive or collisionless drift modes and trapped-electron instabilities. Linear theory has been used to describe the onset of the instabilities, while the magnitude of the diffusion coefficient has been related to the nonlinear saturation of the plasma turbulence [132]. These results, and similar results from octopole experiments [133], suggest that a deterioration of confinement may also be encountered in highly collisionless tokamak plasmas, as predicted by the theory (Section III.B.1b).

3. Outlook for Future Tokamaks

According to the neoclassical model, the energy confinement in a typical tokamak reactor would be better than required by several orders of magnitude; roughly the same is true for the “empirical” pseudoclassical model. Accepting that the neoclassical model does not fit the dominant losses in experimental tokamaks, and that the pseudoclassical model may not be an adequate scaling law, the tokamak approach still has a large margin of safety against deterioration of confinement in future devices. Even conservative empirical extrapolations from present experimental trends (Section III.B.2), and even conservative theoretical estimates based on known micro-instabilities (Section III.B.1b), are consistent with the confinement requirements of typical large-scale tokamak reactor designs.

A “power-amplifier” fusion reactor can be achieved on passing Lawson’s criterion (Fig. 17), but toroidal fusion reactor design normally calls for the attainment of the “ignition condition,” where the reacting plasma becomes self-heating, and large power gains are possible. The respective criteria are plotted in Fig. 17 as functions of $n\tau$ and T_e , for a pure DT mixture and 40% thermal

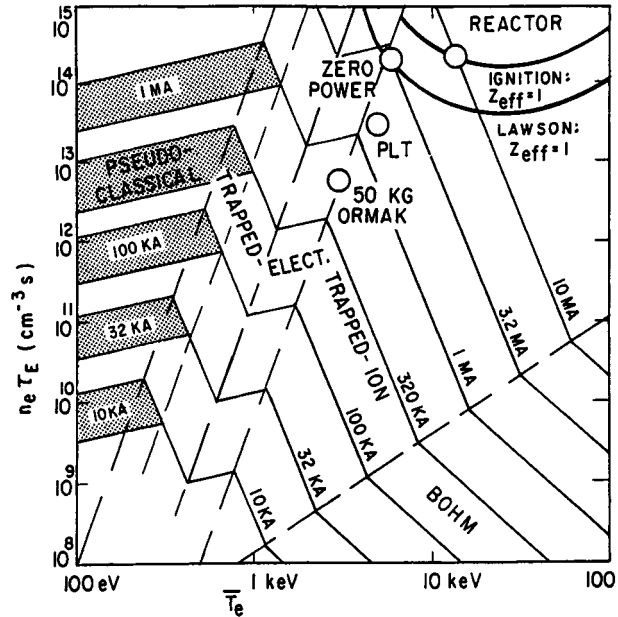


Fig. 17. Lawson $n\tau$ -diagram, with predictions for various tokamak currents, assuming $B_t = 50$ kG, $\beta_{pe} = 1.0$, $R/a = 3$, $Z_{eff} = 1$ and $T_e = T_i$. Hypothetical points are given for power-producing and zero-power reactors, as well as for (quite optimistic) neutral-beam-heated regimes in PLT and High Field ORMAK.

conversion efficiency. (Note, incidentally, that the term “ignition temperature” is sometimes used to mean the minimum temperature at which ignition is possible, i.e., for $n\tau = \infty$.) Illustrative points are indicated for a possible reactor, and for a preceding “zero-power” experiment.

The Lawson diagram has been plotted in terms of mean electron temperature, since confinement is generally more sensitive to T_e than to T_i ; in large future experiments, mean parameter values are expected to move close to peak values, and electron and ion temperatures should become virtually the same. The quantity Z_{eff} refers to the resistivity enhancement $\langle Z \rangle$; in reactor experiments this should be roughly the same as the Bremsstrahlung enhancement $\langle Z_s \rangle$.

The rough theoretical estimates made in Section III.B.1.b for transport in various parameter ranges are expressed below in terms of the (central) $n\tau$ -product, with the density n eliminated on the right-hand side of the equations, in terms of a given β_{pe} . Currents are in MA, (mean) temperatures in keV, $n\tau$ -values in cm⁻³ s. We define $b_t = B/50$ kG and $A = R/3a$. In the formulas of Section III.B.1.b, we have set $r_n = r_T = a$, $r = 2/3a$. We have calculated the confinement time from the simple estimate $\tau = a^2/4D$. The shear is defined as $B_p(a)/2B$. We obtain for the various regimes:

$$(A) n\tau = (1.2 - 2.9) \times 10^{14} \frac{I^2 \bar{T}_e^{1/2}}{Z_{eff}}, \quad (32)$$

PSEUDOCLASSICAL

$$(B) n\tau = 5.9 \times 10^{14} \frac{I^4 b_i^2 \beta_{pe}^2 Z_{eff} A^{3/2}}{\bar{T}_e^{11/2}}, \quad (33)$$

TRAPPED-ELECTRON

$$(C) n\tau = 1.1 \times 10^{13} \frac{I^2 \bar{T}_e^{1/2} A^{1/2}}{Z_{eff}}, \quad (34)$$

TRAPPED-ELECTRON

$$(D) n\tau = 3.2 \times 10^{16} \frac{I^4 b_i^2 \beta_{pe}^2 Z_{eff} A^{5/2}}{\bar{T}_e^{11/2}} \left(\frac{1}{2} + \frac{\bar{T}_e}{2 \bar{T}_i} \right)^2, \quad (35)$$

TRAPPED ION

where letters (A)–(D) refer to the regimes discussed in Section III.B.1.b. At temperatures below those of range A—a situation untypical of tokamaks - one encounters Bohm diffusion in the stellarator. At temperatures above those of range D, one would expect to encounter the trapped-particle interchange mode (E), and enter a Bohm-like scaling (with a geometrical improvement factor that we will neglect for simplicity—cf. Sec.III.B.1.b.)

The predictions of these equations have been laid out in Fig. 17 for the case $b_i = 1$, $A = 1$, $\beta_{pe} = 1$, $Z_{eff} = 1$, and $T_e = T_i$. The $n\tau$ -values are expected to follow the solid lines: beginning at low T_e in the pseudoclassical regime, progressing successively through the trapped-electron, and trapped-ion regimes, and arriving finally at Bohm. Note that the broad confinement picture is given by the Bohm, pseudoclassical and trapped-ion scaling laws, with the two line segments due to the trapped-electron regime representing a “detail.” The entire picture of Fig. 17 is of course idealized, since an actual tokamak plasma will typically contain several different regimes simultaneously within its profile, as well as modifications due to atomic effects; accordingly, the sharp corners in the figures are expected to be well-rounded in practice.

Figure 17 is specialized to large future tokamaks. We suppose that the “poloidal electron β ,” β_{pe} , can be raised to unity by auxiliary (non-ohmic) heating. This implies a total β_p of two, which is marginally compatible with present MHD theory for the indicated aspect ratio of $R/a = 3$. In the absence of impurities, we then find that 3.2 MA should be sufficient for the illustrative feasibility experiment, and 10 MA, for the reactor. The points of interest are seen to lie slightly within the trapped-ion region.

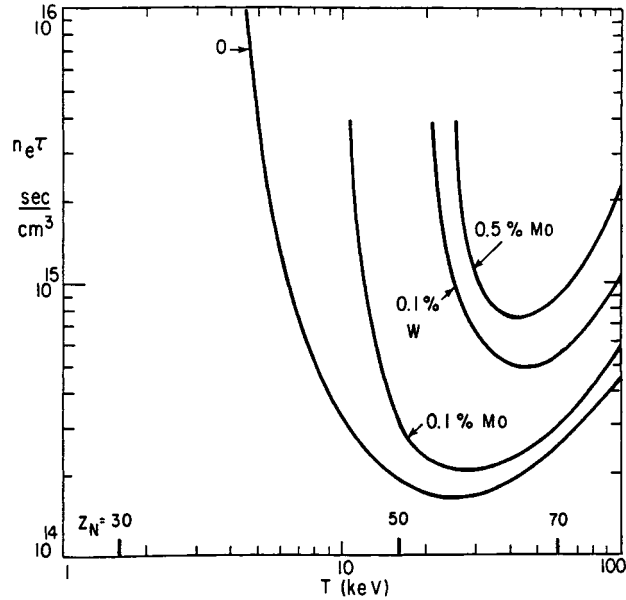


Fig. 18. Ignition condition for DT with various percentages of impurity contamination [100]. The tungsten case allows for line radiation; the molybdenum or niobium case assumes complete stripping. Recombination radiation has been included.

On Fig. 17 we have also plotted hypothetical points for PLT (1.6 MA) and High Field ORMAK (500kA), assuming that the plasma in these devices could be heated to $\bar{T} = 5$ keV and $\bar{T} = 3$ keV, respectively, by means of neutral beams. In placing these points on the present graph, we treat the hypothetical case $\beta_{pe} = 1$ and $Z_{eff} = 1$. The location of these hypothetical operating points, slightly within the trapped-ion regime is similar to the location of the reactor illustrations; hence the experimental realization of these points would be of decisive significance for reactor projections.

It is important to note that the presence of as little as one tungsten ion for 10^3 hydrogenic ions ($Z_{eff} \sim 5$) shifts the Lawson and ignition criteria significantly toward higher temperatures [134]. This is due partly to Bremsstrahlung, partly to line radiation, and partly to the reduction in the number of hydrogenic ions for a given β_{pe} . The confinement predictions in the trapped-ion regime could be somewhat improved by an enhanced Z_{eff} , but these gains are offset by the shift of the ignition condition to higher $n\tau$ and higher temperatures (Fig. 18). Synchrotron radiation losses, which we have been neglecting, also become more troublesome in the higher- T_e regimes (cf. Section III.B.1.c). A contamination of ~ 2 parts per 10^3 of tungsten ($Z_{eff} \sim 10$) would rule out ignition altogether. Lighter atoms are less damaging than tungsten; however, if present in sufficient numbers to

give the same effective Z , they similarly raise the ignition condition.

When Eqs. (32–35) are replotted for parameters characteristic of the ST or T-4 devices, rather than of a reactor, ($b_t\beta_{pe} \sim 0.3$, $A \sim 2.5$, $Z_{eff} \sim 4$, $T_e \sim 3T_i$) the low-current, high-density points tend to fall into the “pseudoclassical” regime, and the high-current, low-density points into the trapped-electron regime. For ORMAK and ATC the characteristic parameters are slightly different again ($b_t\beta_{pe} \sim 0.1$, $A \sim 1$) and the operating range extends deeper into the trapped-electron regime. None of these experiments comes close to the trapped-ion regime, which is thought to be most relevant for reactor purposes. The compressed ATC plasma does penetrate into the second half of the trapped-electron regime (C); the same is expected to be true for High-Field ORMAK and PLT in their Ohmic-heating phase ($b_t\beta_{pe} \sim 0.1$, $A \sim 1$, $T_e \sim T_i$), provided that Z_{eff} can be kept small.

We note, finally, that experiments with very large tokamaks may encounter some entirely new problems, for example the long-time persistence of nonequilibrium current distributions, due to the skin effect [135]. As was noted in Section III.B.2, skin-relaxation is not yet a serious problem in present-day tokamaks. In the PLT device, however, the *classical* skin relaxation time for $Z = 1$ would be of order 1 minute, and in a reactor it would typically be an hour or more. If a strong skin current is set up initially by raising the current more rapidly than the skin-time, an MHD unstable configuration results [136,137] (see Section III.A); the MHD instability would tend to speed up the skin relaxation process, but may also tend to give undesirable side-effects. The same remark holds for neutral gas effects [138] and hypothetical microscopic instabilities that might act to relax the skin current by anomalous resistivity or anomalous electron viscosity [139,140]. The skin effect in large tokamak may have to be suppressed artificially by special moving-limiter techniques (see Section III.D.).

The principal conclusions of this section are:

- a. A tokamak fusion reactor is expected to operate somewhat within the trapped-ion regime. According to the theory, it will require about 10 MA to reach ignition in a hydrogenic plasma—or appreciably more, if impurities are worse than one tungsten nucleus per 1000, or equivalent low- Z impurities ($Z_{eff} \gtrsim 5$). Combining the present results with those of Section III.A, we note that a 10 MA tokamak reactor of 3:1 aspect ratio and 50 kG toroidal field would have a minor radius of 360 cm for a safety factor of $q(a) = 3$. This is an acceptable number, but we note that

improvements in $q(a)$ or β could significantly reduce the required size and/or field strength.

- b. Since there is yet no direct experimental investigation of the trapped-ion mode regime, our reactor estimates may well be inaccurate: to test the severity of the trapped-ion regime is thus of crucial importance to the CTR program.

C. Heating

1. Ohmic Heating

The tokamak plasma current has the basic function of providing the rotational transform needed for plasma equilibrium. In experiments to date, the plasma current has had the incidental function of heating the plasma ohmically to temperatures of order 1 keV. In larger and better-designed tokamaks, one can expect somewhat higher temperatures to be reached. It would even be possible, in principle, to reach ignition conditions with ohmic heating alone—if one makes the assumption that roughly neoclassical or pseudoclassical confinement will hold in highly collisionless plasmas.

The degree of optimism required for consideration of an Ohmic-heated tokamak reactor substantially exceeds that required for ordinary tokamak reactor estimates (see Section III.B.3), which assume some form of auxiliary heating. This can be seen in terms of an elementary calculation. Noting that the Ohmic heating power must exceed the Bremsstrahlung loss, and assuming that the effective Z is about the same for the resistivity and the Bremsstrahlung, one finds:

$$nT_e < 2.4 \times 10^{12} \text{ J keV/A cm.} \quad (1)$$

Current densities envisaged in standard tokamak reactor designs are of order $J \sim 100 \text{ A/cm}^2$. Consequently, for $T_e \sim 10 \text{ keV}$, we have only $n \lesssim 3 \cdot 10^{13} \text{ cm}^{-3}$. These parameters are quite consistent with achieving ignition in the neoclassical or pseudoclassical picture, since $n\tau$ is then independent of n . The numbers, however, imply that one is actually deep into the trapped-ion-mode regime, while requiring confinement times of order $\tau \sim 10 \text{ sec}$ to reach ignition. This is a rather implausible scenario from the point of view of instability theory (Section III.B.1b). In addition, synchrotron radiation becomes an unusually serious problem at such low densities (Section III.B.1c).

It is useful to note that the consideration of Ohmic heating, Bremsstrahlung cooling, and plasma energy loss at a rate Z_{eff} times hydrogenic pseudoclassical diffusion gives the simple formula

$$\beta_{pe} \equiv \frac{8\pi n_e T_e}{B_p^2} = \frac{1}{2} [1 + (I/1.6)^2]^{-1/2} \quad (2)$$

where I is in MA. From this we see that large Ohmic-heated tokamaks must operate at β_{pe} -values well below the levels permitted by MHD theory. The probable confinement disadvantages of operating a large tokamak experiment with Ohmic heating, at the β_{pe} -level given by Eq. (2), rather than with auxiliary heating, at $\beta_{pe} \sim R/2a$, are readily apparent in terms of the discussion of Section III.B.3, especially in connection with Fig. 17.

To optimize the plasma nT_e -values obtainable by ohmic heating [Eq. (1)], one could go to very high magnetic fields, but the technological possibilities are somewhat limited. Another possibility is to take advantage of noncircular cross sections (Section III.A.1). The current density of an elliptical tokamak is given by

$$J = \frac{B_t}{2\pi Rq} \frac{\ell_1^2 + \ell_2^2}{2\ell_1\ell_2} \quad (3)$$

(for uniform J). If the safety factor q can remain fixed as we go to $\ell_1 \gg \ell_2$, then large increases in J are evidently possible. In the simple elliptical tokamak, it turns out that q must, however, be increased to preserve flute stability, and so there is no net increase in J . In other configurations, for example in the D-shaped or doublet configuration of Fig. 5, an appreciable enhancement of J can theoretically be realized [141].

In a sense, therefore, the use of strongly noncircular configurations would make the possibility of Ohmic heating to ignition more realistic. We note, however, that the principal motivation for going to strongly noncircular cross sections is to raise the MHD limit on the β -value so as to facilitate attainment of ignition (Section III.A.3). If this MHD effect can be demonstrated successfully, there would presumably not be much interest in lowering the β -value again so as to be able to use ohmic heating—unless this is the only available heating method.

2. Injection

At present the most promising method of heating toroidal plasmas is by injection of a beam of energetic neutrals into a plasma. This method has become technologically feasible with the rather recent development of inexpensive, high power neutral beam modules [141a,142]. Since the beam power absorbed by the plasma can be comparable to the ohmic heating power, these beams are expected to cause significant heating. Neutral beams also provide a particle source to offset diffusion losses and could be used to maintain an electric current in the plasma [143,143a,144]. This method of heating is

currently being tested in the ORMAK, ATC and CLEO experiments and is being planned for the TFR, JFT-II, T-6, DITE and W-VII stellarator experiments.

A neutral beam injector consists of only a few basic parts. First, there is a plasma source of either the duoPIGatron [141a] (ORNL) or filament [142] (Berkeley) type. Ions are extracted from the plasma meniscus accessible through a multiple-aperture (~ 200 – 300 , 3–4 mm diameter holes) plate. Then they are accelerated in a multiple aperture accel-decel electrode system to energies of say 25 keV. Next, the ions go into a charge-exchange neutralization cell which contains a neutral gas (typically H_2). At the end of this cell about 60–80% of the ions have been converted to energetic neutrals, which are then injected into the plasma. (Any remaining ions at the end of the charge-exchange cell are bent out of the beam path by the magnetic field. Also, streaming of the neutralizing gas and impurities have been shown to be sufficiently low so that their effects on the plasma can be made negligible [141a].) The most powerful neutral beam modules developed so far [141a,142] are capable of delivering about 125 kW to the toroidal plasma confinement region through a 9 cm diameter hole at a distance of 1 meter from the source. More power can be obtained by using a number of such modules—up to four are planned for ORMAK. The overall electrical efficiency of the injection system from power supply to energetic neutral beam in the plasma is 50–60%. This already very high efficiency and the beam module size may be able to be increased with further design improvements.

As the energetic neutrals from the beam penetrate into the confined plasma they suffer charge exchange ($\sim 75\%$) or ionization ($\sim 25\%$ from both electrons and protons) collisions [145,146] with background plasma. The mean free path for “ionization” of an energetic hydrogen neutral is given by

$$\lambda = \frac{1}{n_e \sigma} = \frac{5.5 \times 10^{13} \times E_o}{n_e} \quad (3)$$

where λ is in cm, E_o is the energy of the neutral in keV, n_e is in $\#/cm^3$ and for σ we have used the formula given by Sweetman [146], which is valid from about 20 to 100 keV. For deuterium [146] the numerical coefficient in Eq. (3) is reduced by a factor of 2 and the energy range for applicability becomes 40 to 200 keV. In typical injection experiments $E_o \sim 25$ keV, $n_e \sim 3 \times 10^{13}$ and hence $\lambda \approx 50$ cm. This length is comparable to the plasma diameter, but less than the length of a chord roughly tangent to the plasma center. Thus, maximum beam absorption ($\approx 90\%$) is obtained by tangential injection, and this method is generally preferred in the present experiments.

After being “ionized”, the fast ions from neutral beam injection circulate around the torus with particle orbits similar to those in Fig. 9. For tangential injection in the direction of the ohmic heating current (co-injection) the fast ions are typically injected into “passing” orbits that are confined within the plasma. However, for counter-injection a fraction of the fast ions are injected into “passing” orbits that hit the limiter or liner. In the latter case there is net charge built up in the plasma and hence a radial electric field. The net radial potential drop over the outer region of the plasma can be larger than the kinetic energy of the electrons, a typical level for the potential in a quasi-equilibrium tokamak. However, since the dynamics of the limiter-plasma transition region are not well understood, it is not clear what effect, if any, this will have on the plasma.

The plasma heating comes about from the slowing down of the fast ions by collisions with the background plasma ions and electrons. The time for complete thermalization of a fast ion is [147,148]

$$\tau = \frac{t_s}{3} \ell n [1 + E_o/E_c]^{3/2} \sim 10^{-2} \text{ sec.} \quad (4)$$

where $t_s = \frac{m_f}{m_e} \frac{1}{v_{ei}} = \frac{0.12 (T_e/1 \text{ keV})^{3/2}}{Z (n_e/10^{13} \text{ cm}^{-3})}$ [cf. Eq. (III.B.11)]

is the slowing down (momentum-exchange) time, and $E_c = 14.8 \text{ KT}_e$, with m_f , being the fast ion mass. For injected neutral energies

$$E_o \lesssim 2.4 E_c \sim 35 \text{ KT}_e, \quad (5)$$

a condition that is satisfied in most present experiments, the fast-ion energy, when integrated over the total slowing down process, is transferred preferentially to the plasma ions. Conversely, for higher E_o most of the energy goes to the electrons. A process that competes with plasma heating for the fast-ion energy is charge-exchange of the fast ions on the neutrals in the plasma (see Sec. III.B.1.c). This process produces fast neutrals that have a significant probability of escaping from the plasma and depositing their energy in the containment vessel walls. For most present tokamak experiments, the lifetime of the fast ions against charge exchange [$\tau_{cx} = (n_o \sigma_{cx} v)^{-1} \sim 10\text{-}20 \text{ msec}$] is comparable to, or perhaps longer than, their slowing-down time [$\sim 10 \text{ msec}$, cf. Eq. (4)]. Hence, the charge-exchange process is not a serious limitation on this heating method.

In addition to the desirable heat and particle inputs, neutral injection may have deleterious effects on plasma equilibrium and confinement in a tokamak. Plasma perturbations (in addition to the net charge noted above) arising from neutral injection [144] are caused primarily by the presence of a fast-ion group and by the momentum

imparted to the plasma by beam absorption. After an initial transient, the total fast-ion density accumulated in the plasma is

$$n_f(r, \theta) = \frac{I_o \tau}{(2 \pi R_o) (\pi a^2) e} H(r, \theta) \sim 3 \times 10^{11} / \text{cm}^3 \quad (6)$$

where I_o is the neutral beam current and $H(r, \theta)$ is an order-unity spatial shape factor [144a] that depends on the detailed injection geometry. As the fast ions slow down they impart momentum to the background plasma and, in combination with it, produce a current [144]. Although this current is larger than the neutral-beam current by the “stacking factor,” given by the ratio of slowing down time to transit time around the machine, it is typically smaller than the ohmic-heating current. Thus, it is not expected to cause any significant plasma perturbation. The momentum imparted by the beam absorption causes a toroidal plasma rotation and a concomitant radial electric field [144], which may grow monotonically with time for unidirectional injection. Since in present experiments this plasma velocity is expected to be less than the sound speed, this is not expected to be a significant perturbation. In addition, it has been proposed that the toroidal flow can be impeded by at least three processes: 1) injection of an opposing beam to cancel the *net* momentum (however, this still leaves some distributed toroidal flows; also, introducing a counter-streaming beam can create problems of net charge buildup and a concomitant radial electric field—see above.); 2) the bumpiness of the toroidal field caused by the discreteness of the coils [149]; and 3) charge exchange of the plasma ions, since this process causes the ions to lose their directed momentum and can thereby relax radial electric fields [150]. Finally, since the energy density in the fast ions can be comparable to that in the background plasma to be heated, plasma microinstabilities may be induced by this new source of free energy. For tangential injection, the fast-ion distribution is sufficiently smooth and the parallel electron Landau damping sufficiently strong so that apparently no new instabilities are triggered. Nevertheless, the fast-ion group modifies or excites the drift wave instabilities [151,152] (cf. Sec. III.B.1.b). However, the net effect of these modifications is difficult to assess, since the role of drift waves in toroidal plasma confinement is not well understood. In summary, for tangential neutral beam injection at a level sufficient to cause significant plasma heating the plasma perturbations appear to be small, except for the possible development of radial electric fields greater than those in quasi-equilibrium tokamaks without injection—the net effect of which is unclear.

Perpendicular injection, which is being planned in the French TFR experiment, can cause a number of types

of perturbations even though it imparts little, if any, toroidal momentum to the plasma. As with tangential counter-injection, a significant fraction of the fast ions are injected into unconfined orbits that strike the limiter or liner. In general, as long as the injectors are tilted slightly off perpendicular so that the ions are not injected into super-bananas caused by magnetic ripples (cf. Sec. III.B.1.a), the perpendicularly injected fast ions have trapped-particle orbits (cf. Sec. III.B.1.a). The restricted region of space traversed by these ions and the loss of a fraction of the fast ions from the confinement region causes, as with tangential injection, buildup of electric fields in the plasma [144], the net effect of which is unclear. For perpendicular injection, a number of ion loss-cone type modes similar to those possible in mirror-confined plasmas [153], may be stimulated. The net effect, if any, of these modes is probably just to shorten the slowing down time and increase the fraction of the fast ion energy transferred to the ions. Perpendicular injection may also aggravate the trapped-ion modes (cf. Sec. III.B.1.b) since the fast ions are injected into trapped particle orbits. Indeed, perpendicular injection might become one of the principal tools for studying trapped-ion modes.

Recently, tangential neutral beam heating has been tested in the ATC [153a] and ORMAK [153b] experiments. The plasma ions were heated by a roughly predictable 25%, at a beam power level of some 30–70 kW. Apparently the beam injection was not accompanied by deleterious effects on plasma confinement, any marked plasma rotation (as judged from the rotation rate of magnetic field oscillations), or any measurable high-frequency noise. Previously [154], neutral-beam injection into CLEO had been unsuccessful in producing significant ion heating. However, in CLEO fast ions were apparently confined and slowing down, and the predicted ion temperature rise of about 10% may have been the limit of detectability. Thus, from the low-power-level results of neutral-beam heating tests it seems that this approach may well turn out to be the very effective and important heating method it has been touted to be.

As plasmas increase in size, density, and temperature, it will be desirable to increase the beam energies. It is clear from Eq. (3) that penetration into reactorlike tokamaks ($a \sim 200$ cm) at reactorlike densities ($\approx 2 \cdot 10^{14}$ cm⁻³) requires extremely high-energy beams. Raising the source voltage has both advantages and disadvantages. First, there is the fact that for well-collimated beams the maximum ion beam current is limited to the scaling $V^{3/2}/d^2$, where V is the acceleration voltage and d is the electrode spacing—the Child-Langmuir space-charge-limited current [155]. The power thus increases with increasing energy, though it is not expected to increase

as fast as $V^{5/2}$, because of the greater electrode spacing required to avoid electrical breakdowns, and the increased heat loads. It may not be desirable to go to energies above 50–100 keV with positive ion beams, because the charge-exchange cross sections, and consequent efficiencies in the neutralization cell, decrease rapidly in this range (see Fig. 19). For these high energies it may be necessary to develop negative ion sources and accelerators based on the relatively high efficiency D^- stripping reactions in this energy range (see Fig. 19).

Let us consider in greater detail the problem of beam penetration into the discharge. For tangential injection inside the magnetic axis it has been found [144a] that the competition between exponential beam attenuation and a geometric peaking effect (due to the fact that fast ions produced near the magnetic axis are distributed over a smaller flux surface area than those near the outside) causes the beam energy to be deposited preferentially near the plasma center as long as $a/\lambda \leq 4$, where a is the plasma radius. For perpendicular injection, which may be desired because of the easier access, the criterion is probably comparable. Thus, we may presume that in order to preferentially deposit energy in the plasma center we require $\lambda > a/4$. If $n \sim 5 \times 10^{13}/\text{cm}^3$ as achieved in the present experiments and a ~ 200 cm, we see from Eq. (3) that this would require only $E_o \approx 100$ keV for deuterium injection, which might be done with a modest scale up of the present positive ion beam sources. However, if $n \approx 2 \times 10^{14}/\text{cm}^3$, as is generally assumed in reactor confinement estimates (see Section III.B.3), then we require $E_o \sim 400$ keV, and hence negative-ion sources would probably be needed.

A possible alternative solution is to combine neutral-beam injection with compression (Section III.C.3). One would then inject into the low density precompression plasma (see Section V.C.3), with an attendant improvement in overall heating efficiency, as well as the possibility of penetrating to the plasma center with a 50-keV range beam, even for compressed plasma densities of $n \sim 3 \cdot 10^{14}$ in reactor size.

Finally, we note that the neutral-beam injection technique makes possible the “wet-wood burner” approach [156] to a fusion reactor. A typical illustration of this scheme [157] is the injection (or injection plus compression) of a deuterium beam, with a resultant trapped energetic deuteron population of ~ 200 keV, in a “target plasma” of moderately hot electrons (e.g., 2–5 keV) and of tritium ions at optional temperature. The principal advantage of the wet-wood burner is that the zero-power condition can be crossed under considerably less demanding confinement conditions than are imposed by the conventional Lawson criterion—as well as consider-

ORNL-DWG 72-14228

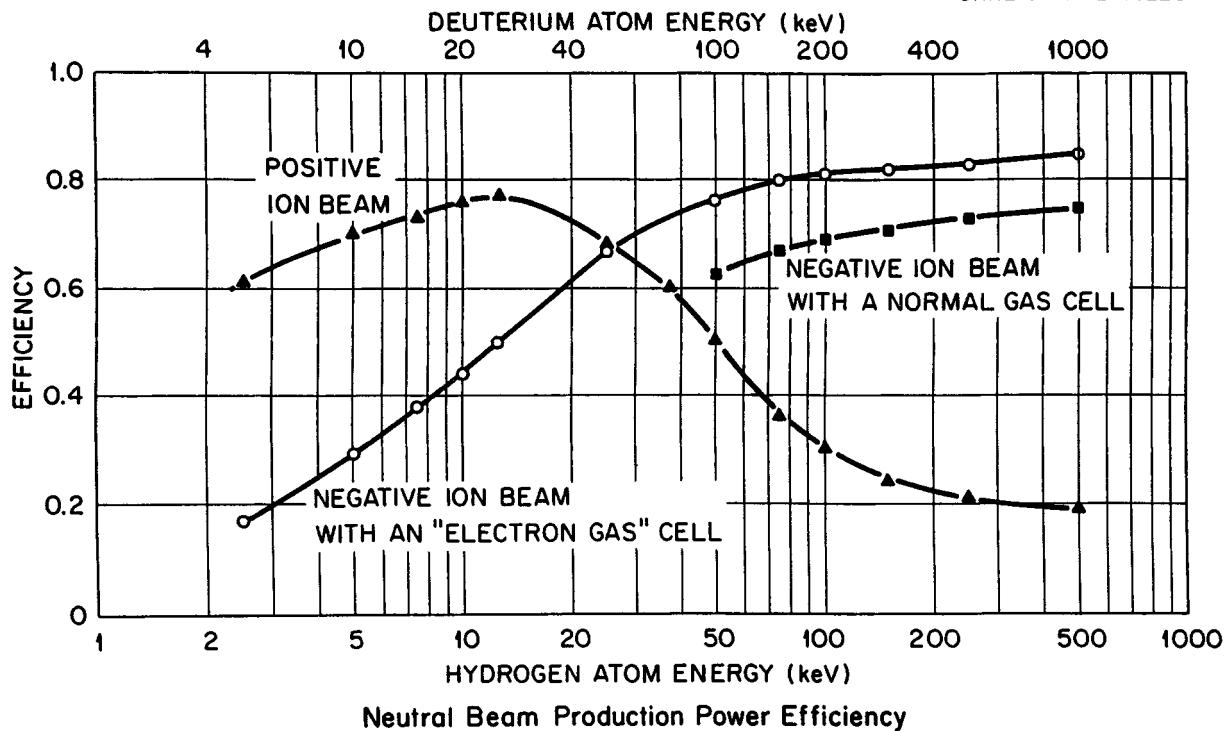


Fig. 19. Efficiency of conversion of a charged beam to a neutral beam by passage through a charge neutralizing cell. The source efficiency is included in the overall efficiency values shown. (Courtesy of L. D. Stewart, ORNL).

ably weaker conditions on plasma temperature. Also, in present day, or next-generation experiments, much larger neutron yields could be obtained by the wet-wood method than by the conventional approach of heating the bulk ions. For example, in the ATC device, Ohmic heating plus compression of a deuterium plasma produces neutron emission rates below 10^8 /sec; initial auxiliary heating with a hydrogen beam, followed by compression, produces over 10^9 /sec; and injection of an initial deuterium beam at 14 keV produces yields of well over 10^{10} /sec in the compressed plasma [153a]. The inherent limitation of the wet-wood burner scheme is that it can reach only moderate power-amplification factors (somewhat like a mirror-machine reactor), rather than giving arbitrarily large amplification factors, like a conventional toroidal reactor as it approaches the ignition condition.

In summary, injection of energetic neutral beams into tokamaks is presently the most promising plasma heating method because: 1) the technology and hardware for present and next generation experiments exist or can be accomplished with only modest extrapolations; and 2) initial injection experiments on ATC and ORMAK have given encouraging results. In order to use this heating method in reactor sized devices it will probably be necessary to develop high energy (200 keV-1 MeV) nega-

tive ion sources in order to have sufficient beam penetration to preferentially heat the plasma center.

3. Wave Heating

Heating plasmas via the absorption of energy in the form of plasma waves offers two features which have important consequences in the low-density fusion research program. First, in the near future, 1-10 megawatts of power will be available in off-the-shelf technology in the frequency ranges appropriate to plasma heating. Ten megawatts exceeds by a factor of five the estimated Ohmic heating in PLT while 1 megawatt is 4 times greater than Ohmic heating in ST. This means that besides providing a demonstration of ion heating, electron heat transport can be studied as a function of temperature. Secondly, for a reactor regime, wave heating methods provide ready penetration of the energy to the plasma center, adequate power to achieve ignition, and, like neutral beams, might be used to maintain steady-state toroidal currents in a tokamak.

The principal difficulty that wave heating methods face is the design and operation of the wave coupling structures which have to be designed for and tested in the specific plasma confinement configuration in which

they are going to be used. Furthermore, there is presently no experience as to how the loading or electrical breakdown problems will scale as the reactor regime is approached. However, general scaling arguments indicate that the breakdown problem will be less severe in very large devices but that the heat load on the walls may be important. In common with neutral beams, most of the technological effort to date has been directed towards heating existing devices and those planned for the near future. For these devices, experience with the C-Stellarator [158,159] has shown that rf energy in the ion-cyclotron frequency range can be transferred to the plasma at 1 megawatt power levels without breakdown problems.

Basic research has carried the wave heating field to the position where theory and experiment have established sufficiently encouraging results to allow high-power heating experiments on present tokamaks to be designed with good confidence that they will succeed. Experiments in both mirror and toroidal geometries have demonstrated techniques whereby effective coupling to the plasma can take place. In toroidal plasmas where confinement is good, experiments are beginning to show promise over a wide range of frequencies. For example, magnetosonic heating has doubled the ion temperature in a small Soviet tokamak [160] (to 200 eV) with an efficiency of 40% and no deleterious effects on plasma confinement. Future progress in wave heating will depend on mounting a vigorous program of high-power heating experiments on tokamaks, together with tests of wave couplers and theories on the effect of wave absorption, etc.

Wave heating experiments have been carried out in four frequency ranges:

- a) Transit-time magnetic pumping; $\omega \ll \Omega_i \sim 2\pi \cdot (100 \text{ kHz})$
- b) Ion-cyclotron and magnetosonic waves; $\omega \approx \Omega_i \sim 2\pi \cdot (50 \text{ MHz})$
- c) Lower hybrid resonance frequency regime; $\omega \sim \omega_{pi} \sim 2\pi \cdot (1 \text{ GHz})$
- d) Electron cyclotron and upper hybrid frequency regime; $\omega \approx \Omega_e \approx 2\pi \cdot (30 \text{ GHz})$

The sections below will make it clear that the ion-cyclotron and lower-hybrid frequency regime are presently the most attractive for high-power wave heating of tokamaks. In these regimes, generation of radio-frequency power can be carried out with 60–70% efficiency [161,162], matching the performance of positive-ion neutral beam sources (see Fig. 1). Power at any conceivable level is readily available. The approximately 50% wave coupling efficiency measured in recent experiments on the ST is comparable with neutral beam performance when charge

exchange losses of the energetic ions are taken into account.

Let us discuss the progress made in the four frequency ranges.

a) Transit-time magnetic pumping; $\omega \ll \Omega_i$.

The recent experimental results of Millar [163] at Culham have shown a confinement time decreased by a factor of two to roughly half of the heating time. Private conversations reveal that this is an ac effect, with dc magnetic ripples of the same magnitude not affecting the confinement time. This discouraging result combined with the fact that the wave energy density must be substantially larger than in the ion-cyclotron frequency range to achieve the same heating rate suggest that transit-time magnetic pumping is probably not an attractive approach to tokamak heating. Nonetheless, it is planned for the WEGA experiments in Europe and perhaps this experiment can be designed to give improved results.

b) Ion-cyclotron and magnetosonic waves; $\omega \sim \Omega_i$.

High-power heating experiments have been carried out on the Model-C Stellarator [158,159], while only low-power experiments [164,165] have been performed on the ST to date. Promising results have also been obtained on the Uragan [166,167] stellarator at Kharkov and on a small tokamak at Khurchatov [160]. Let us briefly discuss these results as they pertain to planned tokamak heating experiments.

Ion-cyclotron waves were generated in a straight-section of the C-Stellarator and propagated to a magnetic beach where they were absorbed [158,159]. What we have learned from these experiments are: 1) wave couplers operating at the 1 MW level can be designed and function with efficiencies greater than 50%—in agreement with theory; 2) wave absorption by ions on a magnetic beach approached along the magnetic field (nonaxisymmetry) heated the ions throughout the entire machine to 500 eV but the energy confinement time remained at its Bohm value. With a local magnetic beach, the ion heating time was shorter than the isotropization time and the ions developed a very anisotropic ($T_{\perp} \gg T_{\parallel}$) velocity distribution which apparently was unstable to the temperature anisotropy microinstabilities [168]. Low-power wave coupling experiments [164,165] on the ST tokamak have demonstrated wave-coupling efficiencies up to 50% and modest ion heating $\Delta T_i \approx 25 \text{ eV}$ appropriate to the power (15 kW) which the present small access ports allow. Both ion-cyclotron and magnetosonic waves were generated in this tokamak geometry where the ion-cyclo-

tron resonance plane is axisymmetric and vertical and hence completely different from the C-Stellarator magnetic beach. A high-power launcher with access ports large enough to couple 1 MW is ready and will be installed in December 1973.

At Kharkov, ion-cyclotron waves doubled the ion temperature (to 400 eV) in the Uragan Stellarator [166,167] ($n = 3 \cdot 10^{12} \text{ cm}^{-3}$) without producing anomalous plasma losses. While theory suggests that ion-cyclotron waves may not be the optimum choice for heating tokamaks which have an order-of-magnitude higher density, the Uragan results do demonstrate that rf methods can heat plasma without spoiling confinement. Magnetosonic wave heating experiments (which are attractive for larger, high-density tokamaks) have had a similar success at Khurchatov, doubling the ion temperature (to 200 eV) in the small tokamak, TM-1-VCh [160,169], and increasing the ion temperature in the TO-1 tokamak [170]. A magnetosonic wave can be readily launched by the same wave generator and coupling structure as the torsional ion-cyclotron wave, and both waves are included in the term ICRH.

ICRH heating methods *may* always require some form of launching coil inside, or at the boundary, of the vacuum vessel, where they will be subject to radiation damage and perhaps be the source of impurities. Solution of this problem is one of the many materials problems that will be encountered and may not be qualitatively worse than others. However, it is hoped that development will show that rf energy can be introduced by waveguides, horns, etc., circumventing such materials problems.

c) Heating near the lower hybrid frequency.

There are two approaches to heating in this frequency regime: First, when the maximum lower hybrid frequency (approximately the ion plasma frequency in typical tokamaks which have $\omega_{pe} \lesssim \Omega_e$) exceeds the wave frequency, linear mode conversion takes place at a point where the wave frequency equals the lower hybrid frequency. At this point, the wave is transformed into an ion plasma wave and is effectively absorbed. On the other hand, when the wave frequency exceeds the maximum lower hybrid frequency in the torus, one can couple to an electrostatic normal mode of the plasma which induces parametric instabilities and concomitant heating at a low threshold. In this mode the heating is expected to be largely (but not overwhelmingly) electron heating.

Linear mode conversion [171–173] is invoked as the absorption mechanism in recent experiments at Khurchatov, Leningrad, and Princeton. The Khurchatov [173] experiment produced 100 eV ions in a linear mirror geom-

etry. The Leningrad [174] experiment noted the formation of an energetic ion tail but no increase in diamagnetism in a small tokamak.

Parametric instabilities [175,176] near the lower hybrid frequency have been found to lead to excellent energy absorption in the FM-1 multipole [177] and small linear experiments [178,179] at Princeton, where the instabilities have been measured in some detail and at Kharkov [180] where their presence has been assumed.

Currently, we judge the parametric instability mode of heating to be more favorable.

The principal questions in lower hybrid heating are: (1) whether the good coupling observed in small devices will continue on larger tokamaks, (2) what is the optimum wave coupling structure, (3) what are the relative merits of linear mode conversion vs. parametric instabilities at high power levels, and (4) what theory governs the saturation of parametric instabilities and nonlinear heating. The planned high-power experiments on ATC and Alcator [172] should help answer the questions.

d) Electron cyclotron and upper hybrid frequency heating.

Here, two regimes must be distinguished: $\omega_{pe}^2 > \Omega_e^2$, $\omega_{pe}^2 < \Omega_e^2$. For low density plasmas ($\omega_{pe}^2 < \Omega_e^2$), there have been a number of experiments carried out in a mirror geometry [181]. Effective heating has been found in all the experiments. The results suggest that stochastic heating [182] predominates. That is, the energy increases by resonant heating, but with a random phase between v_{\perp} and E at each transit of the particle through the resonance zone. While this heating method has been used in toroidal configurations [183,184], it has not been fully exploited because of anticipated concerns about available power at the resonant frequencies (~ 10 - 100 GHz) and the questionable interest in low plasma density. The enlightened technological program of tube development at ORNL has provided power at consistently higher frequencies as needs arise, with cw power at 10.6, 18, 36, and 55 GHz presently available at kilowatt levels. Projected devices to deliver much higher power levels at very high frequencies ($\approx 120 \text{ GHz}$) are possible in principle at this time and can be developed given an adequate technological support level.

For the high density (or weak magnetic field) regime $\omega_{pe}^2 > \Omega_e^2$, linear experiments [183] have shown coupling of the applied power to the plasma and conversion into plasma waves which may then be dumped into particle energy. Alikaev [185] has been most successful in demonstrating the applicability of this technique by heating

electrons in TM-3 up to about 1 keV for densities in the range of $n_e > 10^{12}/\text{cm}^3$.

The possibility of using high-frequency power not as a major power source, but rather as a plasma control or augmentation mechanism may be an attractive alternative. For instance [186], it may be possible to control either the temperature or density gradients or pitch angle distribution by the application of rf or microwave power. This might be done as a supplement to or as a catalyst for increased efficiency, of ohmic, beam, or compressional heating.

Some experiments have shown useful (if somewhat negative) results. The use of low-frequency resonant and non-resonant power has caused mirror plasmas to be ejected into the loss cone [187,188]. The use of low-frequency power has caused electron runaway on Stellarators [189]. The use of microwave power at frequencies near ω_{pe} has caused electron heating on the high-energy tail of the distribution [190,191]. These techniques may be useful, for example, in controlling the number of particles in banana orbits in tokamaks.

In summary, the wave heating field has, through a combination of experiments and theory, established the principles on which high-power heating experiments can be designed. The principal short term goal is to vigorously pursue high-power heating experiments on large tokamaks which have demonstrated good confinement. The emphasis is on going to as high powers as possible (i.e., 1-10 MW range) both to take advantage of the power sources which are available and to investigate the power limitations of wave coupling structures.

4. Compression

The most successful past instances of plasma heating to high temperature and density in controlled fusion research have made use of the adiabatic compression technique [193,194]. The idea is to preheat the plasma by some dissipative mechanism in a relatively weak magnetic field, then carry out a (reversible) adiabatic compression to a higher final field strength.

In the case of tokamaks, it is possible to compress the plasma either by increasing the toroidal magnetic field strength B_t in time [195]; or by increasing the vertical field B_v , thus displacing the plasma inward in major radius R ; or by any combination of these two methods [196] (Fig. 20). The initial plasma can be heated either ohmically, as usual, or by one of the auxiliary heating methods described in the present Section. If the compression can be carried out more rapidly than the plasma energy loss time, it acts as a multiplier of the initial heat energy input.

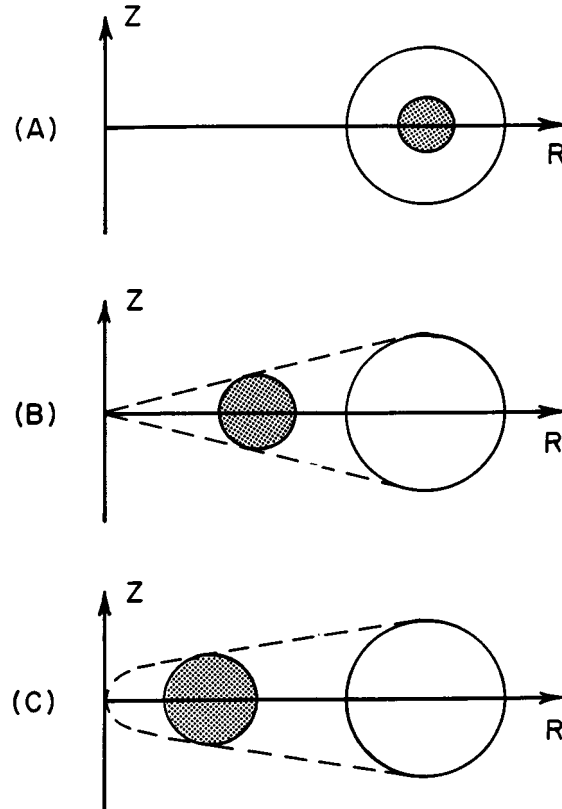


Fig. 20. (A) Compression by raising B_t ; (B) by raising B_t and B_v , so as to preserve the aspect ratio; (C) by raising B_v for fixed B_t . The volume compression factor is four in all cases.

In order to determine whether adiabatic compression is advantageous in tokamaks, one must compare the results of initial heating, followed by compression, with the results that could have been obtained by applying the same heating method in an ordinary tokamak operating in the same volume and at the same final field strength. For ohmic initial heating, it then turns out that compression by raising B_t alone (Fig. 20(A)) is disadvantageous for improving the plasma energy density. This is because B_t , and therefore J , is weak in the precompression stage; the corresponding loss of initial energy density is not fully compensated by the compression. A related disadvantage is that the aspect ratio R/a of the compressed discharge tends to become unfavorably large. On the other hand, compression by changes in both B_t and R can be such as to leave R/a constant (Fig. 20(B)). In that case, an improvement over simple ohmic heating can be obtained, as also in the case where B_t remains fixed in time, and the compression is in R alone (Fig. 20(C)).

The case of compression only in R has the great practical advantage that the process involves the pulsing of magnetic energies comparable to those in the *poloidal*

field, rather than comparable to the 10^2 times larger energies in the *toroidal* field. This consideration makes R-compression the favored candidate for application in large future tokamaks-and even in present-day experimental devices. Our subsequent discussion will therefore be specialized to this case (Fig. 20(C)).

Compression in R by a factor C^{-1} moves the plasma into a region of C times higher B_t , and thus causes the minor radius to compress by a factor of $C^{-1/2}$. The net effect is a volume compression by C^{-2} or a density increase by C^2 . If the compression is slow compared with the particle collision times (the usual case) the temperature rises as $C^{4/3}$. The q -value remains fixed during compression, while the aspect ratio decreases as $C^{-1/2}$. The plasma β_p rises as $C^{1/3}$, while β rises as $C^{4/3}$. In the case of an ohmic-heated plasma with pseudoclassical loss rate, the compression is only marginally advantageous [197]. Much greater advantages can be realized with respect to the more relevant problem of helping ohmic heating overcome radiation cooling [197], so as to reach ignition (Section III.C.1). If the object is to reach maximum $n(T_e + T_i)$ in a final tokamak configuration of given aspect ratio and $B_t =$ field strength, then any degree of compression is advantageous; a factor $C = 3$ would yield an improvement of 4.3 in $n(T_e + T_i)$.

The combination of ohmic heating with compression can be considered a feasible solution of the problem of heating tokamaks to ignition (see Section IV.C.3). If other preheating methods work moderately well, the task of reaching ignition by compression is facilitated. If other heating methods work extremely well, they may indeed be able to do the entire job of reaching ignition in an uncompressed tokamak plasma. As we shall see in Section IV.C.3, however, a moderate compression can have significant practical advantages even when combined with heating methods that could do the job "in principle" by themselves.

The compression technique at present enjoys a unique status among auxiliary tokamak heating methods, from the point of view of experimental verification. It has been tried at a high power level on the ATC device [198,199], and found to work essentially as predicted. The smallness of the ATC device causes the energy confinement time τ_E to be roughly comparable to the compression time (~ 2 msec); hence there is some cooling during compression, and the full theoretical factor-of-3 temperature rise is not obtained for the electrons. Nonetheless, the final plasma parameters for compression of an ohmic heated plasma with $C = 2.3$ ($n \sim 10^{14} \text{ cm}^{-3}$, $T_e \sim 2.5$ keV, $T_i \sim 600$ eV) represent a "tokamak record" for both electron and ion energy density. There is every reason to believe that the ATC technique would work equally well in much larger sizes, and that the temperature

multiplication could then be made substantially greater, owing both to improved adiabaticity and the possibility of increasing the compression ratio C . The combination of neutral beam preheating with compression also appears to be working well. Final ion temperatures of 750eV have been reached [199], and the method could readily be extended both in ATC and in larger devices.

5. Turbulent

The objective of turbulent heating (very large electric fields) is to heat a plasma quickly to very high temperatures, where its subsequent decay is hopefully much slower. In general the heating has been demonstrated experimentally in low-density ($\leq 10^{12}/\text{cm}^3$), small ($a \leq 10$ cm) toroidal plasmas, with resultant keV temperatures [200,201]. However, the transition to long-term confinement is yet to be demonstrated.

Qualitatively, the basic theory of this process is that very large externally created electric fields cause a relative drift velocity between ions and electrons that is large compared with their thermal speeds. This causes two-stream (or really Buneman-type) instabilities, which heat the electrons (and perhaps [202] the ions as well), until the electron thermal velocity exceeds the relative drift velocity between the ions and electrons. Then, an ion acoustic wave instability occurs which heats the ions, apparently by wave trapping of the cold ions.

Since the rapidly rising electric field must penetrate into a preionized plasma, there is some question about the skin penetration time scale and process-how turbulent is the resistivity? Also, the current would appear to be peaked near the plasma edge, rather than at the center, and this type of configuration is generally thought to be unstable to localized tearing modes (see Sec. III.A). Since the heating is essentially by an anomalous resistivity, and the other (cross-field) transport processes are probably similarly anomalous, this process is much like ohmic heating in that it can heat up only to a given β_p . The theoretical estimates [203] are $\beta_p \sim R_o/4a$, which is comparable to the result for ohmic heating in the absence of radiation cooling and for pseudoclassical transport. The hypothetical advantage of turbulent heating relative to ohmic heating is that the process occurs so rapidly that radiation losses are negligible. In attempting to reach thermonuclear ignition this can be a critical point (cf. Section III.C.1).

D. Boundary Effects

1. The Steady-State Discharge

Typical present day tokamak discharges maintain themselves in steady state for periods typically five to

ten times longer than either the particle loss time τ_p or the energy loss time τ_E . A brief recapitulation of the energy and particle economy in steady state will be helpful in understanding the problems of wall erosion and impurity influx discussed in the following sections.

Plasma escaping from the tokamak discharge flows to a metal limiter (usually a tungsten or molybdenum ring encircling the minor plasma cross section at a single location around the major periphery). On reaching the limiter, the plasma is neutralized and then largely re-injected into the discharge. The neutral atoms injected at the limiter appear to be fairly energetic [204], with an appreciable component in the energy range of 10–30 eV. Accordingly, they can penetrate several centimeters into the discharge before being reionized by the plasma electrons or charge exchanged with ions at the local ion temperature. Aside from the local neutral influx at the limiter, there is a wall evolved neutral influx distributed uniformly around the major periphery which typically introduces a comparable total number of neutrals into the plasma. The mean energy of the wall-evolved neutrals is lower than those refluxing from the limiter, but is still in the several eV range. The penetration depth into the discharge before ionization or charge exchange is typically a few centimeters. For typical plasma conditions existing in the outer few centimeters of a tokamak plasma the probability of charge exchange is several times that of ionization and therefore a substantial fraction of the incident neutrals are reflected by the process of charge exchange. Because the plasma ions are typically more energetic than the incident neutrals, this same charge exchange process provides a flux of more energetic neutrals directed into the plasma where subsequent charge exchange with even more energetic ions produces more energetic neutrals, some of which leave the plasma and some of which penetrate further into the plasma. The net result of this charge exchange process is that one sees a flux of energetic neutrals emerging from the plasma with a large peak at the low energies corresponding to surface ion temperatures and a smaller tail corresponding to the central ion temperature.

The energy balance of the tokamak in steady state is provided by ohmic power input and by heat loss to the limiter and the chamber walls. As discussed in Section III.B.2, some tokamak discharges appear to lose most of their heat to the limiter. This is the case for “standard operation” in T-3 [204a], T-4, [204b], and ST [204c], as inferred from spectroscopic and bolometric measurements. Direct calorimetric measurements on limiter heat load have not been published for these devices. Rough calorimetric estimates, based on the number of discharges required to bring a thermally isolated limiter to the point

of red heat in the ST tokamak, however, support the spectroscopy-based estimates [204d]. Accurate calorimetric measurements made with a movable limiter in the ORMAK machine show that only a small fraction of the power input to the plasma flows to the limiter. Extensive calorimetric and bolometric measurements on the TM-2 device [204e] show that only in low density discharges does more than 50% of the power flow to the limiter; the remainder of the plasma power is removed by the dual processes of plasma impurity line radiation and charge exchange. In summary, the apparent trend is for high-current-density discharges to heat the limiter, but for lower-current-density, higher-particle-density regimes to lose their heat to the wall by atomic processes. In the extreme form of the radiation-cooled regime, fast visual observation shows a thin “bright ring” of cold plasma surrounding the discharge, well-detached from limiter contact; this ring shrinks with time and brings on the disruptive instability [204f] (Section III.A., III.B.2).

It is interesting to note that the longevity of the tokamak steady state appears to benefit from a number of natural feedback mechanisms. The initial plasma density typically rises (or drops) to an equilibrium level determined by the balance of plasma outward convection and neutral influx. In some experiments the plasma density remains high for many particle containment times. This indicates that most particles diffusing from the plasma are returned to the plasma as neutrals. In other experiments the plasma density is a continuously decreasing function of time showing that some of the particles which diffuse from the plasma are trapped on the limiter or the walls of the discharge chamber and are not reintroduced as neutrals. In the former case the plasma density equilibrium is found to be quite stable against perturbation (e.g., by pulsed gas loads); it is clear that the influx of cold neutrals exerts a regulatory function. The plasma heat load to the limiter also appears to be regulated by a feedback mechanism: if the limiter is locally overheated, it emits impurities that cause the plasma to channel a greater fraction of its power to radiation, rather than to limiter heating. A related phenomenon is the ability of the discharge to recenter itself in the vacuum chamber when the equilibrium B_v -field is inadequately controlled: if the plasma current or pressure becomes excessive, the major radius increases, the outer limiter is touched, impurities are injected (often with attendant minor disruptive instabilities), and the resultant loss of current and plasma energy restores the plasma to a well-centered position.

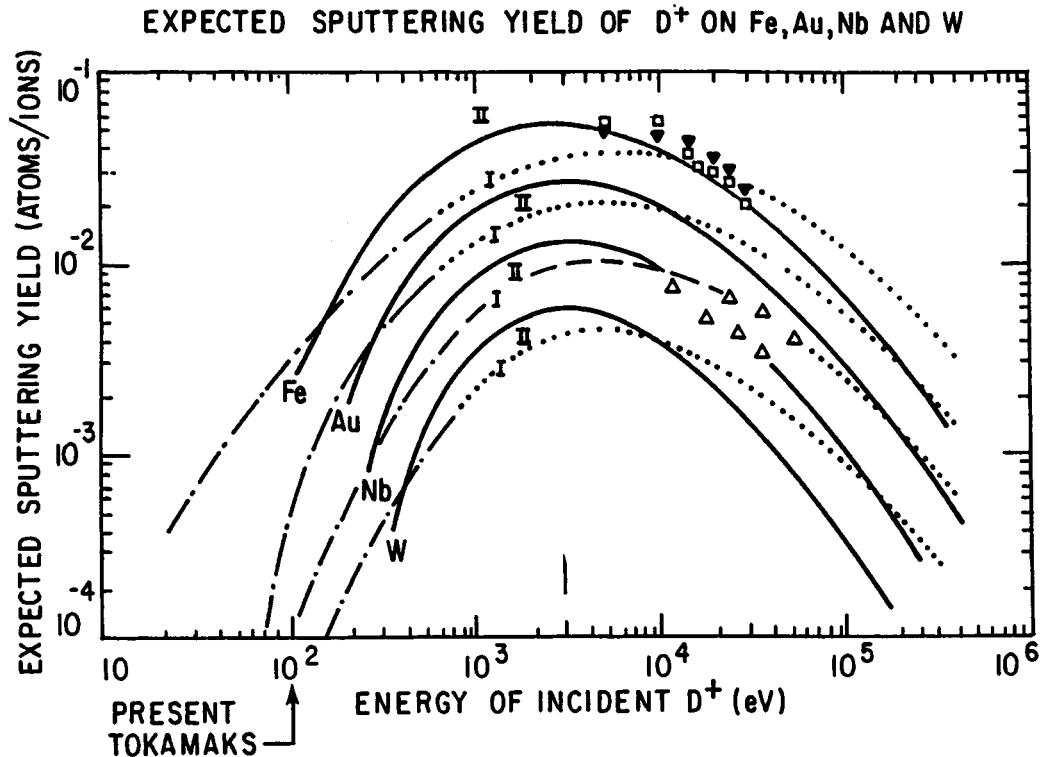


Fig. 21. Expected energy dependent yield of sputtered atoms for D^+ bombarding iron, gold, niobium and tungsten at normal incidence. Curves labeled I are inferred from data taken by D. Rosenberg and G. Wehner [11] for He^{++} sputtering of the four materials at low energies and from data taken by A. Summers, N. Freeman and R. Daly [12] Δ , for He^{++} sputtering of niobium. Curves labeled II were inferred from data on D^+ sputtering of niobium also by Summers, *et. al.* Δ , D^+ sputtering of stainless steel by M. I. Guseva [13] ∇ , and B. M. U. Scherzer [14] \square , and by extrapolations performed by R. Behrisch [2] of D^+ sputtering of niobium. (These data were compiled and analyzed by S. A. Cohen.)

2. Injection of Impurities

The recycling of the tokamak plasma is inevitably accompanied by the ingestion of some impurities. There are a number of identifiable mechanisms.

An important channel for impurity evolution from the chamber wall is bombardment by plasma ions, if they can reach the wall, or else by charge-exchange neutrals [205,206]. The number of neutral wall atoms expected to be sputtered per incident plasma ion or charge-exchange neutral is not well known but is illustrated for purpose of discussion for several wall materials in Fig. 21. In the energy range of 100–1000 eV, we see that roughly 5×10^{-5} iron atoms are sputtered per eV of incident particle energy. For present day tokamaks, with an average ion energy of approximately 300 eV, we see that a fractional contamination of approximately 0.1% iron could be achieved during a single ion energy confinement time, even if only 10% of the average ion energy impinges on the wall. Metal ion contaminations of 0.1% and up are indeed observed in present day tokamak discharges. However these arguments are mainly qualitative. A detailed

understanding of the origin of high Z impurities in tokamak discharges is still lacking. Considerable experimental evidence is being accumulated with respect to the impurity inward diffusion phenomenon mentioned in Section III.B.1.,2. If the impurities do in fact diffuse to the center of the discharge the above arguments lead to an impurity concentration much higher than is actually observed in any tokamak.

In larger, hotter tokamaks of the future, the sputtering problem could become considerably more severe. The increase in size as such will not affect the fractional impurity evolution during an energy containment time, but the increase of mean ion temperature to on the order of 10 keV should make the impurity evolution approximately 30 times worse, unless the fraction of the ion energy impinging on the wall by charge exchange can be reduced. Cooling the plasma-edge ions by means of a “neutral blanket” does not appear promising, if its only effect is to transfer the energy flowing out of the plasma in the form of a few high energy ions into a larger flux of lower energy ions. However, if a neutral blanket had

the effect of transferring this ion energy to the electrons because of the improved electron-ion temperature equilibration found in larger plasmas, the plasma energy would be lost through the electron channel and reduced sputtering would result.

There clearly is much to be gained by proper choice of wall materials. Gold-plating has been found useful in ORMAK, and niobium or tungsten are expected to be even better (Fig. 21). The sputtering problem is, of course, much worse in "steady state" operations, where impurities might tend to accumulate (See Section III.B.1,2), than in a "pulsed" operation where the plasma is held for only one particle confinement time.

Aside from wall-sputtering due to neutrals and plasma ions, there is a similar sputtering process due to plasma ions impinging on the limiter; this is probably the dominant source of heavy impurities in present-day tokamaks. (In discharges with an appreciable run-away electron component, the vaporization of the limiter surface by intensive heat loads due to electron beam pulses plays an even more dramatic role.) As noted in the previous section, impurity injection from the limiter may actually be useful in minimizing limiter damage. In the most high-powered present-day experiments, one can calculate that the absorption of the plasma energy (typically in the kilojoule range) will produce surface melting temperatures, unless the energy is distributed more or less uniformly over the limiter area. Unfortunately, the heat distribution is often nonuniform, as evidenced by the common visual observation of transient white-hot spots on the limiter [206a]. In larger, hotter tokamaks of the future, containing many megajoules of plasma energy, the problem of local limiter vaporization should become extremely severe.

3. Magnetic Limiters and Divertors

It is possible to define the discharge location and size by means of a magnetic—rather than a mechanical—aperture. This is illustrated by several examples in Fig. 22. Outside the magnetic separatrices of these configurations, the magnetic field lines are not closed, but lead away from the plasma; hence, the electron temperature and plasma conductivity tend to be relatively low on these outer field lines [207], and the discharge current tends to channel, instead, on the inside of the separatrices.

The magnetic limiter configurations of Fig. 22 bear an obvious resemblance to the configurations discussed in Section III.A.1, in connection with MHD stability. The proper operation of a magnetic limiter requires that the discharge should strike initially in a well-centered location, and that it should be stable against the axisymmetric

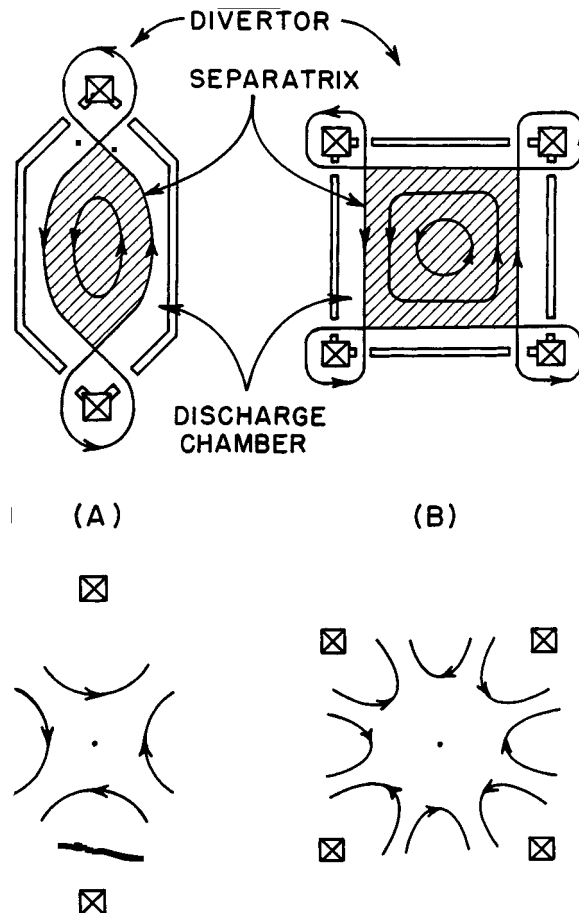


Fig. 22. (A) Elliptical and (B) rectangular divertor structures produced by superposition of quadrupole and octopole fields on the tokamak discharge.

MHD ($n = 0$) modes. For these purposes, the applied quadrupole field (Fig. 22(A)), which is used to make the elliptic configuration, is poorly suited; but the octopole of Fig. 22(B) would be expected to be satisfactory. One notes, incidentally, that a stellarator configuration should be even more effective than an octopole in encouraging initial discharge formation away from mechanical limiters; this approach is being investigated on the Pulsator device in Garching, Germany [208].

Beginning with the idea of a magnetic aperture limiter, it is logical to proceed to a regular divertor: the field lines beyond the separatrix are guided away from the main discharge chamber, into a separately pumped divertor chamber. It is then to be hoped that most of the escaping plasma will not return as neutral gas to the discharge chamber, and that the sputtered atoms resulting from impact of the escaping plasma on divertor walls will also be deposited within the divertor. Here it should be noted that if one wishes to maintain a quasi-steady-state plasma,

one must inject neutral atoms to replace diffusion losses and thus all sputtering will not be eliminated. A secondary advantage of the divertor is that impurities that have entered the tokamak discharge, are pumped, on termination of the discharge, into the divertor chamber, rather than redeposited on the discharge chamber wall. In the case of the Model C Stellarator divertor [209], the experimental result was a precipitous drop of such surface contaminants as oxygen and carbon. Finally, in a sufficiently large device, the “scrape-off” region outside the separatrix will ionize entering heavy atoms and may “flush” them into the divertor, rather than permitting them to enter the discharge proper, where they would diffuse inward and accumulate. However, this latter effect seems difficult to achieve in a practical device.

Actual experimental divertor operation thus far is limited to stellarators and floating-ring devices. The stellarator divertor [209]—unlike the divertors in Fig. 22—passes the short way around the plasma torus, and diverts the main magnetic field. The floating-ring device divertor [210*a,b*] is axisymmetric, like the tokamak divertors in Fig. 22. A small new tokamak device with a single axisymmetric divertor is being built by the authors of Ref. 8. There is also the possibility of a “bundle divertor [212],” which represents a small local detouring of the main tokamak flux; unlike the other examples, this topology necessarily introduces plasma leaks to the wall, and its effect on the tokamak discharge is not clear as yet.

4. Outlook for Future Tokamaks

The emergence of the tokamak device as the most effective means for generating hot toroidal plasma in the laboratory is apparently due in part to the convenient self-regulating interaction of the discharge with its environment: neutral recycling, controlled impurity injection, etc. However, the attainment of adequate plasma purity in future devices—as well as the protection of mechanical structures from plasma erosion—may require some radical changes away from the “natural” tokamak operation (e.g., the use of magnetic limiters, gas blankets or divertors).

If the neutral plasma recycling is interrupted by means of a divertor, the plasma density will decline with a lifetime τ_p . In large tokamak devices of the future, where τ_p is expected to be of the order of 0.1-10 sec (cf. Section III.B.3), the decay of the plasma density may be tolerable.

An alternative approach might be to cool the plasma edge by means of judiciously chosen impurity ions: the idea would be to find a regime where the radiation from partly stripped ions at the plasma edge would remove the

heat outflow without causing wall damage, while the impurity radiation from the plasma interior would remain sufficiently low to permit ignition. In view of the tendency toward impurity concentration in the tokamak discharge (Section III.B.1,2), such a regime could not maintain itself in steady state; whether a practical transient solution exists, remains to be seen.

Still another way of escaping the wall-contact problem may be to use the compression technique (Section III.C.3) to place the plasma transiently away from any limiter. It has been suggested [213] that this technique could serve in a pulsed reactor (during one confinement time τ_p), in place of a divertor arrangement.

In summary, we find that present-day tokamak plasma boundary interactions seem unsuitable for future reactor purposes, though improvements can undoubtedly be made by better choice of wall materials. Alternative technological arrangements exist in principle—and are even expected to have favorable consequences for tokamak stability and confinement—but their effectiveness remains to be demonstrated experimentally.

IV. KEY OBJECTIVES OF THE TOKAMAK PROGRAM

A. Configurational Optimization

1. Testing MHD Stability

A promising start has been made on the theoretical understanding of gross tokamak stability. As we have seen in Section III.B.3, reactor expectations for tokamaks are very sensitive to the attainable β value. As shown in Section III.A, the magnitude of β in turn depends on the attainable values of the safety factor q and of β_p . Accurate experimental determinations of q_{min} (the lowest q -value attainable at the plasma edge without impairing confinement) and β_{pmax} are therefore of prime importance in setting the size and cost of reactor-oriented tokamak experiments.

Considerable experimental information on q_{min} is already available: it appears that a value of ~ 2.5 - 3.5 is compatible with reasonably optimal energy confinement in present-day tokamaks. This determination needs to be repeated and documented in much greater detail in larger, hotter tokamak experiments, where atomic “boundary effects” are less important, and where the radial profiles of current and conductivity are accordingly closer to the intended reactor situation. These studies have been done primarily in large aspect ratio devices ($R/a \approx 7$). They

are now being carried out for plasma aspect ratios nearer to the range of reactor interest, which is $R/a \approx 3$.

Virtually no experimental information is yet available on β_p *max*. Configurations with high β_p -values can be produced transiently by reducing the discharge current; a better method would be compression in *minor* radius. The only really satisfactory test, however, will be to use intensive auxiliary heating (e.g., neutral beams) to raise β_p in quasi-steady state, until limiting MHD instabilities (or loss of equilibrium) are encountered. Again, this investigation should be carried out at realistically low values of R/a , to verify whether the predicted MHD limit of β_p *max* $\sim R/a$ can be reached.

A desirable objective with respect to satisfactory MHD properties in a conventional tokamak would be to operate simultaneously at $R/a \sim 3$, at $q \sim 3$ (or lower), and at $\beta_p \sim 3$ (or higher); if this can be demonstrated experimentally, the plasma β -value will be about 4%—a practical regime for tokamak reactor purposes. An approach toward this objective will be made in High Field ORMAK and in PLT.

2. Improvement of the β -Value

Whether or not the MHD performance of the conventional tokamak meets present expectations, there is much to be gained by special techniques for lowering q and raising β_p —provided that they do not introduce auxiliary plasma troubles or impractical technological requirements.

In future tokamak plasma experiments, further progress can probably be made in reducing the q -value by optimization of the conducting-shell stabilization technique. For reactor purposes, this seems a somewhat impractical approach, unless the neutronics wall-design considerations and the MHD considerations should happen to be compatible. Attention should therefore be paid to the possibility of reducing q by magnetic feedback stabilization of the slow-growing kink-like oscillations. This will be studied experimentally in the ATC device.

One of the best hopes for raising the MHD β -limit is the use of non-circular tokamak minor cross sections. Again there would be some added technical problems in making the required magnetic field and coil structures compatible with reactor operation. On the other hand, some form of noncircular shaping is needed just to provide a magnetic limiter and divertor (Section III.D) and so it seems reasonable to utilize the same technique to optimize β .

At present the only experimental component of the U.S. tokamak program aimed at MHD studies on noncircular cross-sections is the Doublet II device at General

Atomic. The importance of this area, especially in conjunction with the divertor problem, suggests much more extensive experimental investigation.

B. Understanding Plasma Transport and Scaling Laws

1. Entering the “Collisionless Regime”

In the context of tokamak plasma confinement, there are several important criteria for collisionlessness. When the electron mean free path first becomes longer than the major circumference, the plasma enters the standard “pseudoclassical” range of present-day tokamak operation. For mean free paths substantially longer than this, (i.e., hotter plasmas), electrons and ions can become effectively trapped in local magnetic mirrors. In the case of the neoclassical theory, there results a criterion on T_i such that the ion heat diffusion will be in its most collisionless (“banana”) form (Section III.B.1a). In the case of anomalous transport considerations, one has a minimum criterion on both T_e and T_i for entry into the “trapped-ion” or “collisional-trapped-particle” regime, which is expected to be characteristic of tokamak reactor operation (Section III.B.1b). Since neoclassical transport is smaller than the currently estimated trapped-ion-mode transport by several orders of magnitude, the possible consequences of the latter are of main practical concern in connection with tokamak reactor planning.

As noted in Section III.B.3, no present-day tokamak experiments are operating in the relevant trapped-ion-mode regime. Appropriately collisionless plasmas can be achieved in internal-ring devices (Section IV.C). Evidence of highly anomalous plasma loss has indeed been observed. However, much more detailed studies are required to identify the transport mechanisms and insure that accurate analogies can be drawn. The addition of intensive auxiliary heating to present tokamaks could also make the trapped-ion-mode regime accessible. Both electron and ion temperatures need to be raised appreciably, and impurity content needs to be held down. While this might be achieved in ORMAK or in ATC, there is concern that enhancement of energy transport, as the trapped-ion regime is approached, might make heating more difficult, as well as enhancing impurity evolution. The complicating factor is the possible onset of the “trapped-electron-mode” at somewhat lower temperatures—perhaps even in present-day experiments. This could be an inconvenient obstacle to entry into the trapped-ion-mode regime, which is the most relevant for reactor purposes. Thus it seems likely that experiments

at least of the order of High Field ORMAK or PLT will be needed to explore the reactor-relevant “collisionless regime.”

We note, incidentally, that two of the smaller present-day U.S. tokamak experiments have an interesting potential for increasing our understanding of the collisionality question. If the Texas Turbulent Torus succeeds in rapid plasma heating to multi-keV electron and ion temperatures at low plasma density, the subsequent plasma decay process could take place in the trapped-ion-mode regime. Conversely, if the Alcator reaches high-field operation, it will be able to produce multi-keV plasmas at unusually high plasma densities, and thus should be able to explore the possibility of minimizing trapped-particle effects by operating in a high-density regime (i.e., high-field or high- β tokamak modes).

2. Scaling with Size

All theoretically known plasma diffusion processes—whether classical or anomalous—lead to confinement times that increase at least according to the scaling $\tau \propto a^2$. (The trapped-ion mode scaling is $\alpha \perp a^4$.) Scaling with size alone would certainly be more meaningful and confidence-inspiring than extrapolating over appreciable factors in various plasma parameters, such as the temperature. The most promising experimental strategy for obtaining an estimate of reactor-size requirements, is therefore to aim at the achievement of reactor-type plasma temperature, density, and purity in the smallest size tokamak devices that will do the job. Once this stage is achieved, tokamak development toward an actual reactor can proceed with greatly enhanced confidence and sense of technical direction.

At present it is not yet clear what size tokamak facility will be required for a minimum demonstration of reactor plasma parameters. Estimates range from High Field ORMAK or PLT, on the optimistic side, to several times larger devices. Especially if a divertor system is to be incorporated in future tokamak experiments, the large-size estimates would seem to be more realistic. Instead of increasing plasma size, one can also improve prospects for attaining higher temperatures by raising the magnetic field strength. This is illustrated by Eqs. 32-35 of Sec. III.B.3. where size and poloidal field appear only in the form of their product, $I \propto a B_p$. For this reason, most tokamak plans for the future envisage toroidal fields of ≥ 50 kG at the plasma (≥ 90 kG peak field at the coil). If technical problems can be overcome, tokamak experiments at even higher fields might prove fruitful in permitting reactor-type plasma parameters to be obtained in relatively small size. Actual tokamak reactor coil systems,

however, cannot be expected to operate much above 50 kG at the plasma—at least until significant new advances take place in the technology of large superconducting coils.

3. Understanding the Physics of Transport

The preceding two sections have taken a phenomenological approach to the problem of tokamak confinement: experiments should aim to enter the “collisionless regime,” and preferably to attain the characteristic plasma parameters of a reactor—then one can extrapolate τ with size. While this is a reasonable strategy, it would be clearly more desirable to be guided by physical understanding of the tokamak transport. Only if the physics is known can one be certain about extrapolating over large factors; *if* the physics is known, one may be able to take effective measures to optimize confinement. In this sense, discovery of the mechanics of the transport in present-day and future tokamak plasmas would provide the most helpful “benchmark” of all for the tokamak research program.

Direct measurements on fluctuations in a hot plasma can be carried out by scattering of visible and infrared light and microwaves, as well as with energetic ion beams. The application of such diagnostics to tokamak plasmas is still only in its initial stages. Much intensive effort along these lines—as well as much greater support for the development of new diagnostic ideas—is warranted by the potential usefulness of the results. A corresponding intensification of theoretical work on the trapped particle instabilities in present experiments is also very necessary. The requirements in this area have recently been reviewed in detail [218]. Closer interaction between experimentalists and theorists should be encouraged to promote the detailed testing of hypothetical loss mechanisms, such as the trapped particle modes, to inject the stimulus of experimentally observed anomalies into the process of theoretical tokamak modeling and vice versa.

C. Heating

1. Injection

The key heating objective is to show that neutral beams can heat toroidal plasmas significantly. Some progress towards this goal has been made in the recent injection heating experiments in ATC and ORMAK—see Sec. II.C.2. As part of this objective it must be shown that the plasma perturbations (see Sec. II. C.2) produced by increasing the neutral beam power do not pose any serious

limitations on this injection method for larger and more reactor-like plasma and neutral beam regimes. The current experiments in the ORMAK and ATC devices are directed toward this objective. These heating experiments are important since: 1) it is vital to have a practical supplement to ohmic heating in order to explore higher temperature confinement and higher- β stability questions, and 2) the insight gained by using auxiliary power sources of variable strength to heat the plasma should be very helpful in understanding plasma confinement.

2. Wave Heating

In most frequency ranges, the initial objectives (i.e., qualitative agreement with predicted coupling of applied power to wave energy and, ultimately, to plasma energy) have been demonstrated. The remaining questions relate to limitations on attainable energy and the effect of heating on confinement. The coupling efficiencies depend on the plasma properties such as nonlinearities; when high powers are effectively coupled into high-density plasmas, problems that are not yet contemplated could well occur. Crucial tests in this regard for the ion cyclotron resonance heating will be undertaken in early 1974 on the ST device, when ~ 1 –2 MW of rf will be supplied to the coil structure. High power tests of the lower hybrid heating concepts will be carried out in 1974–1975 on the ATC and Alcator.

Given the success of those initial high power experiments, the next objective should be to exploit the very high powers (1–10 MW) available in radio-frequency sources. The objectives are threefold: (1) to provide a demonstration that auxiliary heating can be used in large amounts to initiate (and perhaps maintain) thermonuclear burning in a marginal device, (2) to help achieve high β_p values, and (3) to study wave coupling phenomena at very high powers.

3. Compression

As we have seen in sections III.C.1 and 3, the probability of reaching ignition by ohmic heating alone is finite but small in ordinary tokamaks; it improves considerably with the help of adiabatic compression, and should also improve with the use of noncircular cross-sections. For the same total coil volume, compression may be useful in overcoming radiation loss limitations on plasmas produced in the entire volume. Compression could also be combined advantageously with other heating techniques. In the case of neutral beam injection into large tokamaks, one problem is that higher energy neutral beams are needed to penetrate into the center of the plasma (see

Section III.C.2), and the construction of efficient neutral beam sources then becomes more difficult. Even a modest R-compression ratio C is helpful here, since the product na scales as $C^{3/2}$. Furthermore, the compression amplifies the initial energy input by a factor of $C^{4/3}$, thus making the energetic efficiency of the source a less critical consideration.

4. Turbulent Heating

The goals here are: 1) demonstrate heating to keV temperatures in a high-density ($n \gtrsim 2\text{--}3 \times 10^{13}$) plasma, and 2) demonstrate that it is possible to transform the turbulently heated plasma into a plasma that can be confined in a toroidal system over a long time (e.g., 10 msec) in a manner which is scalable to larger devices. While the first of these goals has been demonstrated in CLIMAX at low densities, it has not yet been demonstrated at the high densities relevant in tokamaks. This is one of the key objectives of the TTT program. Since there are a number of questions concerning the transition from turbulent, short-time energy confinement, to quiescent, long-time energy confinement, a demonstration of this possibility would be most encouraging. This is the ultimate and perhaps most formidable objective of the TTT program.

D. Solution of Boundary Problems

1. Physics of Particle-Surface Interactions

Considering the rather decisive role played by particle-surface interactions in present-day tokamaks, surprisingly little is known about the physical nature—or even the cross section—of these interactions. Some basic data, for example, on sputtering, can be found in the existing technical literature, but most of the specific questions that need to be answered for tokamak purposes will require dedicated measurement efforts on the part of the tokamak research program.

For example, relatively few details are known about sputtering by low-energy hydrogen atoms (or ions) incident on typical present-day tokamak wall materials, such as stainless steel, gold, tungsten, and ceramic. Detailed knowledge of these effects is of rather critical importance in understanding tokamak discharges.

To put the comparison of tokamak data on a more systematic basis, it would clearly be important to eliminate the “hidden variable” of surface contamination by direct monitoring of contaminants, for example by on-line Auger spectroscopy, conducted as part of the standard experimental diagnostics. Even for future devices with

divertors, the study of surface-interaction cross sections and monitoring of surface conditions will remain of substantial importance.

2. Limiter and Divertor Development

As has been pointed out in Section III.D., the long-range prospects of the tokamak discharge seem to depend on getting away from the present primitive environment, into a situation free from direct mechanical contact with the hot plasma. Only in this way can one confidently expect to reduce plasma impurities—and especially heavy impurities—from their present typical levels to desirable levels from the reactor point of view.

The implementation of tokamak experiments with magnetic limiters, and preferably with divertors, is therefore a matter of considerable long-range importance. Just how critical this feature may become, even to the attainment of hot plasmas in moderate-sized tokamak devices, will soon become clear with the initiation of the High Field ORMAK and the PLT. In the short run, some improvements in mechanical limiter technology may prove helpful: for example, the use of rotating horizontal rails to help distribute the heat load, and the use of fast-opening limiters to minimize skin effect in large plasmas. Such limiter innovations are planned for initial operation in the PLT device. The possibility of compressing the discharge transiently away from limiter contact (letting it expand freely) also has some potential, usefulness. This will be explored in ATC.

We note that if a divertor system is required, it is an important element in determining size and cost. The minimum volume of a toroidal-field coil system could easily be raised by a factor of two or more as a result of the divertor addition. In the event that noncircular cross section permits enhanced β -values, this economic disadvantage of divertors would, of course, be offset by the ability to operate at reduced toroidal field strength. Detailed investigation of these possibilities is obviously of major importance in determining the magnitude and technical design of future tokamak facilities.

SUMMARY AND CONCLUSIONS

Confinement of thermonuclear plasma in tokamak toroidal magnetic containers is a highly promising approach to the realization of fusion reactors for central-station electrical generating plants. This report is devoted to a technical review of the present status and key near-term objectives of this program.

The ultimate goal of the program is the successful development of a thermonuclear reactor based on the physics principles of low density closed systems. In striving towards this goal, the program would be expected to pass successive milestones in confinement physics, thermonuclear breakeven, and engineering, including:

1. Demonstration of confinement and heating in the plasma physics regime of a fusion reactor.
2. Demonstration of thermonuclear burn sufficient to yield net energy gain.
3. Demonstration of the engineering elements necessary for a reactor.

Recent experimental results have laid the basis for a systematic advance toward Milestone No. 1, with excellent chances of success. In describing the present status of the program, it is useful to separate the physics problems into four distinct areas:

A. *Configurational Stability*. This area deals with the gross (MHD) equilibrium and stability of the toroidal magnetic container. In the case of tokamaks, the basic equilibrium and linear stability theories are well understood and are found to be in general agreement with experiment. Theory and present experiments indicate, but do not prove yet, that reactor requirements can be met.

B. *Plasma Transport and Scaling*. This area deals with microscopic plasma transport and the scaling laws derived therefrom, which limit the energy confinement time of the plasma in a configuration that is grossly stable. The dominant component of tokamak energy transport is clearly nonclassical (i.e., predominantly due to cooperative phenomena rather than classical Coulomb scattering); however, the present experimental trend would suggest that reactor confinement requirements can probably be met. Theory suggests, for the most probable cooperative transport case (trapped-particle modes), that confinement is likely to be adequate for reactor purposes. The state of understanding is not sufficient, however, to determine at this time the minimum size of the device required for passing Milestone No. 2.

C. *Heating*. Ohmic heating occurs naturally in the tokamak configuration and serves to raise the plasma to the keV temperature range. Auxiliary heating will be required to achieve ignition. Of the three main heating methods currently under experimental study, compressional heating has now been demonstrated successfully and neutral beam heating and wave heating are showing encouraging initial results. The multiplicity of possible heating techniques, coupled with initial success of a variety of heating experiments, leads to considerable optimism for a successful solution of the plasma heating problem.

D. *Boundary Effects.* The interaction of hot plasma particles and plasma-emitted neutral particles with the material boundary leads to the injection of nonhydrogenic atoms into the plasma. Only a low level of such impurities could be tolerated in a reactor. Present plasma impurity levels in tokamaks are worrisome, and it may be necessary to reduce them in future devices. Techniques for control of boundary effects remain to be explored systematically on the tokamak.

Given this basically encouraging outlook, it is nonetheless apparent that additional work remains to be done before Milestone No. 1 will be attained. To help clarify the tasks ahead, Section IV of the present report is addressed to the formulation of key near-term objectives in each of the four problem areas defined above. These are summarized below:

A. *Configurational Optimization.* The key near-term objectives in this area are:

1. Determine the stable limits on plasma current and pressure (cf. the parameters q and β_p of Section III.A.1), and their dependence on radial profiles. In the U. S. program, special reliance is being placed on the ATC and ST at PPPL, and ORMAK at ORNL, to contribute information towards fulfillment of this key objective.
2. Understand the advantages and disadvantages of noncircular cross-sections. Tokamaks with certain noncircular cross-sections may introduce significant advantages relative to conventional tokamaks, for example, by permitting use of a higher β value (ratio of plasma pressure to magnetic pressure). The stability limits and confinement properties of such configurations must be assessed before the overall effect can be judged. In the U. S. program, the Doublet II device at Gulf General Atomic is providing results relevant to this key objective.

B. *Understanding Plasma Transport and Scaling Laws.* The key near-term objectives in this area are:

1. Attain, experimentally, regimes of sufficiently high electron and ion temperatures to assess the effect of trapped particle instabilities on plasma confinement.
2. Determine the scaling laws for optimal design of devices capable of passing Milestone No. 2.
3. Further develop the underlying physics understanding of plasma transport.

The U. S. program is at present relying primarily on the ORMAK and the ATC to advance towards these objectives. Several additional U. S. experiments—TTT

at the University of Texas, Alcator at MIT and internal ring devices at General Atomic, PPPL, and the University of Wisconsin—are also expected to provide important information. The High Field ORMAK tentatively scheduled for FY 1975 operation, and the Princeton Large Torus scheduled for completion in FY 1976, should provide definitive data on scaling.

C. *Heating.* Four heating techniques are being developed for use in large toroidal systems: neutral-beam injection, compression, wave heating, and turbulent heating. Compressional heating was demonstrated recently on the ATC, though not in a plasma of sufficient size to yield ignition temperatures. High-powered neutral injection heating, wave heating and turbulent heating are expected to be demonstrated in FY 1974—respectively, on the ORMAK and ATC, on the ST, and on the TTT. The key near-term objectives in this area are the demonstration of neutral-beam heating and wave heating.

D. *Solution of Boundary Problems.* Studies on the nature and origin of impurities are made on the ST, ATC and on the ORMAK. However, the U. S. at the present time has no major machine devoted primarily to the solution of plasma boundary problems. The key near-term objective in this area is to assess the need for, and development of, techniques for tokamak impurity control. An obvious approach appears to be the development of magnetic divertors. A second important technique is the improvement of wall materials. The divertor techniques tend to impose noncircular cross-sections (cf., A above) or non-axisymmetry.

At present, the key near-term objectives of the program are being addressed by means of relatively small research devices, each designed for a special purpose. The largest U. S. tokamak now under construction, the PLT device, is expected to demonstrate in a single device several of the above key objectives. As the program continues to progress, it will become increasingly necessary to use larger facilities, with the capability of demonstrating the whole set of key objectives together.

ACKNOWLEDGMENTS

Input to this report, is acknowledged from the following: S. C. Brunett, J. B. McBride and N. A. Davies, *U.S. Atomic Energy Commission*; K. Bol, S. A. Cohen, R. A. Ellis, M. B. Gottlieb, D. J. Grove, E. Hinnov, J. C. Hosea, J. L. Johnson, D. M. Meade, E. B. Meservey, F. W. Perkins, J. A. Schmidt, W. Stodiek, S. von Goeler, from the Princeton Plasma Physics Laboratory; L. A. Berry, R. A. Dory, A. C. England, J. T. Hogan, G. G. Kelley, M. Roberts, L. D. Stewart, M. Murakami, N. H.

Lazar, from the Oak Ridge National Laboratory; D. W. Kerst and J. C. Sprott, from the University of Wisconsin; C. W. Hartman, J. Killeen, and L. D. Pearlstein, from the Lawrence Livermore Laboratory; M. Rosenbluth, Institute for Advanced Study; B. Coppi, Massachusetts Institute of Technology; W. E. Drummond, K. Gentle, P. Nielsen, A. Ware, from the University of Texas; H. Grad, New York University; and T. Tamano, Gulf General Atomic.

Electrostatic potential also azimuthal angle..... ϕ
 Shear strength also toroidal angle θ
 Growth rate..... γ
 Diffusion coefficient..... D
 Heat transport coefficient..... χ
 Energy containment time τ_E
 Debye shielding length..... λ_D
 Magnetic moment..... μ
 Collision frequency ν

PARTIAL GLOSSARY OF TERMS

Major radius R_o
 Plasma radius..... α
 Limiter radius α_L
 Radial dimensions of noncircular cross-section ℓ_1, ℓ_2
 Inverse aspect ratio..... $\epsilon = a/R$
 Toroidal magnetic field B_t
 Poloidal magnetic field B_p
 Vertical magnetic field B_v
 Safety factor $q = \epsilon B_t/B_p$
 Shear length..... L_s
 Gyromagnetic frequency Ω
 Gyromagnetic radius ρ
 Trapped particle bounce frequency..... ω_b
 Trapped particle banana width..... Δr_T
 Fraction of particles trapped f_T
 Plasma current I, I_p
 Impressed voltage..... V
 Plasma temperature T
 Ratio of plasma pressure to magnetic field pressure $\beta = 8\pi n(T_e + T_i)/B^2$
 Resistivity η
 Effective Z due to impurities..... Z_{eff}
 Effective Z from resistance measurements..... $\langle Z \rangle$
 Effective Z from x-ray measurements... Z_x
 Resistivity anomaly A_R
 Plasma density n
 Particle mass..... m
 Speed of light c
 Ion sound speed..... V_S
 Current drift velocity..... u
 Plasma thermal velocity V_T
 Curvature drift velocity..... V_D
 Diamagnetic drift velocity V_d
 Wave number..... k
 Curvature drift frequency..... ω_D
 Drift wave frequency ω^*

REFERENCES

1. S. Yoshikawa (1964). *Phys. Fluids* **7**, 278.
2. V. D. Shafranov (1970). *Sov. Phys.-Tech. Phys.* **15**, 175.
3. H. P. Furth, P. H. Rutherford, H. Selberg, (1973). *Phys. Fluids* **16**, 1054; similar calculations may be found in W. Grossmann and S. Ortolani, IPP Report 1/32, Garching Munich (1973).
4. V. D. Shafranov and E. I. Yurchenko, (1968). *Nuclear Fusion* **8**, 329; also L. S. Solovov, V. D. Shafranov, and E. I. Yurchenko, *Nuclear Fusion*, Special Supplement 1969, English Trans. of Russian Papers, p. 25, (IAEA, Vienna).
5. J. D. Callen and R. A. Dory (1972). *Phys. Fluids* **15**, 1523.
6. J. Freidberg, *et. al.* (1973). VI European Conference on Controlled Fusion and Plasma Phys., Moscow.
- 6a. D. Dobrott and M. S. Chu (1973). *Phys. Fluids* **16**, 1371.
7. L. A. Artsimovich (1972). *Nuclear Fusion* **2**, 215.
8. J. C. Hosea, *et. al.*, Plasma Physics and Controlled Nuclear Fusion Research (IAEA, Vienna, 1971), Vol. II, p. 425.
9. K. Bol, *et. al.*, *Phys. Rev. Lett.* **29**, 1495 (1972), D. Stevens, *Phys. Fluids*, to be published.
10. L. I. Artemenkov, *et. al.* (1973). *JETP Letters* **17**, 179.
11. A. Gibson, *et. al.*, Garching/Munich Conference, 1973, Pauer B16-I.
12. V. Mirnov, I. V. Semenov (1971). *JETP* **33**, 1134.
13. J. C. Hosea, *et. al.* (1973). *Phys. Rev. Lett.* **30**, 839.
14. F. C. Jobses and J. C. Hosea, Garching/Munich Conference, 1973, paper B 14.
15. K. Bol, *et. al.*, Garching/Munich Conference, 1973, Paper B 12.
16. P. H. Rutherford and H. P. Furth (1965). Conference on Plasma Theory, Kiev, U.S.S.R., October 1971. B. Coppi, *Phys. Fluids* **7**, 1501 (1964), *Phys. Fluids* **8**, 2273.
17. D. L. Bowers, *et. al.* (1971). *Plasma Physics* **13**, 849.
18. H. P. Furth, (1973). Garching/Munich Conference, 1973, Paper B9-I.
19. V. S. Vlasov, *et. al.*, VI European Conference on Controlled Fusion and Plasma Phys., Moscow, p. 55.
- 19a. D. Dimock, *et. al.* (1973). *Bull Amer Phys. Soc. II*, **18**, 1253.
20. V.A. Vershkov, *et. al.*, (1973). Kurchatov Inst. Preprint IAE-2241 (1973), MATT TRANS-113.
21. E. Hinnov, *et. al.*, Garching/Munich Conference, 1973, Paper B 13.
22. S. von Goeler, *et. al.*, Garching/Munich Conference, 1973, Paper B 25.
23. V. S. Vlasenkov, *et. al.*, Garching/Munich Conference, 1973, Paper B 2.
- 23a. E. Mazzucato, private communication.
- 23b. S. V. Mirnov, (1970). *JETP Letters* **12**, 64.
- 23c. C. Bobeldijk, D. Dimock, and J. C. Hosea, (1971). *Bull. Am. Phys. Soc. II*, **16**, 1232 (1971); PPPL Annual Report MATT-Q-29, p 32.
24. T. Ohkawa, Garching/Munich Conference, 1973, Paper B17-I.
25. A. N. Bortnikov, *et. al.*, Garching/Munich Conference, 1973, Paper B 5.

26. P. H. Rutherford, Garching/Munich Conference, 1973, Paper B 21.
27. M. N. Rosenbluth, *et al.*, Garching/Munich Conference, 1973, Paper B 22.
28. B. B. Kadomtsev and O. P. Pogutse, VI European Conference on Controlled Fusion and Plasma Phys., Moscow, 1973, p. 59.
29. G. Laval, *et al.*, Garching/Munich Conference, 1973, Paper F2-I.
30. T. Ohkawa, private communication.
31. G. Sheffield (1973). PPL Computer Studies, unpublished.
32. B. Coppi, J. M. Greene, and J. L. Johnson (1966). *Nuclear Fusion* **6**, 101.
33. J. M. Greene and J. L. Johnson (1965). unpublished.
34. H. Grad (1967) unpublished (1966); *Phys. Fluids* **10**, 137.
35. For a review of trapped-particle orbits and their effects on plasma microinstabilities see: B. B. Kadomtsev and O. P. Pogutse, (1971). *Nuclear Fusion* **11**, 67.
36. H. Grad (1967). *Phys. Fluids* **10**, 137; H. P. Furth and M. N. Rosenbluth, in *Plasma Physics and Controlled Nuclear Fusion Research* (Proceedings of Novosibirsk Conference, August 1–7, 1968) (IAEA, Vienna, 1969), Vol. I, p. 821.
37. T. E. Stringer, Garching/Munich Conference, 1973, paper F1-I.
- 37a. W. Stodiek, K. Bol, H. Eubank, S. von Goeler and D. J. Grove in *Plasma Physics and Controlled Nuclear Fusion Research* (Proc of Madison Conf., June 17–23, 1971) (IAEA, Vienna, 1971), Vol. 1, p. 465.
38. For a detailed discussion of classical plasma transport see: S. I. Braginskii, in *Reviews of Plasma Physics*, M. A. Leontovich, Ed. (Consultants Bureau, New York, 1965), Vol. I, p. 205.
39. A. A. Galeev and R. Z. Sagdeev (1968). *Soviet Phys. JETP* **26**, 233.
40. M. N. Rosenbluth, R. D. Hazeltine and F. L. Hinton (1973). *Phys. Fluids* **15**, 116.
- 40a. T. Tamano, R. Prater, T. Ohkawa, "Poloidal Bohm Diffusion in Collisionless Plasma," to be published.
41. F. L. Hinton and M. N. Rosenbluth (1973). *Phys. Fluids* **16**, 836.
- 41a. T. Ohkawa, J. R. Gilleland and T. Tamano (1972). *Phys. Rev. Letters* **28**, 1107.
42. M. N. Rosenbluth and A. N. Kaufman (1958). *Phys. Rev.* **109**, 1.
43. R. A. E. Bolton, J. Hugill, D. J. Lees, W. Millar and P. Reynolds, in *Plasma Physics and Controlled Nuclear Fusion Research* (Proceedings of Madison Conference, June 17–23, 1971) (IAEA, Vienna, 1972), Vol. III, p. 79.
44. T. Ohkawa, J. R. Gilleland and T. Tamano (1972). *Phys. Rev. Letters* **28**, 1107.
45. L. A. Artsimovich, A. V. Glukhov and M. P. Petrov (1970). *JETP Letters* **11**, 304.
- 45a. G. G. Kelley *et al.* (1974). Garching/Munich Conference, paper B3-I; L. A. Berry, J. F. Clarke, and J. T. Hogan. *Phys. Rev. Letters* **32**, 362.
46. R. J. Bickerton, J. W. Conner and J. B. Taylor (1971). *Nature, Phys. Sci.* **229** 110; B. B. Kadomtsev and V. D. Shafranov, in *Plasma Physics and Controlled Nuclear Fusion* (Proceedings of Madison Conference, June 17–23, 1971) (IAEA, Vienna, 1972), Vol. II, p. 479.
47. D. J. Sigmar (1973). *Nuclear Fusion* **13**, 17.
48. J. D. Callen, J. F. Clarke and J. A. Rome. Garching/Munich Conference, 1973, paper E 14.
- 48a. L. Spitzer and R. Harm (1953). *Phys. Rev.* **89**, 977; L. Spitzer, *Physics of Fully Ionized Gases* (Interscience, New York, 1964), Chapt. 5.
- 48b. B. Coppi and D. J. Sigmar (1973). *Phys. Fluids* **16**, 1174.
- 48d. D. W. Ross and G. L. Cardwell (1973). *Phys. Fluids* **16**, 1551.
49. A. A. Ware (1970). *Phys. Rev. Letters* **25**, 916; A. A. Galeev (1971). *Soviet Phys. JETP* **32**, 752.
50. D. J. Sigmar and J. F. Clarke, "Neoclassical Transport Theory of Multispecies Plasmas," Sherwood Theory Meeting, Austin, Texas, March 12, 13, 1973 (to be published).
51. V. A. Vershkov and S. V. Mirnov, in Fifth European Conference on Controlled Fusion and Plasma Physics (Grenoble, August 21–25, 1972), Vol. I, p. 1.
52. W. E. Drummond and D. Pines, *Nuclear Fusion* 1962 Supplement, part 3, p. 1049.
53. A. A. Vedenov, E. P. Velikhov and R. Z. Sagdeev (1961). *Nuclear Fusion* **1**, 82; 1962 Supplement, Part 2, p. 465.
54. V. N. Tsytovich (1967). *Soviet Phys.—Uspekhi* **9**, 805; B. B. Kadomtsev, *Plasma Turbulence* (Academic Press, London, 1965).
55. B. Coppi, M. N. Rosenbluth and R. N. Sudan (1969). *Annals of Physics* **55**, 207 (1969); p. 248.
56. T. H. Dupree (1966). *Phys. Fluids* **9**, 1773; **10**, 1049 (1967).
57. A. A. Galeev (1967). *Phys. Fluids* **10**, 1041.
58. See for example: T. H. Stix, *The Theory of Plasma Waves* (McGraw-Hill, New York, 1962), p. 213.
59. W. E. Drummond and M. N. Rosenbluth (1962). *Phys. Fluids* **5**, 1507.
60. See for example: E. K. Zavoiski and L. I. Rudakov (1971). *Soviet Atomic Energy* **23**, 1171.
61. B. D. Fried *et al.*, in *Plasma Physics and Controlled Nuclear Fusion Research* (Proceedings of Madison Conference, June 17–23, 1971) (IAEA, Vienna, 1972), Vol. II, p. 55.
62. J. D. Callen, J. T. Hogan and B. V. Waddell, Garching/Munich Conference, 1973, paper B 23.
63. C. W. Horton, Jr. (1972). *Phys. Rev. Letters* **28**, 1506.
64. T. K. Chu, B. Coppi, H. W. Hendel and F. W. Perkins (1969). *Phys. Fluids* **12**, 203 and references cited therein.
65. B. B. Kadomtsev and O. P. Pogutse, in *Reviews of Plasma Physics*, M. A. Leontovich, Ed. (Consultants Bureau, New York, 1970), p. 249.
66. W. Stodiek, D. J. Grove and J. O. Kessler, in *Plasma Physics and Controlled Nuclear Fusion Research* (Proceedings of Culham Conference, Sept. 6–10, 1965 (IAEA, Vienna, 1966), Vol. II, p. 687.
67. K. M. Young (1967). *Phys. Fluids* **10**, 213.
68. N. A. Krall and M. N. Rosenbluth (1965). *Phys. Fluids* **8**, 1488; see also Ref. 31.
69. O. P. Pogutse (1972). *Nuclear Fusion* **12**, 39.
70. S. Yoshikawa and N. C. Christofilos, in *Plasma Physics and Controlled Nuclear Fusion Research* (Proceedings of Madison Conference, June 17–23, 1971) (IAEA, Vienna, 1972), Vol. II, p. 357, and references cited therein.
71. L. A. Artsimovich (1971). *JETP Letters* **13**, 70.
72. B. B. Kadomtsev and O. P. Pogutse (1971). *Nuclear Fusion* **11**, 67.
73. B. B. Kadomtsev and O. P. Pogutse (1969). *Soviet Phys.—Doklady* **14**, 470.
74. A. A. Galeev, Garching/Munich Conference, 1973, paper E1-I.
75. M. N. Rosenbluth, D. W. Ross, and D. P. Kostomarov (1972). *Nuclear Fusion* **12**, 3.
76. N. T. Gladd and D. W. Ross (1973). *Phys. Fluids* **16**, 1706.
77. W. M. Tang (1973). *Nuclear Fusion* **13**, 883.
78. R. Z. Sagdeev and A. A. Galeev (1972). Comments on Plasma Physics and Controlled Fusion **1**, p. 23.
79. M. N. Rosenbluth, private communication.
80. J. F. Clarke, private communication..
81. J. D. Callen, B. Coppi, R. Dagazian, R. Gajewski and D. J. Sigmar in *Plasma Physics and Controlled Nuclear Fusion Research* (Proceedings of Madison Conference, June 17–23, 1971) (IAEA, Vienna, 1972), Vol. II, p. 451.
82. A. H. Glasser, E. A. Frieman, and S. Yoshikawa, "Stabilization of the Collision-less Trapped-Particle Instability by Shaping of the Tokamak Cross Section", MATT-985, June, 1973 (to be published).
83. M. N. Rosenbluth and M. L. Sloan (1971). *Phys. Fluids* **14**, 1725.
84. J. C. Adam, G. Laval and R. Pellat (1973). *Nuclear Fusion* **13**, 47.
85. B. Coppi and E. Minardi (1973). *Phys. Fluids* **16**, 1021; Garching/Munich Conference, 1973, paper F6-I.

86. D. E. Baldwin and J. D. Callen (1972). *Phys. Rev. Letters* **28** 1686.
87. J. B. Taylor and B. McNamara (1971). *Phys. Fluids* **14**, 1492.
88. M. N. Rosenbluth and C. S. Liu, Fifth European Conference on Controlled Fusion and Plasma Physics, Grenoble, Aug. 21–25, 1972, Vol. I, p. 12.
89. J. B. Taylor, *ibid.*, Vol. II, p. 83.
90. T. Tamano, R. Prater and T. Ohkawa, Garching/Munich Conference, 1973, paper C 4; (1973). *Phys. Rev. Letters* **30**, 431.
91. H. Okuda and J. M. Dawson (1973). *Phys. Fluids* **16**, 1456.
92. T. H. Stix (1973). *Phys. Rev. Letters* **30**, 833.
93. A. P. Vasil'ev, *et. al.* (1960). Nuclear Fusion Supplement, Part 2, 655 (1962); R. F. Post, Riso, International Summer Course in Plasma Physics.
94. H. R. Griem, *Plasma Spectroscopy* (McGraw-Hill, New York, 1964); G. Marr, *Plasma Spectroscopy* (Elsevier, New York, 1968).
95. W. Lotz (1967). *Astrophysical Journal* XIV, 207; and references cited therein.
96. I. Galushkin, *et. al.* (1971). IAEA Madison CN-28/F-6; *Nuclear Fusion* **11**, 597; I. L. Beigman, *et. al.* (1970). *Sov. Astron. J.* **13**, 755.
97. E. Hinnov (1972). MATT-777 (1970); *Plasma Physics* **14**, 755; G. R. Hopkins, G.G.A. report.
98. B. A. Trubnikov (thesis) (AEC-Tr-4073) (1958).
99. D. J. Rose and M. Clark, Jr. (1969). *Plasmas and Controlled Fusion* (MIT Press, Cambridge, Mass., 1961), p. 236; D. J. Rose, *Nuclear Fusion* **9**, 183.
100. M. N. Rosenbluth (1970). *Nuclear Fusion* **10**, 340.
101. J. F. Clarke and R. H. Fowler (1972). *Bull. Am. Phys. Soc.* **17**, 988.
102. B. A. Trubnikov (1972). *JETP Letters* **16**, 25.
103. H. S. W. Massey and E. H. S. Burhop, *Electronic and Ionic Impact Phenomena* (Clarendon Press, Oxford, 1952), p. 232 *et seq*; R. J. Mackin, Jr., (1961). *Nuclear Fusion* **1**, 131; G. H. Dunn and B. Van Zyl (1967). *Phys. Rev.* **154**, 40 and references cited therein; R. J. Colchin (1970). *Nuclear Fusion* **11**, 329.
104. J. F. Clarke and J. T. Hogan, ORNL Annual Progress Report, ORNL-4688, Dec. 31, 1970, p. 56; ORNL Annual Progress Report, ORNL-4793, Dec. 31, 1971, p. 6.
105. L. A. Berry, J. F. Clarke and J. T. Hogan (1974). *Phys. Rev. Letters* **32**, 362.
106. L. A. Artsimovich (1972). *Nuclear Fusion* **2**, 215.
107. W. Stodiek (1972). *V European Conference Controlled Fusion and Plasma Physics* (Grenoble), **II**, 1.
108. D. Dimock, *et. al.*, *Proceedings Fourth International Conference, Plasma Physics and Controlled Nuclear Fusion Research* (IAEA, Vienna 1971), Vol **I**, p. 451.
109. M. Murakami, W. R. Wing, and P. H. Edmonds, "Thomson Scattering Measurements in ORMAK" (to be published).
110. F. C. Jobes, private communication.
111. R. Cano, *et. al.* (1973). *VI European Conference Controlled Fusion and Plasma Physics* (Moscow), **I**, 195.
112. C. Bobeldijk, D. Dimock and J. C. Hosea (1971). PPPL Annual Report, MATT-Q-29 p. 32.
113. D. Dimock, *et. al.* (1973). *Nuclear Fusion* **13**, 271.
114. F. C. Jobes and J. C. Hosea (1973). *VI European Conference Controlled Fusion and Plasma Physics* (Moscow), **I**, 199.
115. E. Hinnov, private communication.
116. K. Bol, *et. al.* *VI European Conference Controlled Fusion and Plasma Physics* (Moscow), Supplementary Paper.
117. S. von Goeler *et. al.* (1973). *Bull. Am. Phys. Soc II* **18**, 1254.
118. E. Hinnov *et. al.*, *ibid.*, 1253.
119. N. J. Peacock, *et. al.* (1969). *Nature* **224**, 448.
120. E. P. Gorbunov, S. V. Mirnov, V. S. Strelkov (1970). *Nuclear Fusion* **10**, 43.
121. L. L. Gorelik, *et. al.* (1972). *Nuclear Fusion* **12**, 185; Culham Conference 1965, Russian Translation 471 (AEC-tr-6760).
122. W. Stodiek, private communication.
123. H. P. Furth, Garching/Munich Conference, 1973, Paper B 9-I.
124. V. A. Vershkov, *et. al.* (1973). Kurchatov Preprint IAE-2291.
125. E. Hinnov, *et. al.* (1972). *Plasma Physics* **14**, 755.
126. Y. N. Dnestrovskii, D. P. Kostomarov (1970). *Atomnaya Energiya* **29**, 434.
127. D. F. Düchs, *et. al.*, Garching/Munich Conference, 1973, Paper B10-I; Plasma Physics Laboratory TM-265.
128. G. G. Kelley, *et. al.*, Garching/Munich Conference, 1973, Paper B3-I; L. D. Stewart, *et. al.*, Papers E 8, E 12; R. A. Dory, *et. al.*, Paper E 13.
129. L. A. Artsimovich, *et. al.* (1970). *JETP Letters* **11**, 304.
130. L. A. Berry, J. F. Clarke, and J. T. Hogan (1974). *Phys. Rev. Letters* **32**, 362.
131. J. Sinnis, *et. al.* (1972). *Phys. Rev. Letters*, **29**, 1214.
132. J. Schmidt, *et. al.* (1973). *Bull. Am. Phys. Soc.* **18**, 1323.
133. R. Prater and T. Tamano (1973). *Bull. Am. Phys. Soc.* **18**, 1255.
134. D. M. Meade, MATT-989 (1973), to be published in *Nuclear Fusion*.
135. D. F. Düchs, *et. al.* (1972). *Nuclear Fusion* **12**, 341.
136. H. P. Furth, P. H. Rutherford, H. Selberg (1973). *Phys. Fluids* **16**, 1054.
137. D. C. Robinson (1973). "A Model for Skin Diffusion," Joint European Tokamak Working Group Report, Technical Annex No. 1, p. 95.
138. J. T. Hogan and R. H. Fowler (1973). *Bull. Am. Phys. Soc. II* **18**, 1308.
139. H. W. Hendel and M. Yamada. Princeton Plasma Physics Laboratory MATT-1015 (1973); Submitted to *Phys. Rev. Letters*.
140. J. Schmidt and S. Yoshikawa (1971). *Phys. Rev. Letters* **26**, 753.
141. V. D. Shafranov and E. I. Yurchenko (1968). *Nuclear Fusion* **8**, 329.
- 141a. L. D. Stewart, R. C. Davis, J. T. Hogan, T. C. Jernigan, O. B. Morgan, and W. L. Stirling, Garching/Munich Conference, 1973, paper E12; W. L. Stirling, R. C. Davis, T. C. Jernigan, O. B. Morgan, J. J. Orzechowski, G. Schilling and L. D. Stewart, paper d-5 at Second Int. Conf. on Ion Sources, Vienna, 1972.
142. K. W. Ehlers and W. B. Kunkel, paper d-3 at Second Int. Conf. on Ion Sources, Vienna, 1972.
143. T. Ohkawa (1970). *Nuclear Fusion* **10**, 195.
- 143a. R. J. Bickerton (1972). *Comments on Plasma Phys. and Controlled Fusion* **1**, 95.
144. J. D. Callen, J. F. Clarke and J. A. Rome, Garching/Munich Conference, 1973, paper E-14.
- 144a. J. A. Rome, J. D. Callen and J. F. Clarke, ORNL-TM-4332, Sept., 1973 (to be published in *Nuclear Fusion*).
145. A. C. Riviere (1971). *Nuclear Fusion* **11**, 363.
146. D. R. Sweetman (1973). *Nuclear Fusion* **13**, 157.
147. D. J. Sigmar and G. Joyce (1971). *Nuclear Fusion* **11**, 447.
148. T. H. Stix (1972). *Plasma physics* **14**, 367.
149. J. W. Conner and J. G. Cordey, Garching/Munich Conference, 1973, paper F 3.
150. J. F. Clarke and D. J. Sigmar (private communication).
151. T. H. Stix, MATT-945, Dec., 1972.
152. P. J. Catto, M. N. Rosenbluth and C. S. Liu (1973). *Phys. Fluids* **16**; 1719.
153. J. G. Cordey and M. J. Houghton (1973). *Nuclear Fusion* **13**, 215.
- 153a. H. P. Furth, 6th European Conference on Controlled Fusion and Plasma Physics, Moscow, July 30–August 5, 1973; K. Bol, *et. al.*, Supplemental paper, *ibid.*; H. P. Eubank, *Bull. Am. Phys. Soc. II*, **18**, 1288; R. Golston, *et. al.* *ibid.*, 1972.
- 153b. C. F. Barnett, *et. al.*, *ibid.*, Supplemental paper.
154. A. Gibson *et al.*, Garching/Munich Conference, 1973, paper B16-I.
155. C. D. Child (1911). *Phys. Rev.* **32**, 492.
156. See for example: F. Powell, California Research and Development Company Report No. LWS-24920, 1953 (unpublished); P. R. Bell, J. S. Luce, R. J. Mackin, Jr., E. D. Shipley, and A. Simon, ORNL-2457 Special Report, 1958; J. R. McNally, Jr. (1971). *Nuclear Fusion* **11**, 187.
157. J. M. Dawson, H. P. Furth and F. H. Tenney (1971). *Phys. Rev. Letters* **26**, 1156.

158. M. A. Rothman, R. M. Sinclair, I. G. Brown and J. C. Hosea (1969). *Phys. Fluids* **12**, 2211.
169. J. C. Hosea and R. M. Sinclair (1970). *Phys. Fluids* **13**, 701.
160. V. L. Vdovin, *et al.* (1973). *Soviet Physics - JETP Letters* **17**, 2.
161. A. Stappans, E. W. McCume, J. A. Ruetz, *Proc. IEEE* **61**, 299 (1973). See especially the discussion on p. 313.
162. T. E. Yinast, D. R. Carter, J. A. Eshelman and J. M. Pawlikowski (1973). *Proc. IEEE* **61**, 357.
163. W. Millar, R. A. E. Bolton, and G. Cattenci, Garching/Munich Conference, 1973, Paper E-6.
164. J. C. Hosea and W. M. Hooke (1973). *Phys. Rev. Letters* **31**, 150.
165. W. M. Hooke and J. C. Hosea, Fifth European Conference on Controlled Fusion and Plasma Physics, Grenoble, August 21–25, 1972, Vol. I, p. 107; MATT 940, November 1972.
166. V. T. Tolok and V. A. Suprunenko, Garching/Munich Conference, 1973, Paper E4-I.
167. A. G. Diky, *et al.*, Garching/Munich Conference, 1973, Paper E 17.
168. C. O. Beasley and J. G. Cordey (1968). *Plasma Physics* **10**, 411 and references cited therein.
169. V. L. Vdovin, *et al.* (1971). *Soviet Physics - JETP Letters* **14**, 149.
170. N. V. Ivanov, I. A. Kovan, and E. V. Los (1972). *Soviet Physics - JETP Letters* **16**, 60.
171. V. E. Golant and A. D. Piliya (1972). *Soviet Physics Uspekhi* **14**, 413.
172. R. J. Briggs and R. R. Parker (1972). *Phys. Rev. Letters* **29**, 852.
173. V. M. Glagolev, N. A. Krivov and Yu. V. Skosyrev, in *Plasma Physics and Controlled Nuclear Fusion Research* (Proceedings of Madison Conference, Madison, June 17–25, 1971) (IAEA, Vienna, 1972), Vol III, p. 559 (Translation: Nuclear Fusion Supplement, 1972, p. 329.).
174. I. P. Gladkovsky, *et al.*, Fifth European Conference on Controlled Fusion and Plasma Physics, Grenoble, August 21–25, 1972, Vol. I, p. 109.
175. W. M. Hooke and S. Bernabei (1972). *Phys. Rev. Letters* **28**, 407.
176. M. Porkolab (1972). *Nuclear Fusion* **12**, 329 and references cited therein.
177. W. Hooke, Symposium on Plasma Heating and Injection, Varenna, Italy, 1972, p. 77.
178. W. M. Hooke and S. Bernabei (1972). *Phys. Rev. Letters* **29**, 1218.
179. T. K. Chu, S. Bernabei and R. W. Motley (1973). *Phys. Rev. Letters* **31**, 211.
180. V. F. Tarasenko, A. B. Kitsenko, V. I. Panchenko and K. M. Stepanov (1973). *Soviet Physics - Technical Physics* **17**, 1599.
181. R. A. Dandl, *et al.* in *Plasma Physics and Controlled Nuclear Fusion Research* (proceedings of Novosibirsk conference, August 1–7, 1968) (IAEA, Vienna, 1969), Vol. II, p. 435; V. V. Alikae, *et al.*, *ibid.*, Vol. II, p. 381 (translation: Nuclear Fusion Supplement, 1969, p. 183); T. Consoli, *ibid.*, Vol II, p. 361 and references cited therein; W. B. Ard, *et al.*, in *Plasma Physics and Controlled Nuclear Fusion Research* (Proceedings of Madison Conference, Madison, June 17–23, 1971) (IAEA, Vienna, 1972), Vol II, p. 619.
182. H. Grawe (1969). *Plasma Physics* **11**, 151.
183. A. N. Anisimov *et al.*, in *Plasma Physics and Controlled Nuclear Fusion Research* (proceedings of Madison Conference, June 17–23, 1971) (IAEA, Vienna, 1972) Vol III, p. 543 (Translation: Nuclear Fusion Supplement, 1972, p. 321). V. I. Arkhipenko, *et al.*, in *Plasma Physics and Controlled Nuclear Fusion Research* (Proceedings of Madison Conference, June 17–23, 1971) (IAEA, Vienna, 1972), Vol III, p. 525 (Translation: Nuclear Fusion Supplement, 1972, p. 311.).
184. C. W. Hartman, O. A. Anderson, D. H. Birdsall, E. B. Hooper, Jr. and R. H. Munger, Garching/Munich Conference, 1973, paper C-6.
185. V. V. Alikae, G. A. Bobrovskii, M. M. Ofitserov, V. I. Poznyak and K. A. Razumova, (1972). *JETP Letters* **15**, 27; at Fifth European Conference on Controlled Fusion and Plasma Physics, Grenoble, Aug. 21–25, 1972, Vol I, p. 108.
186. J. F. Clarke and R. A. Dandl, private communication.
187. S. Puri, private communication.
188. R. A. Dandl *et al.* (1971). *Nuclear Fusion* **11**, 411.
189. G. Grieger, Garching/Munich Conference, 1973, Paper D3-1.
190. H. Dreicer *et al.* (1973). *Phys. Rev. Letters* **31**, 426.
191. T. K. Chu and H. W. Hendel (1972). *Phys. Rev. Letters* **29**, 634.
192. F. H. Coensgen, *et al.*, Plasma Physics and Controlled Nuclear Fusion (Madison 1971), II, 721 (IAEA, Vienna, 1972).
193. S. C. Burnett, *et al.*, Plasma Physics and Controlled Nuclear Fusion (Madison 1971), III, 201 (IAEA, Vienna, 1972).
194. E. L. Berezovsky, *et al.*, Garching/Munich Conference, 1973, Paper B 19.
195. H. P. Furth and S. Yoshikawa (1970). *Phys. Fluids* **13**, 2593.
196. H. P. Furth, Garching/Munich Conference, 1973, Paper B9-I.
197. K. Bol, *et al.* (1972). *Phys. Rev. Lett* **29**, 1495.
198. K. Bol, *et al.*, Garching/Munich Conference, 1973, Paper B 12.
199. H. P. Eubank, *Bull. Am. Phys. Soc. II*, **18**, 1288. To be submitted to *Phys. Rev. Lett.*
200. S. M. Hamberger, J. Jancarik, L. E. Sharp, D. A. Aldcroft and A. Wetherell, in *Plasma Physics and Controlled Nuclear Fusion Research* (Proceedings of Madison Conference, June 17–23, 1971) (IAEA, Vienna, 1972), Vol II, p. 37, S. M. Hamberger and J. Jancarik, *Phys. Rev. Letters* **25**, 999 (1970) and references cited therein.
201. E. K. Zavoisky *et al.*, in *Plasma Physics and Controlled Nuclear Fusion Research* (Proceedings of Madison Conference, June 17–23, 1971) (IAEA, Vienna, 1972), Vol II, p. 3 (Translation: Nuclear Fusion Supplement, 1972, p. 81) and references cited therein.
202. W. E. Drummond, J. R. Thompson, M. L. Sloan and H. V. Wong, in *Plasma Physics and Controlled Nuclear Fusion Research* (Proceedings of Madison Conference; June 17–23, 1971) (IAEA, Vienna, 1972), Vol II, p. 167, and references cited therein.
203. W. E. Drummond (private communication).
204. D. Dimock, *et al.* (1973). *Nuclear Fusion* **13**, 271.
- 204a. L. L. Gorelick, *et al.* (1972). *Nuclear Fusion* **12**, 185.
- 204b. V. A. Vershkov and S. V. Mirnov, Princeton Plasma Physics Laboratory MATT-TRANS 113 (December 1973).
- 204c. E. Hinnov, Princeton Plasma Physics Laboratory MATT-1024 (1974).
- 204d. W. Stodiek, private communication.
- 204e. L. L. Gorelik, *et al.*, Plasma Physics and Controlled Nuclear Fusion Research (Proceedings, Culham Conference, 1965) **2**, p. 647 (IAEA, Vienna, 1966).
- 204f. H. P. Furth, Garching/Munich Conference, 1973, Paper B9-I.
205. R. Behrish (1972). *Nuclear Fusion* **12**, 695.
206. G. M. McCracken, private communication.
- 206a. L. L. Gorelik, *et al.*, Plasma Physics and Controlled Nuclear Fusion Research (Proceedings, Culham Conference, 1965) **2**, p. 647 (IAEA, Vienna, 1966).
207. T. Ohkawa, *et al.*, Gulf-GA-A12603 (1973).
208. Annual Report 1970, Max-Planck Institut für Plasmaphysik, p. 58.
209. A. S. Bishop, *et al.* (1965). *Phys. Fluids* **8**, p. 1541; Princeton Plasma Physics Laboratory MATT-Q-21, pp. 7–19 (1963).
- 210a. Princeton Plasma Physics Laboratory MATT-Q-29, Annual Report 1971, p. 4.
- 210b. T. Tamano, private communication.

211. A. Kitsunezaki, *et. al.*, Garching/Munich Conference, 1973, Paper G2.
212. C. Colven, A. Gibson, and P. E. Stott, Fifth European Conference on Controlled Fusion and Plasma Physics **1**, p. 7 (Grenoble, 1972).
213. M. B. Gottlieb, private communication.
214. D. Rosenberg and G. K. Wehner (1962). *J. Ap. Phys.* **33**, 1842.
215. A. Summers, N. Freeman and R. Daly (1971). *J. Ap. Phys.* **42**, 4774.
216. M. I. Guseva (1962). *Rad. Eng. and Elec. Phys.* **7**, 1563.
217. B. M. U. Scherzer, unpublished (1972).
218. Review of the Research Program of DCTR, Prepared for the CTR Standing Committee Meeting at MIT, April 26–27, 1973, Wash-1271.